

**CHARACTERIZATION OF THE TEXTURE,  
COMPOSITION AND POROSITY OF THE AYMAMÓN  
LIMESTONE FORMATION AND LABORATORY  
DERIVATION OF ELASTIC PROPERTIES AND  
SEISMIC WAVE VELOCITIES**

by

Vanessa Rosario López

A thesis submitted in partial fulfillment of the requirements for the degree of

MASTER OF SCIENCE  
in  
GEOLOGY

UNIVERSITY OF PUERTO RICO  
MAYAGÜEZ CAMPUS  
2008

Approved by:

---

James Joyce, PhD  
President, Graduate Committee

---

Date

---

Wilson R. Ramírez, PhD  
Member, Graduate Committee

---

Date

---

Eugenio Asencio, PhD  
Member, Graduate Committee

---

Date

---

Beatriz I. Camacho, PhD  
Representative of Graduate Studies

---

Date

---

Aaron Cavesie, PhD  
Chairperson of the Department

---

Date

## ABSTRACT

The study area of this project lies in the central portion of northern coastal plain of Puerto Rico, which is characterized by mogote karst terrains that form on the Tertiary Aymamón Limestone Formation. Lowlands between the mogote hills and ridges are covered by Quaternary blanket deposits that obscure and fill underlying sinkholes in the Aymamón Limestone. Subsurface investigations of these features and their potential for collapse rely heavily on seismic surveys. The purpose of this thesis was to investigate the physical properties of the Aymamón Limestone Formation that control its seismic wave velocity to enhance interpretation of subsurface seismic analyses. A test boring (B-1) was drilled at the Monte Verde Urbanization's basketball court at Manatí, in order to correlate the derived MASW seismic velocity profile with the subsurface geology of the site and collect core samples for testing. The boring encountered cavernous porosity at depths between 21.5-27.4 m that precluded core sampling at the target depths. Only two indurated recrystallized limestone fragments with densities of  $2,084 \text{ kg/m}^3$  and  $1,602 \text{ kg/m}^3$ , respectively, were recovered from a depth of 25 meters.

As an alternative Aymamón Limestone core samples from four (4) different core holes (NC-4, NC-5, NC-9, and NC-10) drilled by the USGS were collected in order to characterize their composition, texture and porosity and select sample for testing. Much of the Aymamón Limestone cores from this mogote karst zone are comprised of well-indurated, recrystallized and well-cemented limestones. Samples were mostly packstone and less commonly wackestone and grainstone textures. Most of the porosity is vuggy and mouldic with much less intra-particle porosity. The fossils in the core samples included calcareous algae, benthic foraminifers, and echinoderms that have a calcite skeletal composition and corals, mollusks, and other fragments

that have an aragonite skeletal composition. The micro-porosity percentages for cores NC-4, NC-5, NC-9, and NC-10 were 1.49%, 1.72%, 3.31%, and 2.54%, respectively. The mineralogy of the carbonate samples is dominantly composed of calcite with some samples consisting of high Mg calcite and dolomite.

Four core samples from the original target depths were chosen from the closest NC-5 and subjected to unconfined compression tests to determine their elastic properties and derivative seismic velocities. The samples from 20m and 27.5m consisted of wackestones and those from 21.5m and 23m were packstones. All four samples were composed of calcite or high Mg calcite. Vug porosity dominated the four samples with some inter-particle porosity in the 21.5m sample and both intra-particle and fracture porosity in the 23m sample. The estimated macro-porosity percentages for samples from 20, 21.5, 23, and 27.5 meters deep were 19.33%, 1%, 3.5%, and 39.67%; and the micro-porosity values were 1.69%, 0.88%, 2.15%, and 0.39%, respectively. The density values of the samples from core NC-5 range from 2,295 to 2,510 kg/m<sup>3</sup>. The results of the tested samples showed that Young's modulus ranged from 1.02-3.04 GPa, Poisson's ratio from 0.27-0.37, the shear modulus from 0.5-1.3 GPa, and the bulk modulus from 1.06-2.6 GPa. The Young's modulus and the shear modulus consistently increased with sample depth. The resultant calculated P-wave velocities ranged from 859-1,360 m/sec and S-wave velocity ranged from 446-740 m/sec. Calculated S-wave velocities increased consistently with depth of sample and reached a maximum at the sample with the highest mega-porosity and least density. The test results are consistent with field observations at Monte Verde where cavernous porosity was encountered at depths where seismic profiles increasingly higher shear wave velocities. The association of higher calculated P-wave velocities with lower micro-porosity suggests that

recrystallization of the limestone between mega-pores to a denser mass may be controlling seismic wave velocity in limestones in advanced stages of dissolution.

## RESUMEN

El área de estudio de este proyecto se encuentra localizada en la parte central de la costa norte de Puerto Rico, la cual está caracterizada por terrenos cársicos de mogotes, los cuales se forman en la Formación Aymamón (Terciario). Las tierras bajas entre los mogotes y las cuevas están cubiertas por depósitos de mantos de arena de edad Cuaternaria, los cuales ocultan y llenan los sumideros en la Formación Aymamón. Investigaciones superficiales de estos sumideros y su potencial para colapsar dependen de las mediciones sísmicas. El propósito de esta tesis fue investigar las propiedades físicas de la Formación Aymamón que controlan las velocidades de ondas sísmicas para intensificar la interpretación de análisis sísmicos en la superficie. Un barreno (B-1) fue realizado en la cancha de baloncesto de la Urbanización Monte Verde en Manatí, para correlacionar el perfil de las velocidades sísmicas obtenido de la técnica de MASW con la geología superficial del área y recolectar muestras de roca para realizar pruebas. Durante el barreno se encontró porosidad de caverna a una profundidad de 21.5 a 27.4 metros que impidió el muestreo hacia las profundidades deseadas. Solamente dos fragmentos de roca caliza con densidades de  $2,084 \text{ kg/m}^3$  y  $1,602 \text{ kg/m}^3$ , respectivamente, endurecidos y recristalizados fueron recolectados a una profundidad de 25 metros.

Como una alternativa, muestras de núcleos de roca caliza de cuatro (4) barrenos diferentes (NC-4, NC-5, NC-9, y NC-10) de la Formación Aymamón, realizados por el Servicio Geológico de los Estados Unidos (USGS, por sus siglas en inglés) fueron recolectadas para caracterizar su composición, textura y porosidad y seleccionar las muestras para realizar las pruebas. La mayoría de los núcleos de roca caliza de esta zona cársica de mogotes, están bien endurecidos, recristalizados y bien cementados. La textura presente en las muestras de roca es mayormente “packstones” y menos común “wackestones” y “grainstones”. La porosidad es

mayormente “vuggy” y de molde, siendo menos común la porosidad dentro de las partículas. Los fósiles presentes en las muestras de roca incluyen, algas calcáreas, foraminíferos bénticos y equinodermos, los cuales están compuestos de calcita; y corales, moluscos, y otros fragmentos compuestos de aragonita. Los porcentajes de micro-porosidad para los núcleos NC-4, NC-5, NC-9, y NC-10 fueron 1.49%, 1.72%, 3.31%, y 2.54%, respectivamente. La mineralogía de las rocas es mayormente de calcita con algunas muestras compuestas de calcita magnesiana y dolomita.

Cuatro muestras de roca de las profundidades deseadas fueron escogidas del núcleo NC-5 y fueron sometidas a pruebas de compresión uniaxial para determinar las constantes elásticas las velocidades sísmicas derivadas. Las muestras de 20 m y 27.5 m tienen una textura “wackestones” y las de 21.5 m y 23 m son “packstones”. Las cuatro muestras están compuestas de calcita y calcita magnesiana. La porosidad “vug” es la más común en las cuatro muestras, la muestra de 21.5 m mostró porosidad entre las partículas y la muestra de 23 m mostró porosidad dentro de la partícula y de fractura. Los porcentajes estimados de macro-porosidad para las muestras de 20, 21.5, 23, y 27.5 metros de profundidad fueron 19.33%, 1%, 3.5%, y 39.67%; y los valores de la micro-porosidad fueron 1.69%, 0.88%, 2.15%, y 0.39%, respectivamente. Los valores de la densidad de las muestras del núcleo de roca NC-5 varían de 2,295 a 2,510 kg/m<sup>3</sup>. Los resultados de las muestras de roca muestran que el módulo de Young varía de 1.02-3.04 GPa, la razón de Poisson varía de 0.27-0.37, el módulo cortante varía de 0.5-1.3 GPa, y el módulo de compresión varía de 1.06-2.6 GPa. El módulo de Young y el módulo cortante aumentaron consistentemente con la profundidad de las muestras. Las velocidades calculadas resultantes de la onda P varían de 859-1,360 m/seg y las de la onda S varían de 446-740 m/seg. Las velocidades calculadas de la onda S aumentaron consistentemente con la profundidad de las muestras y alcanzaron un máximo en la muestra que tenía el valor de macro-porosidad más alto y

la densidad menor. Los resultados de las pruebas son consistentes con las observaciones de campo obtenidas en la Urbanización Monte, donde la porosidad de caverna fue encontrada a profundidades donde las velocidades de la onda cortante aumentaron. La asociación de las velocidades altas de la onda P con la baja micro-porosidad sugiere que la recristalización de la roca caliza entre los mega-poros a una masa más densa puede estar controlando las velocidades de ondas sísmicas en la roca caliza en avanzados estados de disolución.

## **DEDICATION**

This thesis project is dedicated to God, for giving me the wisdom and the strength to finish this investigation, and to my parents and brothers, who have offered to me their unconditional support. Also this work is dedicated to my love and best friend, Angel Robles.



## ACKNOWLEDGEMENTS

I would like to deeply thank those persons who helped in one way or another during the time of the investigation of my thesis project, who provided me with useful and helpful assistance.

First I would also like to express my gratitude to my advisor, Dr. James Joyce, whose expertise, understanding, and patience, added considerably to my graduate experience. He went well beyond their duty in helping me with this thesis, reading and copiously commenting on earlier drafts. I appreciate his assistance through these years. I am completely grateful for his help, availability and patience. THANKS!

My thanks must also go to the other two members of my graduate committee, Dr. Wilson R. Ramírez, and Dr. Eugenio Asencio, for the assistance they provided at all levels of the research project. For all their guidance, both with the mechanics of the written text and with the implications that lay therein, I wish to express my sincerest appreciation.

I would also like to thank my family for the support they provided me through my entire life. My parents, Mario and Lillian, whose patience, support, and impeccable understanding allowed me to write this thesis. They have breathlessly awaited this thesis, and they deserve full credit for it. So there is also a “thank-you, mom and dad”. Also warmest thanks must go to my two brothers; Mario I. and Carlos, whose support and assistance also help me to finish this thesis project. In particular, I must acknowledge my boyfriend and best friend, Angel, without whose love, encouragement and assistance, I would not have finished this thesis. He was with me when things went difficult, “thank you my love for your patience and support”.

I would like to express my deeply gratitude to the Robles-Meléndez family, for their unconditionally support and assistance since I start graduate school. Also I must thank the Estrada-Arroyo family, for their assistance during part of the field work.

I must also acknowledge the Civil Engineering Faculty from the Polytechnic University of Puerto Rico, Hato Rey, for the provision of the engineering laboratory facilities and the materials needed for this study. Special thanks go to Eng. Sigfredo Torres and Geol. Jesús Rodríguez from the U.S. Geological Survey, for their help in the finding of research material. My thanks must go to Geo Cim, Inc., (Geol. Alejandro Soto) and Suelos, Inc. (Eng. Carlos Rodríguez). Also, I must thank the University of Puerto Rico Agricultural Experimental Station “Finca La Montaña”, Aguadilla.

In conclusion, I recognize that this research project would not have been possible without the financial assistance of Exxon Mobile. Finally, I would like to express my gratitude to the University of Puerto Rico, Mayagüez, Department of Geology (Teaching Assistantship).

## TABLE OF CONTENTS

	PAGE
List of Figures .....	xiv
List of Tables .....	xvi
List of Graphs .....	xvii
List of Abbreviations .....	xviii
Chapter I: Introduction.....	1
Study Area .....	3
Chapter II: Geological Setting .....	7
General Physiography of Puerto Rico.....	7
North Coast (Karst) Limestone Belt of Puerto Rico .....	11
Chapter III: Methodology .....	14
Drilling and Sampling Activities .....	14
Collection of Rock Samples.....	15
Porosity Quantification .....	15
Thin Section Preparation.....	15
Point Counting Technique .....	15
Micro-Porosity .....	16
Macro-Porosity .....	16
Bulk Density .....	16
Mineral Identification .....	17

Unconfined Compressive Strength (UCS) Test.....	17
Static Testing .....	18
Specimen Preparation .....	18
Testing Setup .....	18
Calculation of Elastic Constants and Seismic Wave Velocities .....	19
Geophysically Determined Elastic Constants and Seismic Wave Velocities .....	22
Cross-hole geophysical studies .....	22
Shear Wave Velocity at Monte Verde .....	22
Chapter IV: Results.....	23
Test Boring.....	23
Rock Core and Thin Section .....	26
Porosity .....	38
Mineral Identification .....	45
Bulk Density .....	46
Elastic Properties of the Aymamón Limestone Core Samples .....	47
Chapter V: Interpretation and Analysis .....	55
Test Boring.....	55
Rock Core and Thin Section .....	55
Mineral Identification .....	56
Bulk Density .....	56
Elastic Properties of the Aymamón Limestone Core Samples .....	57

Comparison of the Calculated Seismic Velocities with MASW and CHS methods ...	58
Chapter VI: Discussions and Conclusions .....	59
References .....	61
Appendixes	
Appendix A     Results of the Unconfined Compressive Strength Test	
Appendix B     XRD Results	

## LIST OF FIGURES

	PAGE
<b>CHAPTER I</b>	
Figure 1.1 Topographic map of the Manatí Quadrangle showing location of Boring B-1 .....	4
Figure 1.2 Aerial photograph showing location of Boring B-1 in the basketball court at the Monte Verde Urbanization, Coto Norte Ward, Manatí.....	5
Figure 1.3 Location of core holes NC-4, NC-5, NC-9, and NC-10 in Topographic Maps of Manatí and Barceloneta Quadrangles .....	6
<b>CHAPTER II</b>	
Figure 2.1 Location of Puerto Rico in the Caribbean region .....	9
Figure 2.2 Principal physiographic divisions of Puerto Rico .....	10
<b>CHAPTER IV</b>	
Figure 4.1 1-D shear wave vs depth profile.....	23
Figure 4.2 Picture of thin section from NC-4 32.3 m showing vug porosity .....	36
Figure 4.3 Picture of thin section from NC-9 14 m showing vug porosity .....	36
Figure 4.4 Picture of thin section from NC-5 20 m showing fracture porosity .....	37
Figure 4.5 Picture of thin section from NC-10 7.9 m showing mouldic porosity .....	37
Figure 4.6 Lithology, texture and micro-porosity percentages of Core NC-4.....	41
Figure 4.7 Lithology, texture and micro-porosity percentages of Core NC-5.....	42
Figure 4.8 Lithology, texture and micro-porosity percentages of Core NC-9.....	43
Figure 4.9 Lithology, texture and micro-porosity percentages of Core NC-10.....	44
Figure 4.10a Core sample NC-5 (depth-20m) .....	48
Figure 4.10b Stress vs Strain loading curve of Core NC-5 20 m .....	48
Figure 4.11a Core sample NC-5 (depth-21.5m) .....	49

Figure 4.11b Stress vs Strain loading curve of Core NC-5 21.5 m .....	49
Figure 4.12a Core sample NC-5 (depth-23m) .....	50
Figure 4.12b Stress vs Strain loading curve of Core NC-5 23 m .....	50
Figure 4.13a Core sample NC-5 (depth-27.5m) .....	51
Figure 4.13b Stress vs Strain loading curve of Core NC-5 27.5 m .....	51

## LIST OF TABLES

<b>CHAPTER IV</b>	<b>PAGE</b>
Table 4.1 Soil Boring Log .....	24
Table 4.2 Descriptions of Core NC-4 .....	26
Table 4.3 Descriptions of Core NC-5 .....	27
Table 4.4 Descriptions of Core NC-9 .....	28
Table 4.5 Descriptions of Core NC-10 .....	28
Table 4.6 NC-4 Thin section Log .....	29
Table 4.7 A NC-5 Thin section Log .....	30
Table 4.7 B NC-5 Thin section Log (Cont.) .....	31
Table 4.8 NC-9 Thin section Log .....	32
Table 4.9 A NC-10 Thin section Log .....	33
Table 4.9 B NC-10 Thin section Log (Cont.) .....	34
Table 4.10 Micro-porosity classification in the Aymamón Limestone Formation.....	35
Table 4.11 Micro-porosity percentages in the Aymamón Limestone Formation.....	38
Table 4.12 Mineralogy of samples determined by XRD technique.....	45
Table 4.13 Mineralogy of thin sections determined by staining technique .....	46
Table 4.14 Bulk densities of NC-5 limestone core samples and Monte Verde core fragments ....	46
Table 4.15 Core sample density, porosity, elastic constants and seismic velocities .....	52
Table 4.16 Comparison of laboratory calculated and MASW analysis seismic wave velocities .	53
Table 4.17 Comparison of laboratory and field values of seismic velocities .....	53
Table 4.18 Comparison of laboratory and field values of elastic constants .....	54



## LIST OF GRAPHS

	PAGE
<b>CHAPTER IV</b>	
Graph 4.1 Graph showing the relation between micro-porosity and depth of core NC-5 .....	39
Graph 4.2 Graph showing the relation between micro-porosity and depth of core NC-9 .....	39
Graph 4.3 Graph showing the relation between micro-porosity and depth of core NC-10 .....	40

## LIST OF ABBREVIATIONS

American Standard for Testing and Materials	ASTM
Bulk Modulus	K
Mega Pascals	MPa
North Coast	NC
Pascals	Pa
Poisson's ratio	$\nu$
Pound square inch	psi
Primary (P) wave velocity	$V_p$
Shear Modulus	$\mu$
Shear (S) wave velocity	$V_s$
Standard Penetration Test	SPT
Unconfined Compressive Strength	UCS
United States Geological Survey	USGS
X-ray Diffraction	XRD
Young's Modulus	E

## **Chapter I: Introduction**

The North Coast of Puerto Rico is characterized by karst landforms developed on Tertiary limestone. The karst processes of dissolution and re-precipitation of carbonate minerals that have formed the characteristic mogotes and sinkholes of these terrains remains active to the present day. Mogotes are haystack-shaped residual hills that remained where water percolates through the limestone to form sinkholes and underground rivers that carve out caves whose collapse may form additional sinkholes.

Sinkholes are important near-surface indicators of active karst features at depth, such as cavities, conduits and solution enlarged fractures. Collapse of sinkholes represents a major geologic hazard in the north coast of Puerto Rico, causing millions of dollars in damage during the rainy season. On November 30, 2002 after an extensive rainy period, houses in the Monte Verde Urbanization, Coto Norte Ward, Manatí; were extensively damage due to the sudden partial collapse around a sinkhole within the community. This event brought to light the problem of the collapse of sinkholes that are hidden below a cover of thick Quaternary sandy and clayey sediments referred to as Blanket Deposits. The difficulty with addressing this problem lies in determining the location of buried sinkholes subject to collapse. Because of the limited scope and sample range provided by standard drilling practices many engineering companies have turned to geophysical methods to delineate buried and covered sinkhole features. The problem of detection is further complicated in urbanized areas where much of the area is covered by pavements and access is limited.

This investigation forms part of a larger geophysical study that is being conducted in an urbanized and developed sector of Manatí to address problems related to karst-sinkhole detection. The Monte Verde Urbanization Site at Manatí was selected for this study because the

2002 collapse and the existence subsequent subsurface geotechnical data collected around the collapse site of it had previously been studied by GeoCim, a Geotechnical and Testing Services Firm located in San Juan. In 2004, they drilled 2 soil borings at Street No. 34 of the Monte Verde Urbanization. The present study focuses on another portion of the urbanization where subsurface collapse has become a serious concern.

The purpose of this thesis was to investigate the physical properties of the Aymamón Limestone Formation that control its elastic shear-wave velocities. In specific this investigation seeks to:

- Determine the elastic constants: Young's modulus, Poisson's ratio, Bulk modulus and shear modulus by static laboratory tests of rock samples of the Aymamón Limestone subjected to uniaxial loading. This study uses core samples drilled in the Aymamón Limestone by the U.S. Geological Survey as part of a comprehensive study of the North Coast Aquifer System.
- Determine rock density and porosity
- Drill a test boring and collect soil and rock samples at the Monte Verde Urbanization basketball court
- Make descriptions and petrographic analyses to better characterize the physical properties of the Aymamón Limestone in order to assess the applicability of the laboratory analyses to interpretation of seismic surveys in the formation as a whole.
- To investigate the physical properties of the Aymamón Limestone Formation that controls its seismic wave velocity, as studied at different locations along the Puerto Rico North Coast.

Samples were obtained from four (4) 30-meters deep core holes (NC-4, NC-5, NC-9, and NC-10) along the north coast of Puerto Rico.

### **Study Area**

The study area of this project comprises the north-central part of the onshore portion of the Puerto Rico North Coast Limestone Belt. This study is based on one borehole drilled at the basketball court at the Monte Verde Urbanization, Manatí, and four (4) core holes (NC-4, NC-5, NC-9, and NC-10) drilled by the US Geological Survey in cooperation with the Puerto Rico Department of Natural Resources as part of a comprehensive study of the North Coast Aquifer System.

The study area is located in the North Coast Limestone Belt. Boring B-1 is included in the Topographic Map of the Manatí Quadrangle from the U.S. Geological Survey (USGS) (Figure 1.1) and also core holes NC-4 and NC-9 (Figure 1.3). Core holes NC-5 and NC-10 are included in the Topographic Map of the Barceloneta Quadrangle from the U.S. Geological Survey (USGS) (Figure 1.3). Karst topography, the result of dissolution of the middle Tertiary limestone, prevails in the areas where the cores were drilled. A detailed description of the site Geology follows in Chapter II.

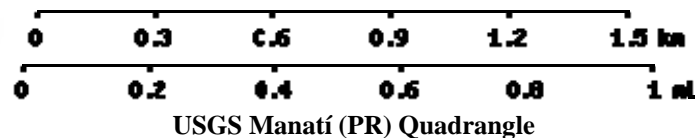
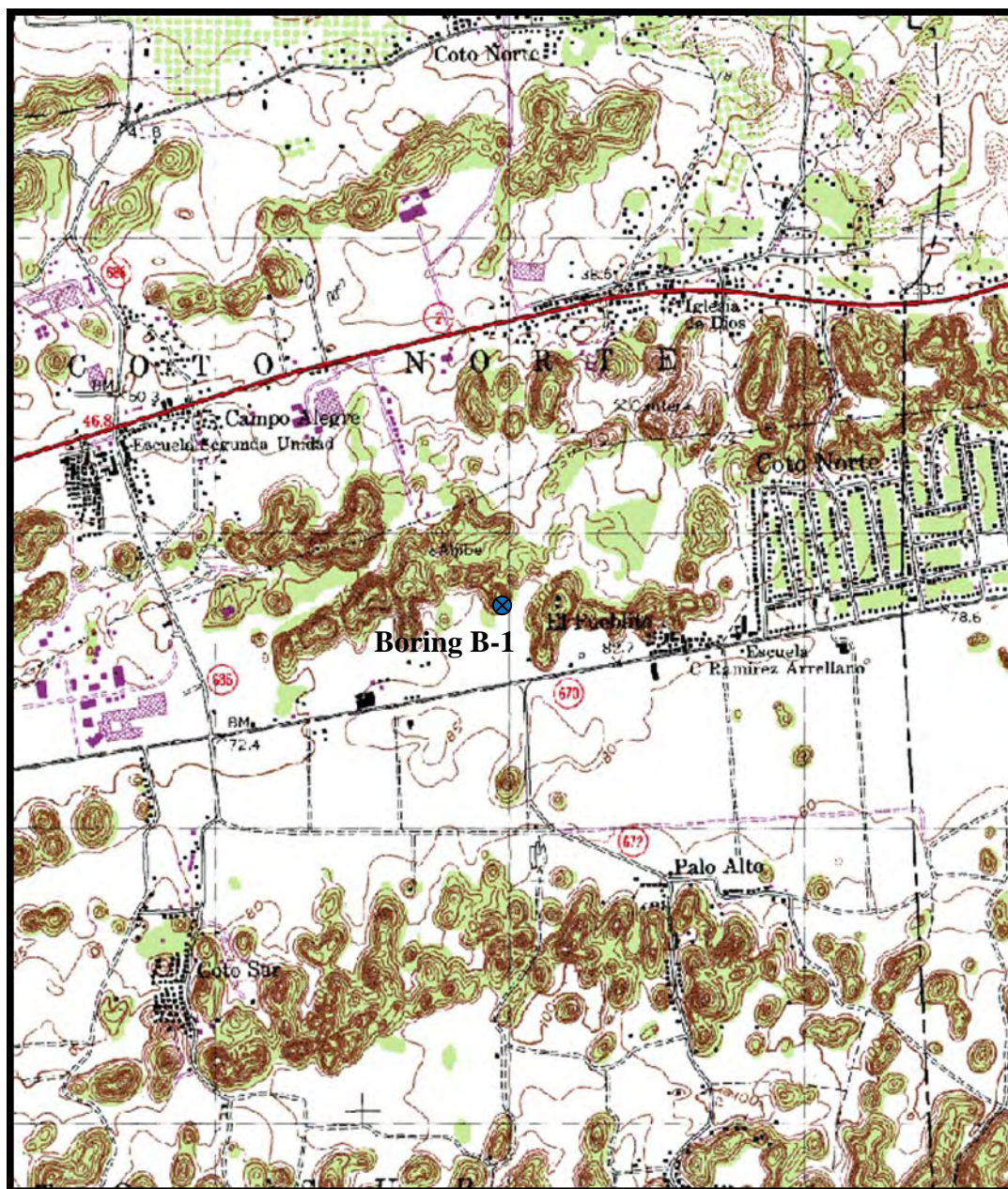
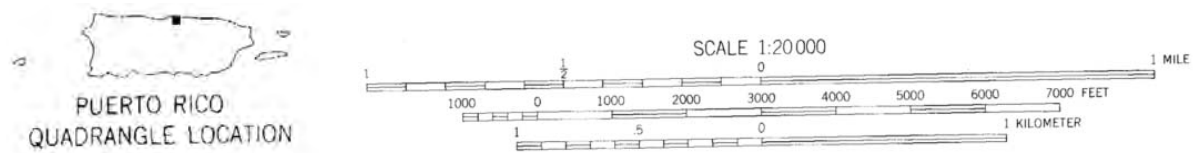
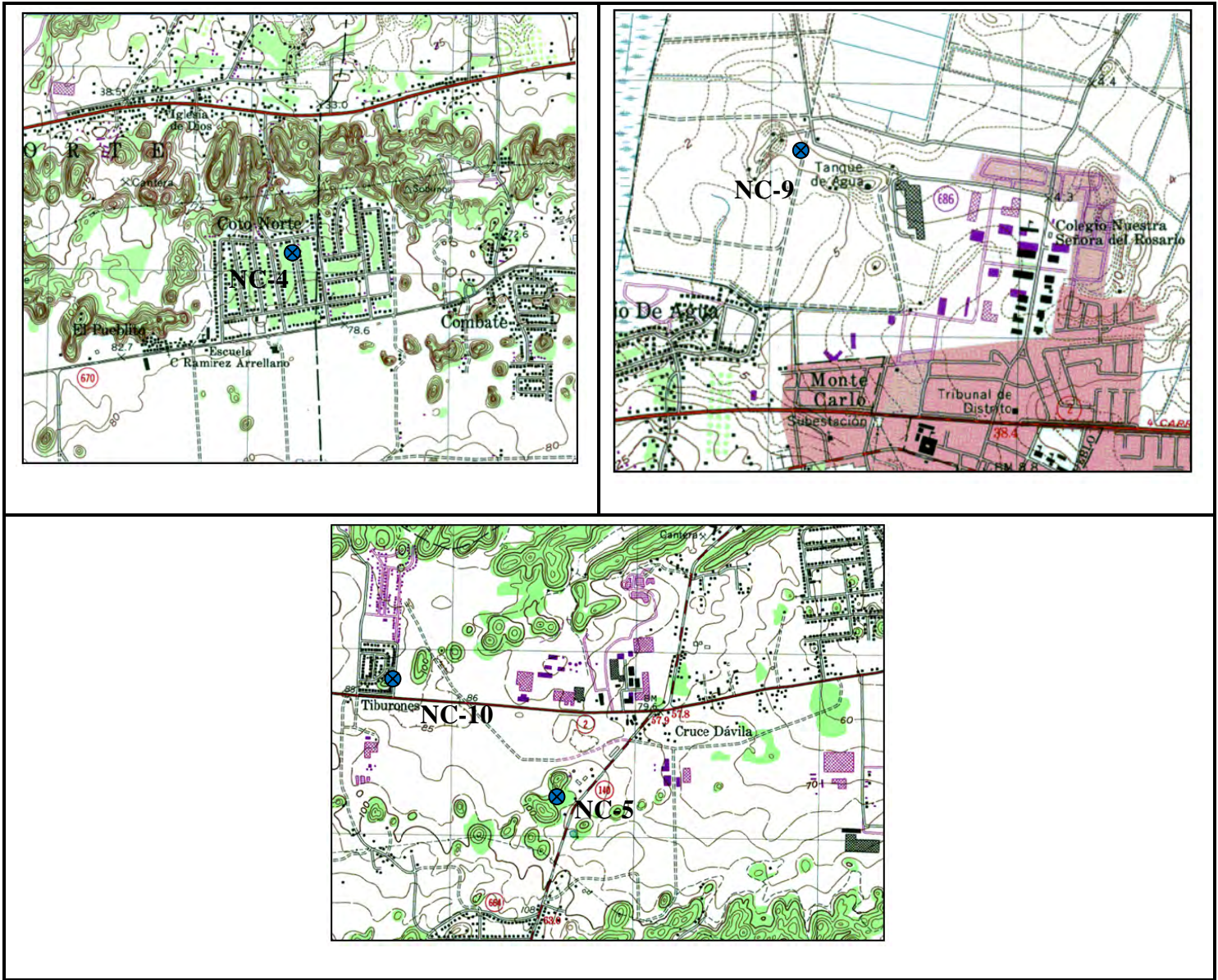


Figure 1.1: Topographic Map of the Manatí Quadrangle showing location of Boring B-1.



**Figure 1.2: Aerial photograph showing location of Boring B-1 in the basketball court at the Monte Verde Urbanization, Coto Norte Ward, Manatí.**





**Figure 1.3: Location of core holes NC-4, NC-5, NC-9, and NC-10 in Topographic Maps of Manatí and Barceloneta Quadrangles.**



## **Chapter II: Geological Setting**

### **General Physiography of Puerto Rico**

Puerto Rico is the easternmost island of the Greater Antilles Arc System and is located in the northeastern Caribbean Sea region between latitudes 17° 30' and 18° 15' and longitudes 64°15' and 66° 30'. It is bounded on the north by the Puerto Rico Trench, on the south by the Muertos Trough, on the east by the Anegada Passage and on the west by the Mona Canyon (Krushensky and Schellekens, 2000) (Figure. 2.1). The island of Puerto Rico is roughly rectangular in shape, extending up to 111 miles (179 km) from east to west and 39 miles (63 km) from north to south. The island can be divided into three main physiographic areas:

- 1) A central east-west mountainous area;
- 2) A limestone belt in the northwest to north-central area; and
- 3) A discontinuous fringe of relatively flat alluvial coastal plains in the south and northeast areas (Figure. 2.2) (Monroe, 1980a).

The Puerto Rico central mountainous interior consists of rocks that are predominantly volcanic and is flanked on the north and south by younger limestone deposits of Tertiary age and by clastic sediments of Quaternary age (Ramírez, 2000) (Figures. 2.2). The most extensive deposits of Puerto Rico are along the north coast in a band that extends from the northwestern corner of the island to the Río Grande de Loíza in the northeastern corner. This band has a maximum width of 14 miles (Monroe, 1980a). In this area along the north coast, a mature tropical karst has developed by dissolution of the limestone. The limestone deposits in the southern part of the island are less extensive and because of a dryer climate, karst features are not as well developed.

About one-fifth of Puerto Rico is covered by limestone. The late Oligocene to Middle Miocene northern limestone belt (Northern Karst Topography Province) extends about 135 km, from Río Grande de Loíza to the west coast in Aguadilla, and reaches a maximum width of about 23 km south of Arecibo (Monroe, 1980b). Limestones in Puerto Rico have been extensively eroded by dissolution and this has contributed to the wide variety of karst relief features, including sinkholes, caverns, *mogotes*, and solution valley. All of these features are well-developed on the north coast limestone. The karst topography province in the north-central and northwestern areas is composed principally of Neogene limestones that are at least 1,700 m thick (Briggs and Gordon, 1961; Monroe, 1980a; Ward *et al.*, *in press*). This sediment accumulated in the North Coast Tertiary Basin during late Oligocene to Pliocene time (Ramírez, 2000).

Quaternary clastic sediments that cover Puerto Rico consist predominately of poorly sorted mixtures of gravel, sand, and finer materials (Quiñones-Márquez and others, 1984). These sediments lie along the north and south coastal plains and in river valleys along the east and west coasts of Puerto Rico.

Coastal plain deposits flank the northern and the southern sides of the island. These coastal plain deposits consist of alluvial fans, coalescing flood plains and beach and lagoonal deposits that have very low relief, with the exception of isolated hills of volcanic, intrusive, or sedimentary bedrock material (Monroe, 1980a & b). An insular shelf extending a few kilometers off the northern coast to a maximum of 15 km off the southern coast surrounds the island. A substantial part of his Puerto Rico insular shelf was subaerially exposed during the Pleistocene (Donnelly, 1964).

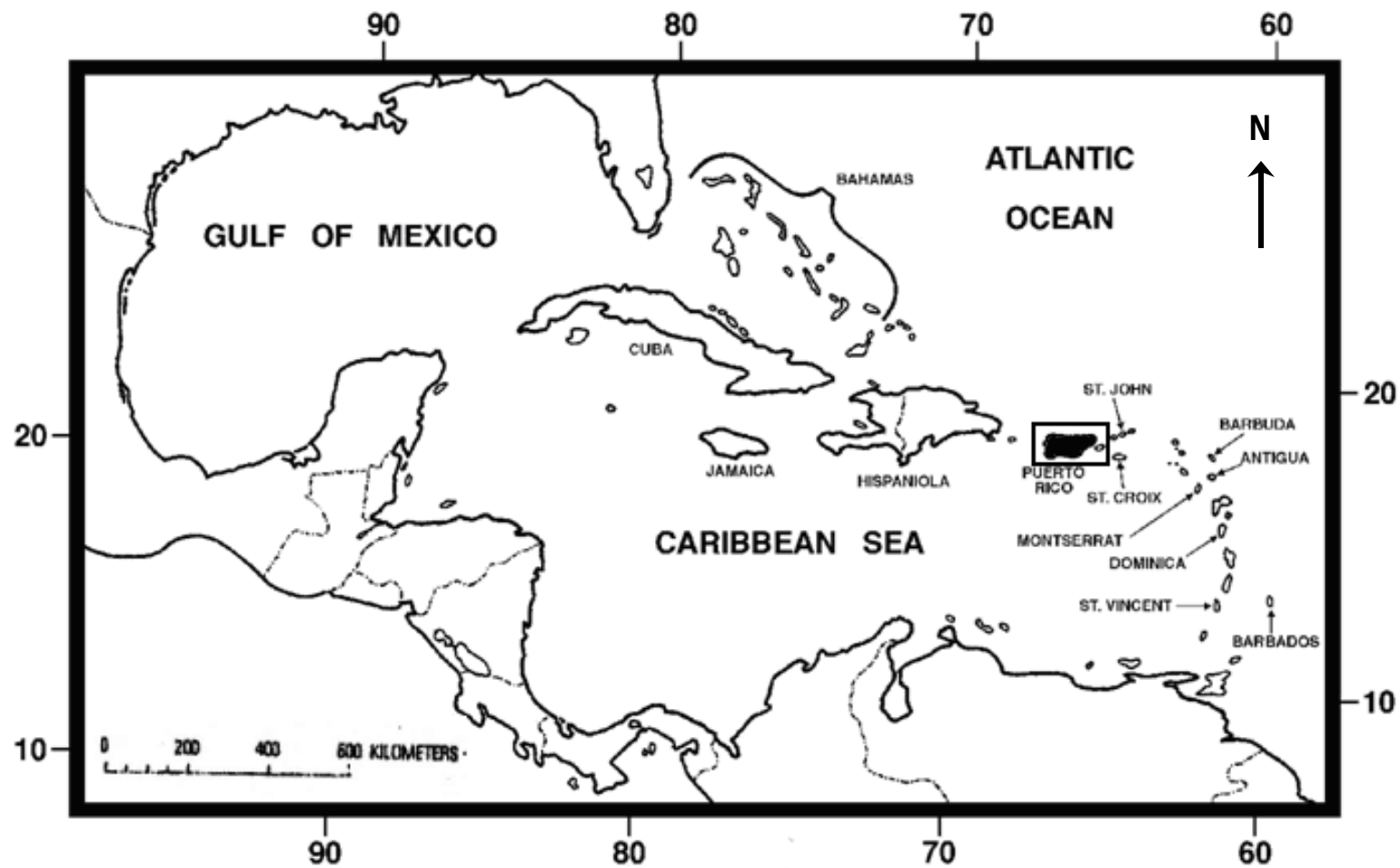


Figure 2.1: Location of Puerto Rico in the Caribbean region.

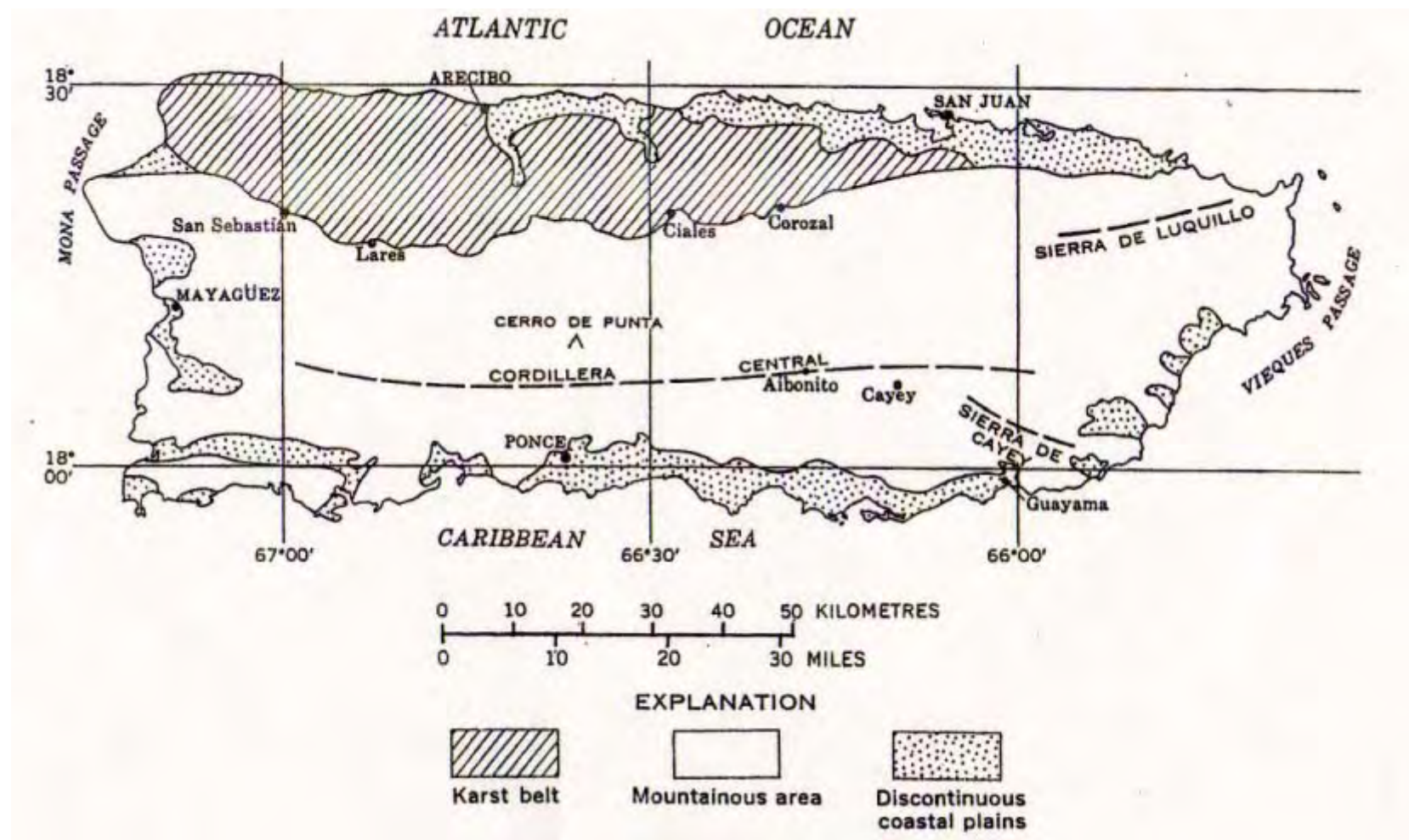


Figure 2.2: Principal physiographic divisions of Puerto Rico (from Monroe, 1976).

## **North Coast (Karst) Limestone Belt of Puerto Rico**

The most important limestone units in the karst terrain of Puerto Rico are the formations of Oligocene and Miocene age in northern and southern Puerto Rico. Limestone rocks vary considerably in susceptibility to erosion (Meyerhoff and others, 1983), and they dip generally north from about 5° along their southern border to less than 1° near the Atlantic Ocean (Monroe, 1976).

The strata have been divided into six formations (Monroe, 1973a), ranging in age from late Oligocene to middle Miocene; four of the formations consist principally of limestone, and the other two contain limestone locally. In ascending order the formations are:

- Lares Limestone,
- Cibao Formation,
- Aguada Limestone,
- Aymamón Limestone and,
- Camuy Formation.

Each of which has distinctively different solution properties (Meyerhoff and others, 1983), which give rise to karst phenomena characteristics of each formation. A sixth unit, the Mucarabones sand, is the eastern lateral clastic equivalent of the Lares Limestone and the lower two thirds of the Cibao Formation (Monroe, 1976).

The karst features of the Aymamón are dominated by the mogotes, which form a tower karst throughout its outcrop belt, except in the northwestern part of Puerto Rico, where the Aymamón consists mainly of chalky material that has been eroded into low west-trending ridges,

possibly in part by marine plantation (Meyerhoff and others, 1983). The relatively unconsolidated Aymamón has been recrystallized (Monroe, 1966) on the surface into a very hard limestone, which caps the mogotes and causes them to stand up above the relatively easily eroded ridges of the Aguada Limestone that form the boundaries of the dolines. Hence, the basal beds of the Aymamón form a very pronounced cuesta scarp that is readily noted on the ground but that is difficult to delineate on topographic maps, because it is masked by the abundant deep closed depressions both to the north and the south. The mogotes rise out of irregular plains floored by generally red to brown argillaceous sand and sandy clay, generally referred to as “blanket sand” after the work by Briggs (1966). Other karst features common in the Aymamón are well-like vertical shafts seen at the sides of mogotes and in places in the areas covered by blanket deposits (Monroe, 1973); caves are present in places, but the Aymamón is generally so unconsolidated, except on the surface, that only a few caves are very long (Monroe, 1976).

The blanket sands fill in the depressions between mogotes and the ridges of mogotes in the northern karst belt between Bayamón and Aguadilla, especially in the northern part of the belt in the outcrop area of the Aymamón Limestone and the Camuy Formation. Blanket sands were named and described in 1962 by Briggs (1966). Briggs described them as composed of quartz sand, clayey sand, sandy clay, and clay, “the dominant constituents of which are angular, sub-angular, and sub-round, medium to fine grains of clear quartz, and reddish-brown to moderate-brown, dark yellowish orange, light-gray, and white, commonly ferruginous kaolinitic clay. Quartz and clay together make up almost all of the blanket sands at most outcrops, but their relative proportions vary greatly.”

Briggs (1966) believed that parent material of the blanket sands, debris from the volcanic interior, was carried to the coastal area by rivers during the long period between deposition of the limestone and its gradual uplift to its present altitude above sea level, probably beginning shortly after deposition of the Aymamón Limestone was completed. He believed that karstification of the limestone has already started at that time, and that longshore currents of the sea distributed the river-transported material over the partly karstified surface, so that the alluvium was trapped in solution depressions that had formed in the limestone surface. After deposition, the volcanic-derived debris was weathered to laterite earth. This theory is supported by the greater abundance of sand over clay in the eastern part of the belt where through-flowing rivers are more abundant, and by the relative scarcity of sand west of the Arecibo area. Briggs's ideas are also supported by the fact that the higher areas of blanket sand farthest from the coast, presumably the older parts, contain much more clay than the lower seaward parts, which indicated greater laterization of these presumably older deposits (Monroe, 1976).

## **Chapter III: Methodology**

### **Drilling and Sampling Activities**

A soil boring and a rock core drilling were conducted on February 27 to March 2, 2007, by GeoCim, a Geotechnical and Testing Services Firm located in San Juan, near the bleachers of the basketball court at the Monte Verde Urbanization, Manatí. The field work consisted of drilling one borehole to a depth of 30 meters (100 feet) below existing ground surface, while securing soil and weathered rock samples. The test hole was drilled by SPT (Standard Penetration Test) sampling to a depth of 21.3 meters (70 feet) to be followed by power auger methods of core drilling, using rock diamond core bits to the 27.4 meters depth. The SPT was performed following ASTM D 1586-99 (ASTM, 1999). Soil samples were taken at every change of the soil profile or at vertical intervals not exceeding 0.46 meters (1.5 feet). The SPT was performed driving a split-barrel sampler to obtain a representative soil sample and a measure of the resistance of the soil to penetration of the sampler. The soil samples collected were described and classified using the Unified Soil Classification System (USCS).

The numbers of blows required for the penetration were recorded and the second and third 6 inches of penetration were added to obtain the standard penetration resistance of the N-value.. These N-values were written in the plastic bottles and in tabular form. A soil boring log of the samples descriptions was prepared.

Drilling and sampling was conducted as follows:

- N<75blows per foot (bpf) in soil with augers and sampling at 5 ft. intervals
- N>75 bpf in soil with augers and sampling at 5 ft. intervals
- In rock with N-size diamond core drilling equipment



The drilling equipment consisted of a Central Mine Equipment Mode-55 (CME-55) drill rig, which was truck-mounted and pulled by F-350 truck. Water was circulated through the core boring to displace cutting; and cool the drill bits which heat up as they cut through the rock. The limestone that underlies the site includes zones of high solution porosity that resulted in the loss of the circulation water into the limestone.

### **Collection of Rock Core Samples**

A total of 21 samples were collected from four (4) different core holes drilled (NC-4, NC-5, NC-9, and NC-10) by the United States Geological Survey (U.S.G.S.) in cooperation with the Puerto Rico Department of Natural Resources (samples numbers begin with the prefix “NC”) at the Aymamón Limestone Formation. Samples were collected to make petrographic analyses and to measure engineering parameters.

### **Porosity Quantification**

#### **Thin-Section Preparation**

The cores were sample when changes in rock type were present and at every 1.5 meters within the thick intervals of rock. Thin sections were prepared by cutting a chip from the carbonate samples taken from the rock cores NC-4, NC-5, NC-9, and NC-10. This was followed by impregnation under a vacuum and heat with blue stained epoxy to augment sample cohesion and to prevent loss of material during the grinding procedure. Each of the samples is mounted on a frosted glass slide and then cut and ground in water to an approximate thickness of 30 to 35  $\mu\text{m}$ .

#### **Point Counting Technique**

Digital images of the thin sections were processed to measure the pore space. The porosity values of the samples were obtained by point counting the images of the thin

sectioned samples, using a computer program - JMicroVision. Three hundred (300) points were counted per thin section obtaining porosity percentages in relation to the total solid volume represented.

### **Micro-Porosity**

Micro-porosity variations within the Aymamón Limestone Formation were characterized by point counting thin sections quantitatively. Twenty-one (21) samples from four (4) core holes (NC-4, NC-5, NC-9, and NC-10) were studied.

### **Macro-Porosity**

The big pores present in the cores were too big to be measure in a thin section. Their influence in the porosity/permeability and strength of the rock may be more significant than the micro-porosity. Most of these big pores are secondary porosity produced by dissolution – vug porosity.

Digital images from four (4) limestone rock samples from core hole NC-5 were taken and processed to extract the macro-pore space of vug porosity. The porosity values of the samples were obtained by point counting 300 points per sample using the computer program - JMicroVision.

### **Bulk Rock Density**

Limestone cylinder samples were weight by placing each rock sample on the balance to determine their mass. Then rock samples were immersed completely in a beaker of water to determine their volume. Rock samples were covered when submerged in water, due to the amount of pores, so the density was not affected. The bulk density of each rock sample was calculated dividing the weight of the sample by its volume, using the following equation:

$$\rho = \frac{m}{v} \quad (\text{Equation 1})$$

where:

$\rho$  = density (Kg/m<sup>3</sup>)

m = mass (Kg)

v = volume (m<sup>3</sup>)

### **Mineral Identification**

Rock samples were analyzed to determine their mineral content by X-ray diffraction (XRD) and by thin section staining techniques. In the X-ray analysis, the amount of high-Mg calcite and calcite was determined as a percent of the total carbonate in the powdered sample. Samples scanned with the X-ray diffractometer, were analyzed and identifications were performed in the computer with XRD dedicated software.

Differentiation of calcite from dolomite in thin sections required the use of staining techniques. In the stained thin section analysis, the presence of high Mg calcite was determined by visually estimating the color of stained carbonate grains in the thin section sample. Thin sections were dipped for one minute into the Alizarin red-S and Potassium ferricyanide solution. The length of the time applied was adequate to obtain differentiation of calcite.

### **Unconfined Compressive Strength (UCS) Test**

During the laboratory work in this investigation we analyzed four core rock samples from Test Well NC-5, to characterized engineering parameters in the Aymamón Limestone Formation. Samples used were retrieved from depths of 20 to 27.5 meters. We determined the elastic constants: Young's modulus, Poisson's ratio, bulk modulus and shear modulus by static laboratory tests of rock specimens subjected to uniaxial loading.

The UCS test was carried out in a press in which a cylindrical limestone rock specimen was placed on a platen and axial load was applied to it by a hydraulic ram. The axial length and diametral swelling of the loaded specimen were recorded, because Young's modulus was determined at the same time as strength was tested. Deformation was monitored by an electrical dial gauge attached to the specimen.

## **Static Testing**

### **Specimen Preparation**

Specimen preparation was performed in the Geochemistry Laboratory at the Department of Geology, UPR-Mayagüez Campus, under American Standard for Testing and Materials (ASTM 4543-04; ASTM, 2004).

The specimens were cut into lengths of 2.8 to 3.94 inches, using a rotator trim saw. Solid cylinders were prepared with a length to diameter ratio of approximately 1.0 to 1.5. Specimen ends were cut parallel to each other, normal to the longitudinal axis and ground smooth.

### **Testing Setup**

Specimen testing was performed at the Polytechnic University of Puerto Rico, Hato Rey, at the Construction Materials Laboratory. The tests were performed on 2.8 inches diameter and 3.94 inches length solid cylinders. At the mid-height of each specimen, an electronic dial gauge was attached along the circumference (horizontal) in order to measure axial deformation. The samples were loaded in compression at a constant strain rate of 2,000 N and at an ambient temperature of 70° F.

A strain-controlled loading frame, having a capacity of 178 kN, was used for the load application. The frame is equipped with a load cell to measure the applied load, and with an LVDT (Linear Variable Differential Transformer) to measure the vertical displacement. Rock specimen was mounted under the loading frame. The load cell and the LVDT were connected to a computerized data logger. All measuring devices were calibrated, and the tests were made according to ASTM Standard D 3148-02 (ASTM, 2002). The applied load, the vertical displacement, and the vertical and horizontal strains were continuously recorded during loading.

### **Calculations of Elastic Constants and Seismic Wave Velocities**

The elastic constants that were determined from the limestone core samples were: Young's modulus, Poisson's ratio, shear modulus and bulk modulus. The density and the compressional and shear seismic wave velocities were also calculated.

The Young's modulus (E) was obtained from the stress-strain response of a cylindrical core of limestone rock subjected to uniaxial compression, using equation 2. The resulting stresses and strains were plotted graphically (Figures 4.9 – 4.12).

$$\text{Young's modulus} = \frac{F/A}{\Delta L/L} = \frac{\sigma}{\varepsilon} \quad (\text{Equation 2})$$

where:

F = longitudinal applied force

A = cross-sectional area of the sample

$\Delta L$  = change in length of the sample

L = original length of the sample

$\sigma$  = axial stress

$\varepsilon$  = axial strain

Poisson's ratio ( $\nu$ ) was determined using an equipment of unconfined compression with an electronic dial gauge attached to the sample to measure the axial deformation in the rock sample.

$$\text{Poisson's ratio} = \frac{\Delta D / D}{\Delta L / L} = \frac{\epsilon_t}{\epsilon_a} \quad (\text{Equation 3})$$

where:

$\Delta D$  = change in diameter

$D$  = diameter of the sample

$\Delta L$  = length of the sample

$L$  = original length of the sample

$\epsilon_t$  = transversal strain

$\epsilon_a$  = axial strain

The shear modulus ( $\mu$ ) is related to the other moduli of elasticity by equation 4, using the values of the Young's modulus and the Poisson's ratio (Isenberg, 1972).

$$\mu = \frac{E}{2(1+\nu)} \quad (\text{Equation 4})$$

where:

$E$  = Young's Modulus

$\nu$  = Poisson's ratio

The bulk modulus ( $K$ ) is related to the Young's modulus ( $E$ ) and Poisson's ratio ( $\nu$ ) as can easily be shown by rewriting the relative volume change in terms of the relative length changes (Equation 5) (Isenberg, 1972). It was calculated using the following equation:

$$K = \frac{E}{3(1-2\nu)} \quad (\text{Equation 5})$$

where:

E = Young's Modulus

$\nu$  = Poisson's ratio

The shear wave velocity ( $V_s$ ) was calculated using the shear modulus and the density values of carbonate rock samples, by the following equation:

$$V_s = \sqrt{\frac{E}{2\rho(1+\nu)}}$$

(Equation 6)

where:

$\rho$  = density of the rock sample

$\mu$  = shear modulus

The primary (P) wave velocity ( $V_p$ ) was calculated using the bulk and shear modulus, and the density value of carbonate rock samples, by the following equation:

$$V_p = \sqrt{\frac{K + 4/3\mu}{\rho}}$$

(Equation 7)

where:

K = bulk modulus

$\mu$  = shear modulus

$\rho$  = density of the rock sample

## **Geophysically Determined Elastic Constants and Seismic Wave Velocities**

### **Cross-hole geophysical studies**

Numerous geotechnical studies have utilized the Seismic Cross Hole method to delineate sinkholes and characterize the compressional and shear seismic wave velocity and elastic properties of the north coast limestones. Suelos, Inc. conducted a cross-hole seismic study in the Aguada Formation in Bayamón and in the Aymamón Formation at Abbott Laboratories, Barceloneta.

### **Shear Wave Velocity at Monte Verde**

As part of a larger geophysical study that is still being conducted at the Monte Verde Urbanization, a Multichannel Analysis of Surface Waves (MASW) data set was gathered near the Test-Boring site. The shear – wave profile was gathered by Rodríguez-Vázquez, H. in 2006 by: (a) Acquiring multichannel records (or shot gathers; (b) Extracting the fundamental surface-wave mode, (lowest frequency at the lowest velocity, dispersion curve,), and; (c) Inverting the curve to obtain a depth versus shear velocity  $V_s$  function. The shear-wave velocity function closest to the test-boring log was used in the interpretation section of this thesis.



## Chapter IV: Results

### Test Boring

Table 4.1 shows the results of the Test Boring drilled at the Monte Verde Urbanization's basketball court. Soil samples were classified and described according to the Unified Soil Classification System (USCS). SPT-N values and shear wave velocities are also shown. A relation between the SPT-N values and the shear wave velocity is also presented. Figure 4.1 shows the profile of the 1-D shear wave vs depth.

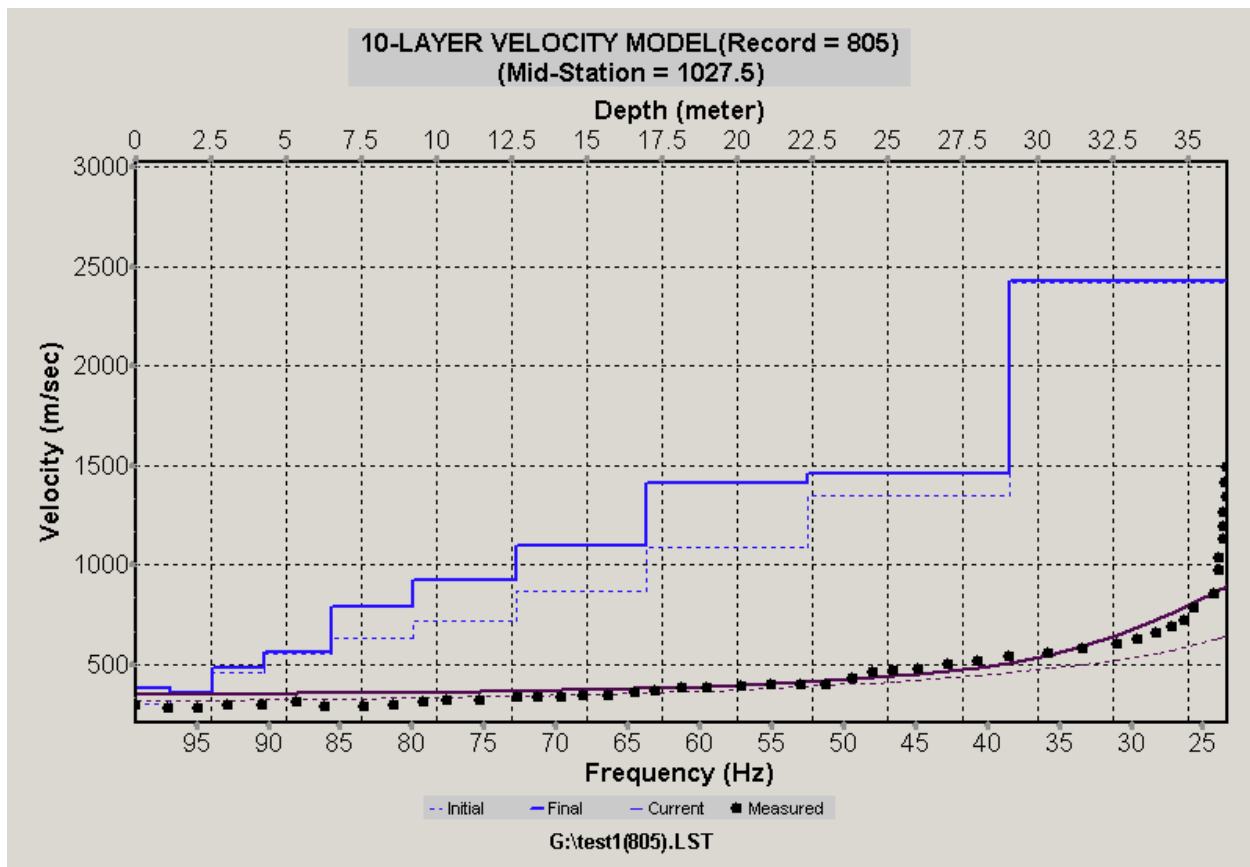




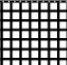
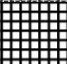
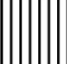
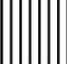






Figure 4.1: 1-D Shear wave vs depth profile.

Table 4.1: SOIL BORING LOG				Project: Test Boring at the Monte Verde Urbanization's basketball court, Manati, PR							
Location: Basketball Court at Monte Verde Urbanization, Road PR-670 Manati, PR							Page 1 of 2				
Drilling Method: Standard Penetration Test							Total depth: 27.4 meters				
Coordinates of Hole: 18° 25' 55.5" N 66° 27' 11.3" W							Date: February 27, 2007				
Sketch / notes:				<div><div><div><div><div></div><div>N</div></div><div></div></div><div><div></div><div>Basketball Court</div></div><div><div></div><div>B-1</div></div></div><div><div>USCS Classification:</div><div>Clay - Cl</div><div>Silt - MI</div><div>Well Graded Gravel - Gw</div><div>Poorly Graded Gravel – Gp</div><div>Silty Gravel – Gm</div><div>Clayey Gravel - Gc</div><div>Well Graded Sand–Sw</div><div>Poorly Graded Sand-Sp</div><div>Silty Sand - Sm</div><div>Clayey Sand – Sc</div></div></div>							
Depth (m)	Boring	Sample	USCS	Description of material		SPT Values	SPT N values	Vs (m/s)	Vs		
									N-Values		
									600	1,200	
									25	50	75
0-0.46	B-1	1	Sc	Clayey sand with silt and some gravel		2-2-3	5				
0.76-1.2	B-1	2	Sc	Clayey sand with some gravel		3-3-3	6				
1.5-2	B-1	3	Sc	Clayey sand with some weathered limestone fragments		8-7-5	12	554			
2.3-2.7	B-1	4	Cl	Clayey sand with weathered limestone fragments		4-7-9	16	366			
3-3.5	B-1	5	Sc	Clayey sand with weathered limestone fragments		43-42-45	87				
4.9-5.3	B-1	6	Sm	Silty sand with weathered limestone fragments		37-6-1	7	339			
5.8-6.2	B-1	7	Sm	Silty sand with weathered limestone fragments		9-10-9	19	624			
7.3-7.8	B-1	8	Gm	Highly weathered limestone fragments		36-50-2	52				
8.8-9.3	B-1	9	Gm	Highly weathered limestone fragments		2-27-32	59	691			
10.4-11	B-1	10	Gm	Highly weathered limestone fragments		10-2-2	4				
12-12.3	B-1	11	Gm	Highly weathered limestone fragments		43-23-13	36	741			
13.4-13.9	B-1	12	Gm	Highly weathered limestone fragments		2-3-13	16				
15-15.4	B-1	13	Gm	Highly weathered limestone fragments		13-15-12	27				

"N" values are the number of blows required to drive the sampling spoon a distance of twelve inches with a 140 lbs hammer falling 30 inches.






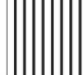






 N-Values  
 Vs – Shear wave velocity

Table 4.1: SOIL BORING LOG			Project: Test Boring at the Monte Verde Urbanization's basketball court, Manatí, PR										
Location: Basketball Court at Monte Verde Urbanization Road PR-670 Manatí, Puerto Rico						Page 2 of 2							
Drilling Method: Standard Penetration Test						Total depth: 27.4 meters							
Coordinates of Hole: 18° 25' 55.5" N 66° 27' 11.3" W						Date: February 27, 2007							
Sketch / notes:				B-1		USCS Classification:							
<div><div>↑ N</div><div>Basketball Court</div></div>						Clay - CI						Clayey Gravel – Gc	
						Silt - MI						Well Graded Sand - Sw	
						Well Graded Gravel - Gw						Poorly Graded Sand – Sp	
						Poorly Graded Gravel – Gp						Silty Sand - Sm	
						Silty Gravel – Gm						Clayey Sand - Sc	
Depth (m)	Boring No.	Sample No.	USCS	Description of material		SPT Values	SPT-N values	Vs (m/s)	Vs				
									600	1,200	N-Values		
									25	50	75		
16.5-16.9	B-1	14	Gm	Highly weathered limestone fragments		4-4-1	5	864					
18-18.4	B-1	15	Gm	Highly weathered limestone fragments		13-27-12	39						
19.5-20	B-1	16	Gm	Highly weathered limestone fragments		50-2 ½	50/2 ½						
21-21.5	B-1	17	Gm	Highly weathered limestone fragments		50-48-17	65						
21.5-22.9	B-1			No recovery. Void				1,257					
22.9-24.9	B-1			No recovery. Void									
24.9-25.9	B-1			4 cm and 6 cm fragments of indurated limestone rock									
25.9-27.4	B-1			No recovery. Void				1,486					
				End of Test Hole – 27.4 m									

"N" values are the number of blows required to drive the sampling spoon a distance of twelve inches with a 140 lbs hammer falling 30 inches.

 N-Values  
 Vs – Shear wave velocity

## Rock Core and Thin Section

Based on core and thin section inspection, a detailed lithological, biological, and petrographic description was constructed for the Aymamón Limestone Formation. To accomplish this task, four previously described cores (NC-4, NC-5, NC-9, and NC-10) were re-sampled. Lithology, fossil assemblage and porosity were examined in cores and thin sections adding details to previous descriptions made by Hartely (1989) and Scharlach (1990). New logs for all cores were produced by compiling new data and observations. A description of the rock (Table 4.2 – Table 4.5) and thin section (Table 4.6 – Table 4.9) log formats and information are presented in the following tables. Table 4.10 shows the different porosity types identified from the carbonate samples. Porosity classification was based on Choquette and Pray (1970) classification system. Texture classification was based on Dunham (1962) classification system.

**Table 4.2: Descriptions of Core NC-4.**

Core: NC-4	
Location: Coto Norte Ward, Manatí, PR	
Coordinates: 18° 26' 05"N 66° 26' 30"W      Elevation: 32.9 m above sea level	
Sampling Date: May, 2007	
Depth (m)	Core Description
32 – 32.9	Pale yellow-orange hard dense crystalline wackestone with silt and clay. Vug and fracture porosity are present.

**Table 4.3: Descriptions of Core NC-5.**

Core: NC-5	
Location: Tiburones Ward, Barceloneta, PR	
Coordinates: 18° 25' 43"N 66° 34' 15"W      Elevation: 95.1 m above sea level	
Sampling Date: May, 2007	
Depth (m)	Core Description
13.7 – 14.6	Pale orange-yellow indurated packstone. Mouldic, vug and shelter porosity are present.
14.9 – 15.8	Pale yellow-creamy well indurated packstone with silt-size skeletal fragments. Vug and fracture porosity.
16.2 – 17	Pale yellow-orange well indurated packstone.
18.6 – 19.5	Pale yellow to creamy well indurated packstone. Fracture porosity.
19.8 – 20.7	Pale yellow-orange-pink well indurated wackestone with silt-size skeletal fragments. Vug porosity.
21- 21.9	Pale orange-pink well indurated packstone. Vug porosity, forams and other skeletal fragments.
22.3 – 23.2	Pale yellow-orange-pink well indurated packstone to grainstone. Vug and fracture porosity, forams and other silt-size skeletal fragments.
24.7 – 25.6	Pale yellow-pink well indurated wackestone. Vug porosity, very fine-grained skeletal fragments.
25.9 – 26.8	Yellow-orange-pink well indurated wackestone. Vug porosity, silt-size skeletal fragments.
27.1 – 28	Pale yellow-pink well indurated wackestone. Shelter and vug porosity, forams and silt-size skeletal fragments.
28.3 – 29.3	Pale yellow chalky wackestone to packstone. Fracture, mouldic and vug porosity, forams and silt-size skeletal fragments.

**Table 4.4: Descriptions of Core NC-9.**

Core: NC-9	
Location: Cabo Caribe Ward, Vega Baja, PR	
Coordinates: 18° 27' 30" N 66° 23' 43" W                      Elevation: 3.5 m above sea level	
Sampling Date: May, 2007	
Depth (m)	Core Description
13.7 – 14.6	Very pale yellow poorly indurated, chalky grainstone. Fracture and vug porosity, forams and skeletal fragments.
14.9 – 15.8	Very pale orange well indurated grainstone. Vug and mouldic porosity, medium-size skeletal fragments.
16.2 - 17	Pale yellow-orange chalky and poorly indurated grainstone. Vug porosity and silt-size skeletal fragments.

**Table 4.5: Descriptions of Core NC-10.**

Core: NC-10	
Location: Tiburones Ward, Barceloneta, PR	
Coordinates: 18° 26' 04" N 66° 34' 45" W                      Elevation: 80 m above sea level	
Sampling Date: May, 2007	
Depth (m)	Core Description
7.6 – 8.5	Pale yellow to creamy dense packstone. Mouldic, fracture and vug porosity. Silt-size skeletal fragments.
8.8 – 9.8	Very pale orange-yellow-pink indurated packstone. Mouldic and vug porosity, silt-size skeletal fragments.
10 - 11	Pale orange-yellow-pink well indurated packstone. Mouldic and vug porosity. Fine-grained skeletal fragments.
25.9 – 26.8	Creamy to white well indurated packstone. Mouldic and vug porosity.
27.1 – 28	White chalky moderately indurated grainstone. Vug porosity, silt-size skeletal fragments.
28.3 – 29.3	Pale yellow-creamy-white well indurated packstone. Vug and mouldic porosity.

**Table 4.6: NC-4 Thin Section Log.**

Core: NC-4																													
Location: Coto Norte Ward, Manatí, PR																													
Coordinates: 18° 26' 05" N 66° 26' 30" W      Elevation: 32.9 m above sea level																													
Sampling Date: May, 2007																													
Depth (m)	Fabric (Dunham, 1962)						Porosity Types (Choquette and Pray, 1970)												Fossils										
	Mudstone	Wackestone	Packstone	Grainstone	Boundstone	Crystalline	Fabric Selective						Non Fabric Selective			Fabric Selective or not			Calcareous algae	Benthonic Foraminifera	Corals	Mollusks	Echinoderms	Skeletal Fragments					
							Interparticle	Intraparticle	Intercrystal	Mouldic	Fenestral	Shelter	Framework	Fracture	Channel	Vug	Breccia	Boring							Burrow	Shrinkage			
32.3		X												X			X								<i>Miliolids</i> <i>Nummulites</i>		Bivalves	X	X

**Table 4.7 A: NC-5 Thin Section Log.**

Core: NC-5																										
Location: Tiburones Ward, Barceloneta, PR																										
Coordinates: 18° 25' 43" N 66° 34' 15" W											Elevation: 95.1 m above sea level															
Sampling Date: May, 2007																										
Depth (m)	Fabric (Dunham, 1962)						Porosity Types (Choquette and Pray, 1970)												Fossils							
	Mudstone	Wackestone	Packstone	Grainstone	Boundstone	Crystalline	Fabric Selective							Non Fabric Selective			Fabric Selective or not				Calcareous algae	Benthonic Foraminifera	Corals	Mollusks	Echinoderms	Skeletal Fragments
							Interparticle	Intraparticle	Intercrystal	Mouldic	Fenestral	Shelter	Framework	Fracture	Channel	Vug	Breccia	Boring	Burrow	Shrinkage						
14			X													X					Goniolithon	Peneroplid Amphistegina Miliolid Nummulites				
15.5			X					X								X					Red algae	Amphistegina Fusulimid Miliolids Discocyclina		Gastropods		
17			X													X					Goniolithon	Amphistegina Miliolids Globorotalia Nummulites		Gastropods		X
18.5			X								X				X	X					Red algae	Miliolids Nummulites Discocyclina		Gastropods		



**Table 4.7 B: NC-5 Thin Section Log (Cont.).**

Core: NC-5																												
Location: Tiburones Ward, Barceloneta, PR																												
Coordinates: 18° 25' 43" N 66° 34' 15" W													Elevation: 95.1 m above sea level															
Sampling Date: May, 2007																												
Depth (m)	Fabric (Dunham, 1962)						Porosity Types (Choquette and Pray, 1970)														Fossils							
	Mudstone	Wackestone	Packstone	Grainstone	Boundstone	Crystalline	Fabric Selective							Non Fabric Selective			Fabric Selective or not				Calcareous algae	Benthonic Foraminifera	Corals	Mollusks	Echinoderms	Skeletal Fragments		
							Interparticle	Intraparticle	Intercrystal	Mouldic	Fenestral	Shelter	Framework	Fracture	Channel	Vug	Breccia	Boring	Burrow	Shrinkage								
20		X															X					<i>Goniolithon</i>	<i>Miliolids</i>			Gastropods	X	
21.5			X				X										X						<i>Amphistegina Miliolids</i>			Scaphopods		
23			X	X				X						X			X					Red algae	<i>Amphistegina Miliolids Peneroplid Fusulinid</i>					
24.5		X															X											X
26		X															X											X
27.5		X															X											X
29		X	X					X									X					<i>Goniolithon</i>	<i>Miliolid Globorotalia Fusulinid Nummulites</i>			Gastropods		

**Table 4.8: NC-9 Thin Section Log.**

Core: NC-9																											
Location: Cabo Caribe Ward, Vega Baja, PR																											
Coordinates: 18° 27' 30" N 66° 23' 43" W Elevation: 3.5 m above sea level																											
Sampling Date: May, 2007																											
Depth (m)	Fabric (Dunham, 1962)						Porosity Types (Choquette and Pray, 1970)												Fossils								
	Mudstone	Wackestone	Packstone	Grainstone	Boundstone	Crystalline	Fabric Selective						Non Fabric Selective			Fabric Selective or not			Calcareous algae	Benthonic Foraminifera	Corals	Mollusks	Echinoderms	Skeletal Fragments			
							Interparticle	Intraparticle	Intercrystal	Mouldic	Fenestral	Shelter	Framework	Fracture	Channel	Vug	Breccia	Boring							Burrow	Shrinkage	
14				X				X									X					<i>Goniolithon</i>	<i>Amphistegina</i>		Gastropods	X	
15.5				X			X	X		X							X						<i>Miliolids, Nummulites, Peneroplid, Fusulinid, Discocyclina</i>				
17				X			X	X									X					<i>Goniolithon</i>	<i>Miliolids Discocyclina</i>		Gastropods		

**Table 4.9 A: NC-10 Thin Section Log.**

Core: NC-10																											
Location: Tiburones Ward, Barceloneta, PR																											
Coordinates: 18° 26' 04" N 66° 34' 45" W											Elevation: 80 m above sea level																
Sampling Date: May, 2007																											
Depth (m)	Fabric (Dunham, 1962)						Porosity Types (Choquette and Pray, 1970)														Fossils						
	Mudstone	Wackestone	Packstone	Grainstone	Boundstone	Crystalline	Fabric Selective							Non Fabric Selective			Fabric Selective or not				Calcareous algae	Benthonic Foraminifera	Corals	Mollusks	Echinoderms	Skeletal Fragments	
							Interparticle	Intraparticle	Intercrystal	Mouldic	Fenestral	Shelter	Framework	Fracture	Channel	Vug	Breccia	Boring	Burrow	Shrinkage							
7.9			X							X							X					<i>Goniolithon</i>	<i>Nummulites</i> <i>Miliolids</i> <i>Fusulinid</i>				
9.4			X					X		X							X					<i>Goniolithon, Lythophyllum</i>	<i>Miliolids, Fusulinid,</i> <i>Nummulites,</i> <i>Amphistegina, Peneroplid</i>		Gastropods	X	
10.9			X							X							X					<i>Goniolithon</i>	<i>Miliolids</i> <i>Nummulites</i> <i>Amphistegina</i>	X		X	
26.2			X					X		X							X					<i>Fusulinid</i> <i>Amphistegina</i>		Bivalves			

**Table 4.9 B: NC-10 Thin Section Log (Cont.).**

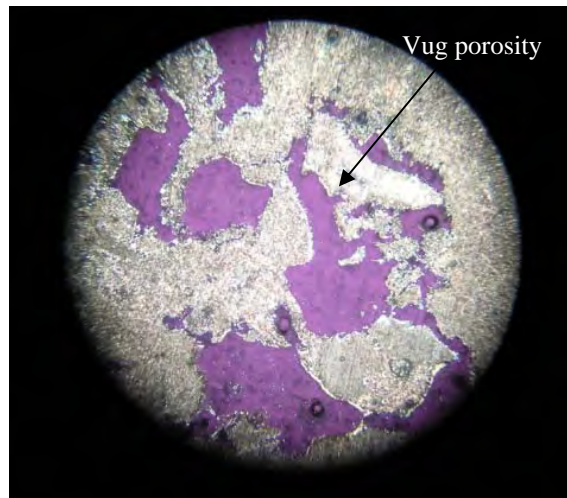
Core: NC-10																											
Location: Tiburones Ward, Barceloneta, PR																											
Coordinates: 18° 26' 04" N 66° 34' 45" W												Elevation: 80 m above sea level															
Sampling Date: May, 2007																											
Depth (m)	Fabric (Dunham, 1962)						Porosity Types (Choquette and Pray, 1970)														Fossils						
	Mudstone	Wackestone	Packstone	Grainstone	Boundstone	Crystalline	Fabric Selective							Non Fabric Selective			Fabric Selective or not				Calcareous algae	Benthonic Foraminifera	Corals	Mollusks	Echinoderms	Skeletal Fragments	
							Interparticle	Intraparticle	Intercrystal	Mouldic	Fenestral	Shelter	Framework	Fracture	Channel	Vug	Breccia	Boring	Burrow	Shrinkage							
27.9				X						X						X							<i>Nummulites Amphistegina Miliolids</i>		Gastropods		
29.2			X					X		X						X						<i>Goniolithon</i>	<i>Fusulinid, Discocyclina Amphistegina Nummulites Miliolids</i>		Gastropods	X	

**Table 4.10: Micro-porosity Classification in the Aymamón Limestone Formation.**

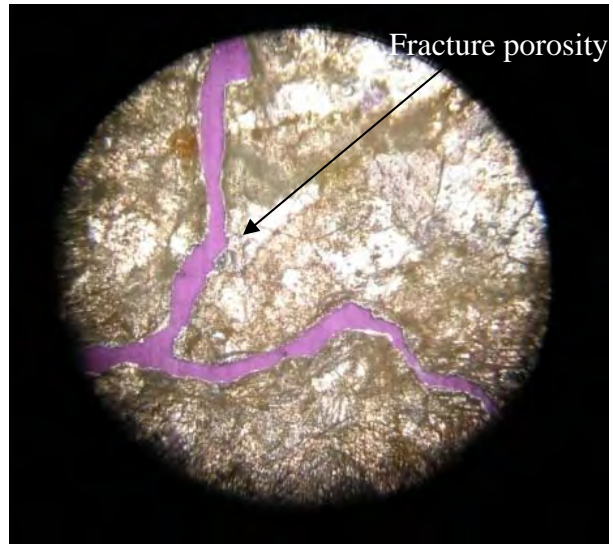
Core	Depth (m)	Porosity Classification (Choquette and Pray, 1970)													
		Fabric Selective							Non-Fabric Selective			Fabric Selective or Not			
		Interparticle	Intraparticle	Intercrystal	Mouldic	Fenestral	Shelter	Framework	Fracture	Channel	Vug	Breccia	Boring	Burrow	Shrinkage
NC-4	32-32.9														
NC-5	13.7-14.6														
	14.9-15.8														
	16.2-17														
	18.6-19.5														
	19.8-20.7														
	21-21.9														
	22.3-23.2														
	24.7-25.6														
	25.9-26.8														
	27.1-28														
	28.3-29.3														
NC-9	13.7-14.6														
	14.9-15.8														
	16.2-17														
NC-10	7.6-8.5														
	8.8-9.8														
	10--11														
	25.9-26.8														
	27.1-28														
	28.3-29.3														



**Figure 4.2: Picture of thin section from NC-4 32.3 m showing vug porosity.**



**Figure 4.3: Picture of thin section from NC-9 14 m showing vug porosity.**



**Figure 4.4: Picture of thin section from NC-5 20 m showing fracture porosity.**



**Figure 4.5: Picture of thin section from NC-10 7.9 m showing mouldic porosity.**

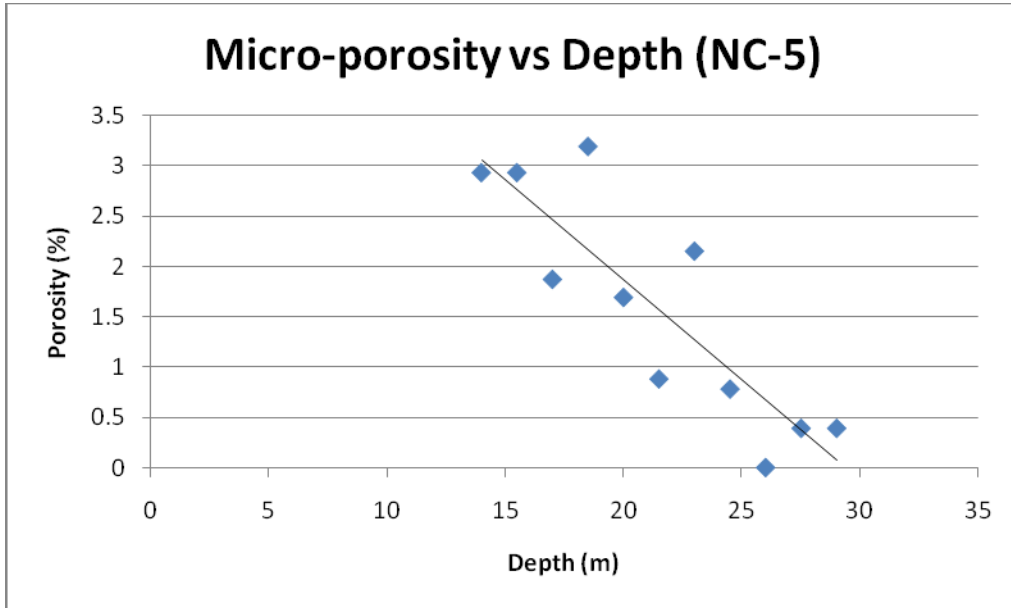
## Porosity

Micro-porosity percentages obtained from point counting thin sections are shown on Table 4.12. Most of the micro-porosity is vuggy and mouldic with much less intraparticle porosity. The micro-porosity percentages for cores NC-4, NC-5, NC-9, and NC-10 were 1.49%, 1.72%, 3.31%, and 2.54%, respectively. Graphs 4.1 to 4.3 show the relationship between micro-porosity and depth for cores NC-5, NC-9, and NC-10.

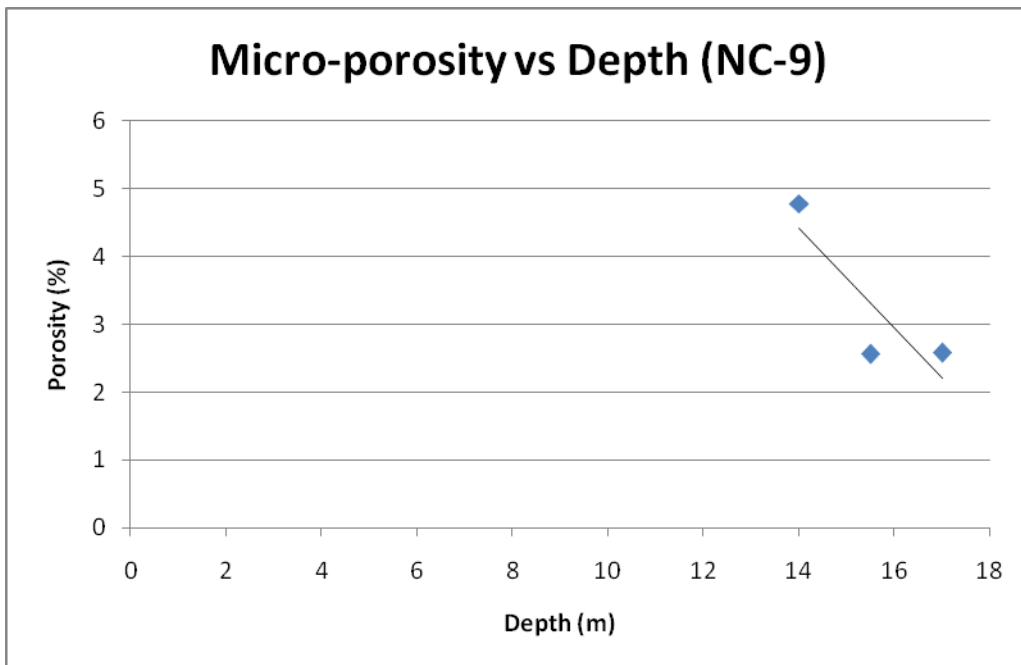
**Table 4.11: Micro-porosity percentages in the Aymamón Limestone Formation.**

Core	Depth (m)	Porosity (%)
NC-4	32.3	1.49
	14	2.93
	15.5	2.93
	17	1.87
	18.5	3.19
	20	1.69
NC-5	21.5	0.88
	23	2.15
	24.5	0.78
	26	0
	27.5	0.39
	29	0.39
	14	4.78
NC-9	15.5	2.56
	17	2.58
	7.9	2.77
	9.4	2.64
NC-10	10.9	2.81
	26.2	2.54
	27.7	1.25
	29.2	3.24

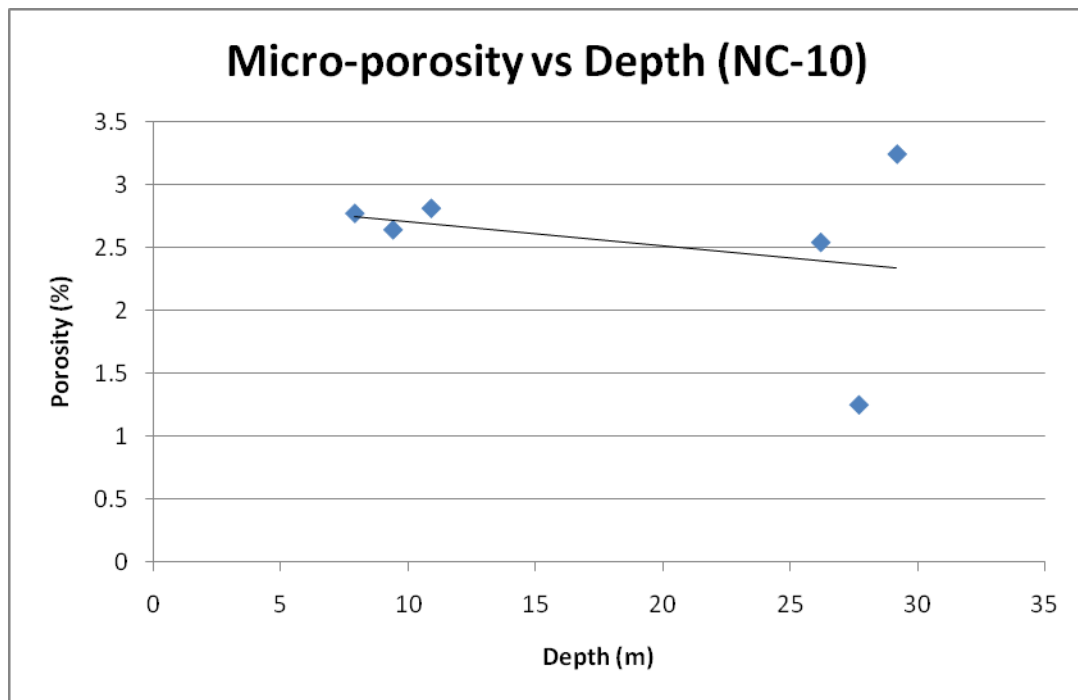




**Graph 4.1:** Graph showing the relation between micro-porosity and depth of core NC-5. As depth increase the micro-porosity percent decrease.



**Graph 4.2:** Graph showing the relation between micro-porosity and depth of core NC-9. As depth increase the micro-porosity percent decrease.

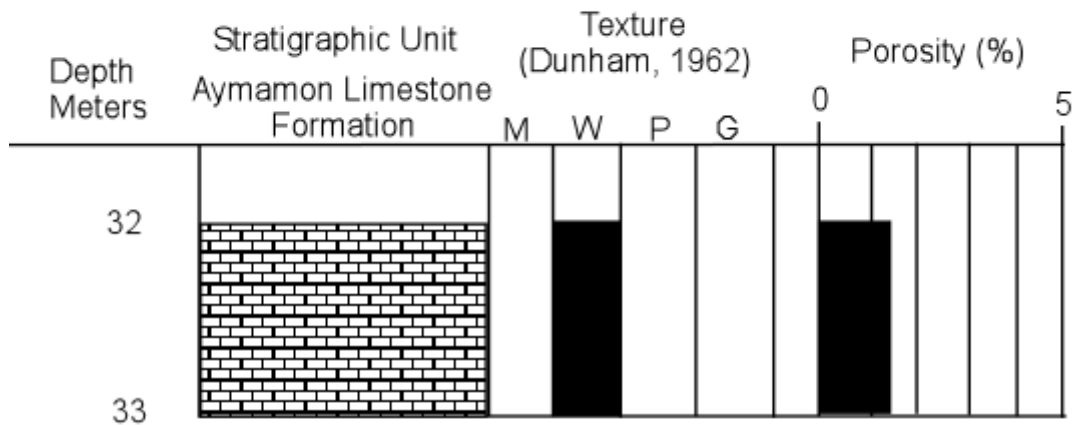


**Graph 4.3: Graph showing the relation between micro-porosity and depth of core NC-10. As depth increase the micro-porosity percent decrease.**

Core hole NC-4, Manati, Puerto Rico

Coordinates: N 18° 26' 05" W 66° 26' 30"

Elevation: 32.9 m above sea level



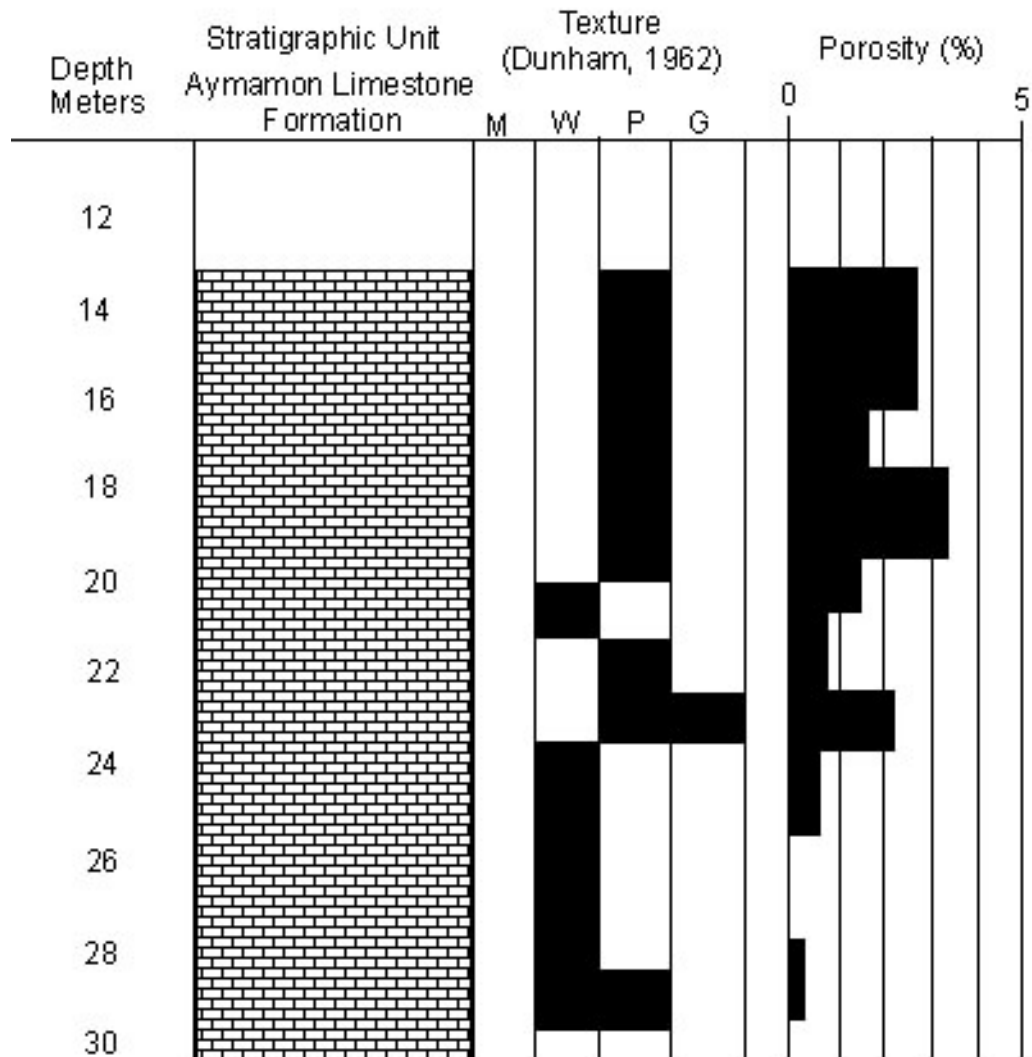
Legend: M-Mudstone  
W-Wackestone  
P-Packstone  
G-Grainstone

**Figure 4.6: Lithology, texture and micro-porosity percentages of Core NC-4.**

Core hole NC-5, Barceloneta, Puerto Rico

Coordinates: N 18° 25' 43" W 66° 34' 15"

Elevation: 95.1 m above sea level



Legend: M-Mudstone  
W-Wackestone  
P-Packstone  
G-Grainstone

Figure 4.7: Lithology, texture and micro-porosity percentages of Core NC-5.

Core hole NC-9, Vega Baja, Puerto Rico

Coordinates: N 18° 27' 30" W 66° 23' 43"

Elevation: 3.5 m above sea level

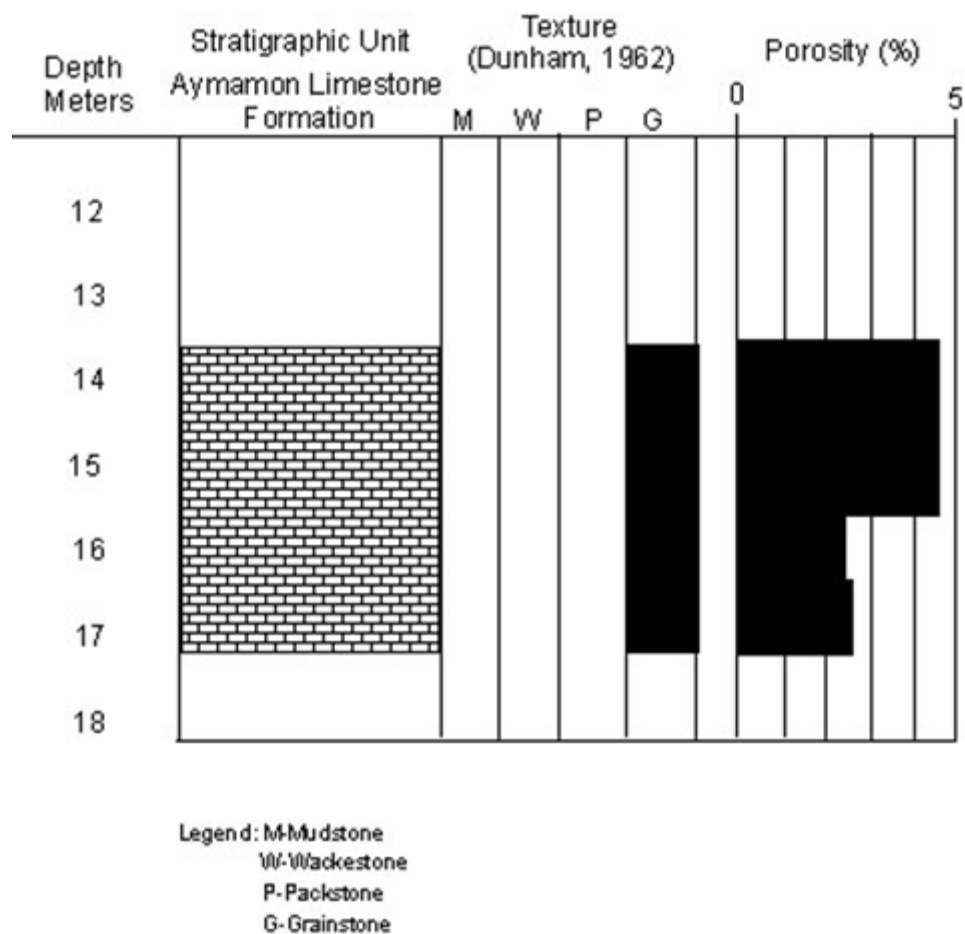


Figure 4.8: Lithology, texture and micro-porosity percentages of Core NC-9.

Core hole NC-10, Barceloneta, Puerto Rico

Coordinates: N 18° 26' 04" W 66° 34' 45"

Elevation: 80 m above sea level

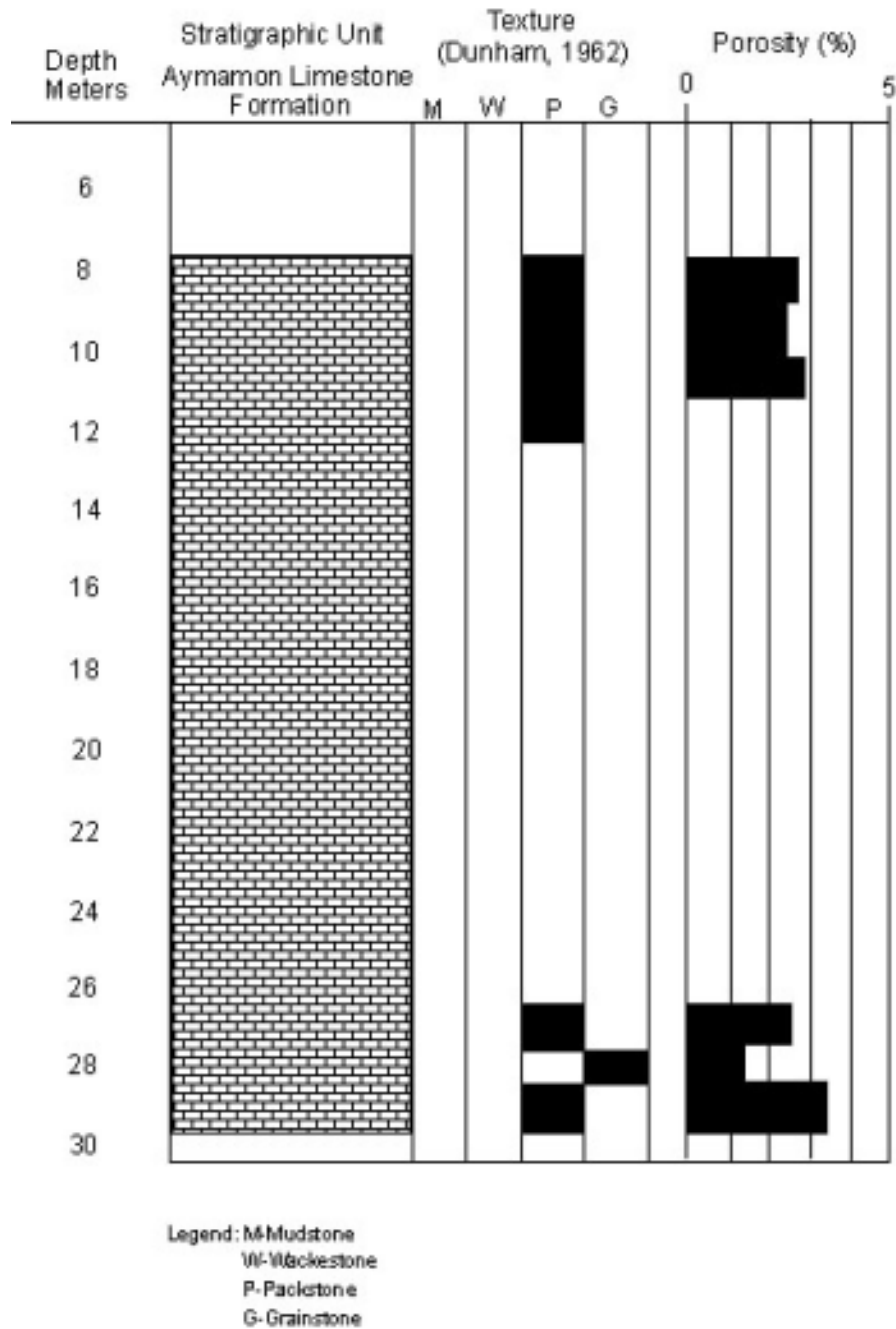


Figure 4.9: Lithology, texture and micro-porosity percentages of Core NC-10.

## Mineral Identification

Twenty one (21) carbonate samples were scanned with an X-ray diffractometer. Mineralogy obtained from the samples by x-ray diffraction is shown in Table 4.12. The graphs of the XRD results are shown in Appendix B. Nine (9) thin sections were stained using Alizarin red-S and Potassium ferricyanide solution. These thin sections were stained to differentiate calcite from dolomite. The mineralogy determined by staining is shown in Table 4.13.

**Table 4.12: Mineralogy of samples determined by XRD technique.**

Core	Depth (m)	Mineralogy
NC-4	32.3	High Mg calcite
	14	Calcite, High Mg calcite & dolomite
	15.5	Calcite
	17	Calcite
	18.5	High Mg calcite & dolomite
NC-5	20	Calcite & dolomite
	21.5	Calcite & dolomite
	23	Calcite & dolomite
	24.5	Calcite
	26	High Mg calcite & dolomite
	27.5	High Mg calcite
	29	Calcite
	14	Calcite
NC-9	15.5	High Mg calcite
	17	Calcite
	7.9	High Mg calcite
	9.4	High Mg calcite & dolomite
NC-10	10.9	High Mg calcite & dolomite
	26.2	High Mg calcite & dolomite
	27.7	High Mg calcite
	29.2	High Mg calcite

**Table 4.13: Mineralogy of thin sections determined by staining technique.**

Sample	Depth (m)	Stain	Mineralogy
NC-10	9.4	Red color	High Mg calcite
NC-10	10.9	Red color	High Mg calcite
NC-10	26.2	Red color	High Mg calcite
NC-5	14	Red color	High Mg calcite
NC-5	18.5	Red color	High Mg calcite
NC-5	20	Red color	Calcite
NC-5	21.5	Red color	Calcite
NC-5	23	Red color	Calcite
NC-5	26	Red color	High Mg calcite

**Bulk Density**

The resulting densities are listed on Table 4.14 along with the porosity estimates for the NC-5 core samples and the core fragments recovered in the Monte Verde boring.

**Table 4.14: Bulk density of NC-5 limestone core samples and Monte Verde core fragments.**

Core	Depth (m)	Weight (Kg)	Volume (m <sup>3</sup> )	Density (Kg/m <sup>3</sup> )	Macro-porosity + Micro-porosity
NC-5	20	0.73799	0.0003	2,460	19.33 + 1.69
NC-5	21.5	0.65257	0.00026	2,510	1 + 0.88
NC-5	23	0.99634	0.0004	2,491	3.5 + 2.15
NC-5	27.5	1.05568	0.00046	2,295	39.67 + 0.39
<b>MV-Boring fragment</b>					<b>Calculated Total Porosity</b>
6 cm	24.9-25.9	0.15632	0.000075	2,084	33.81
4 cm		0.08011	0.00005	1,602	40.67

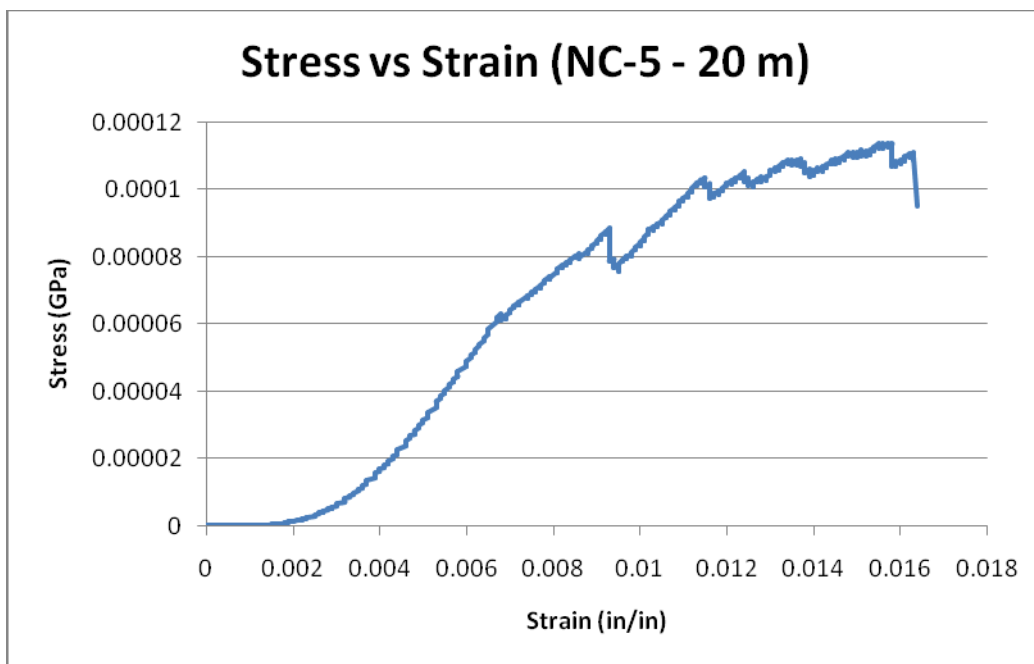


## **Elastic Properties of the Aymamón Limestone Core Samples**

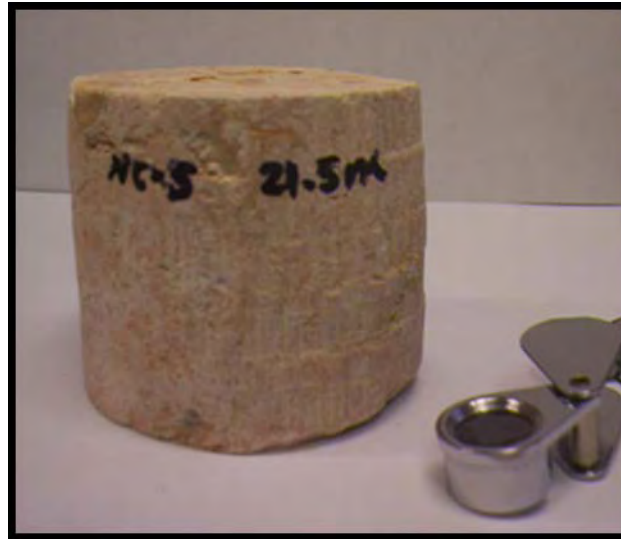
These elastic moduli are what control the velocity of the seismic wave in different materials. Lateral strain gauges were added to the test to determine Poisson's ratio which combined with the elastic modulus allows for the rigidity or elastic shear modulus and the elastic compressibility or bulk modulus to be calculated. The results of the unconfined compression test analyses of the NC-5 core samples are shown graphically on stress versus strain curves in Figures 4.9 to 4.12 and presented in Tables A-1 to A-5 in Appendix A. The resultant calculations of the elastic constants and the seismic wave velocities are shown in Tables A-6 to A-12 in Appendix A. The values of the core sample density and elastic constants are summarized in Table 4.15. The seismic wave velocities calculated using the elastic constants determined from the unconfined compression tests on the NC-5 core samples are also shown on Table 4.15. The calculated shear seismic velocities are compared to the shear wave velocities at the Monte Verde boring and core location determined using the MASW method in Table 4.16. Table 4.17 shows the comparison of the laboratory and field values of the seismic and elastic constants.



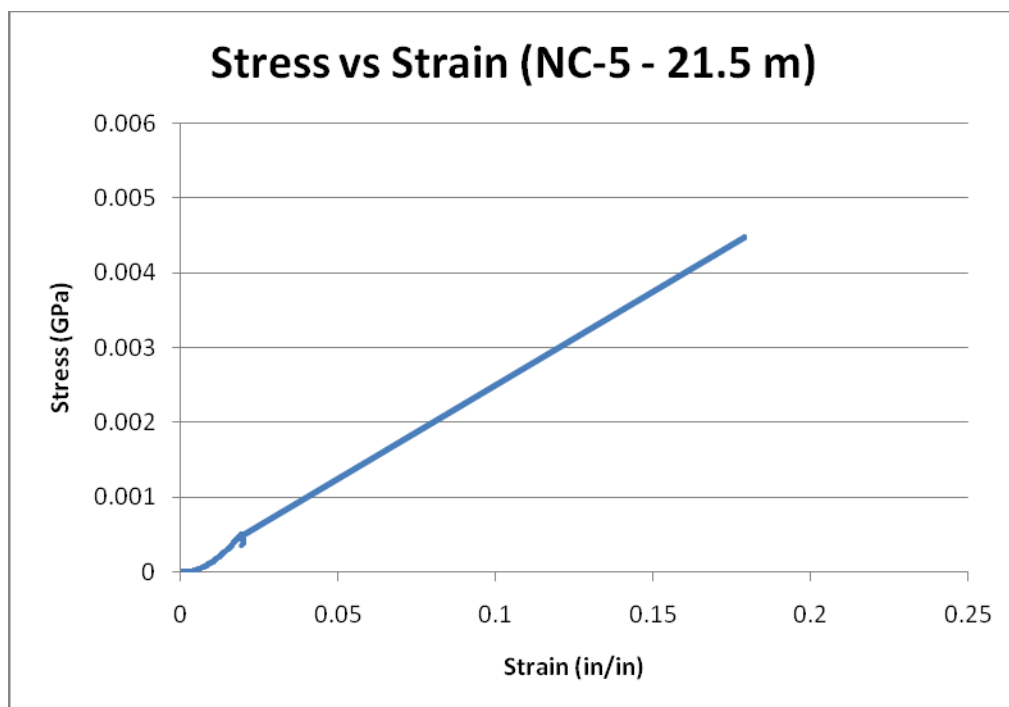
**Figure 4.10a: Core sample NC-5 (depth - 20 m).**



**Figure 4.10b: Stress vs Strain loading curve of Core NC-5 20 m.**



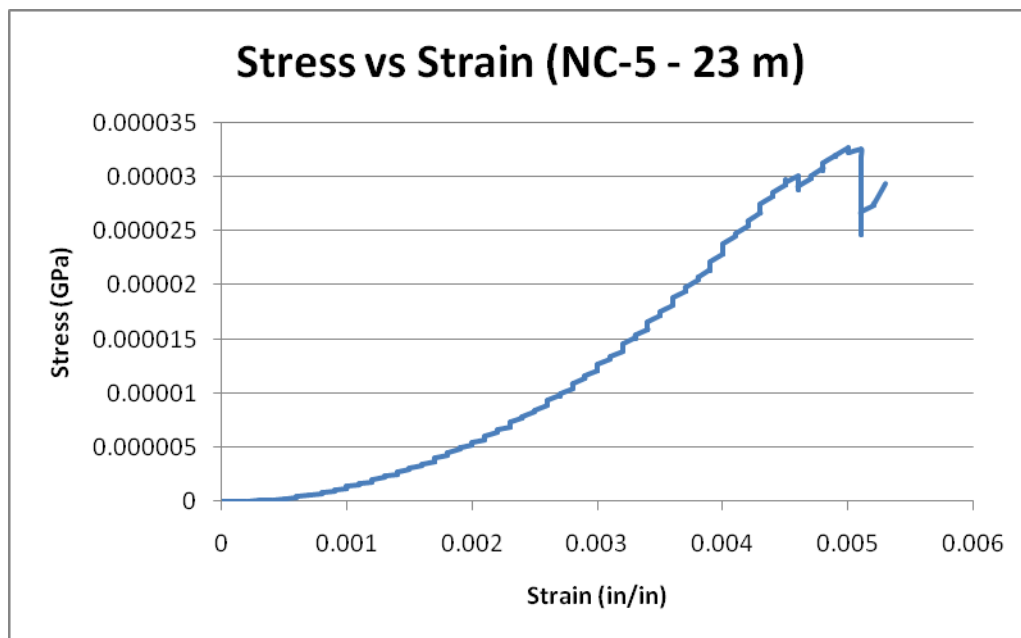
**Figure 4.11a: Core sample NC-5 (depth - 21.5 m).**



**Figure 4.11b: Stress vs Strain loading curve of Core NC-5 21.5 m.**



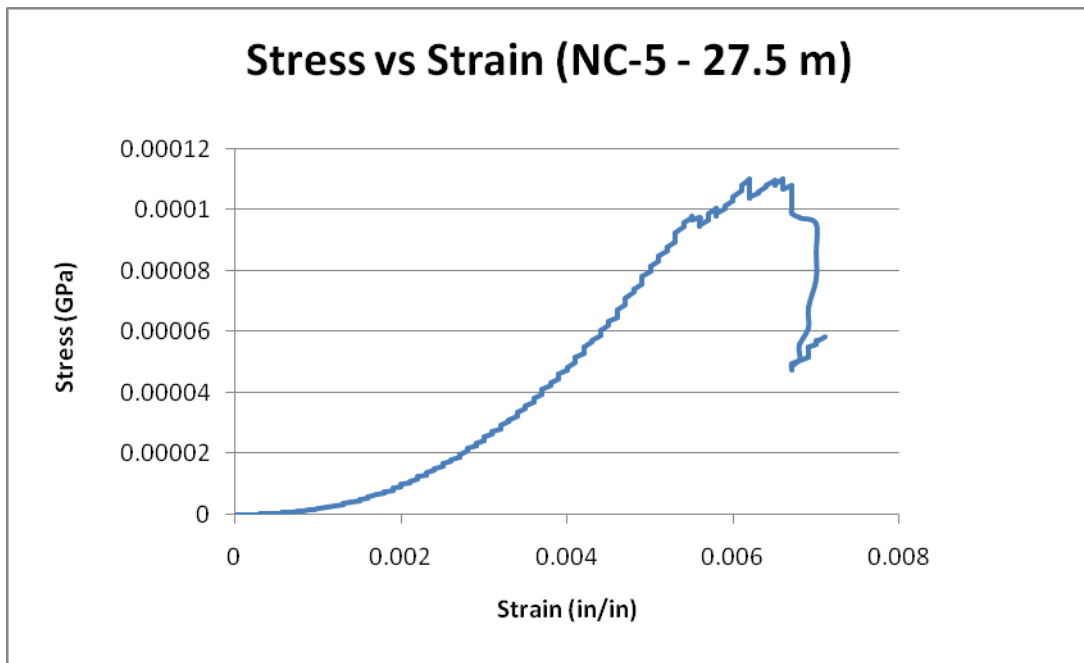
**Figure 4.12a: Core sample NC-5 (depth - 23 m).**



**Figure 4.12b: Stress vs Strain loading curve of Core NC-5 23 m.**



**Figure 4.13a: Core sample NC-5 (depth - 27.5 m).**



**Figure 4.13b: Stress vs Strain loading curve of Core NC-5 23 m.**

**Table 4.15: Core sample density, porosity, elastic constants and seismic velocities.**

<b>Depth (m)</b>	<b>Density (Kg/m<sup>3</sup>)</b>	<b>Macro/Micro Porosity (%)</b>	<b>E (GPa)</b>	<b>Poisson's Ratio (ν)</b>	<b>μ (GPa)</b>	<b>K (GPa)</b>	<b>S-wave Velocity (m/sec)</b>	<b>P-wave Velocity (m/sec)</b>
20	2,460	19.33/1.69	1.02	0.029	0.50	0.36	450	646
21.5	2,510	1/0.88	1.37	0.37	0.50	1.74	446	981
23	2,490	3.5/2.15	1.47	0.27	0.58	1.06	482	859
27.5	2,290	39.67/0.39	3.24	0.29	1.3	2.6	740	1,360

**Table 4.16: Comparison of laboratory calculated and MASW analysis seismic wave velocities.**

Depth-meters	Calculated seismic velocity for tested NC-5 core samples of the Aymamón Limestone		Shear wave velocity derived by MASW
	P-wave velocity	S-wave velocity	S-wave velocity
17	--	--	864
20	646	450	--
21.5	981	446	--
22	--	--	1257
23	859	482	--
27.5	1360	740	--
29	--	--	1486

**Table 4.17: Comparison of laboratory and field values of seismic velocities.**

Location	Measurement	Velocity (m/sec)	
		Lab	Field
Average 21.5m-23m-27.5m Aymamón Limestone Formation Cruce Dávila, Barceloneta Core sample 21.5m	Vp	1,067	--
	Vs	556	--
	Vp	981	--
	Vs	446	--
Aymamón Limestone Formation Abbott Laboratories, Barceloneta	Vp	--	1,066
	Vs	--	--
Aguada Formation (Limestone) Bayamón	Vp	--	1,057
	Vs	--	439

-- Not attempted

**Table 4.18: Comparison of laboratory and field values of elastic constants.**

Location	Measurement	(GPa)	
		Lab	Field
Aymamón Limestone Formation Cruce Dávila, Barceloneta Average-21.5m	E	2.03-1.37	--
	$\nu^*$	0.31-0.37	--
	$\mu$	0.79-0.5	--
	K	1.44-1.74	--
Aguada Formation (Limestone) Bayamón	E	--	1.10
	$\nu^*$	--	0.35
	$\mu$	--	0.41
	K	--	--

-- Not attempted

\*Poisson's ratio is unitary



## **Chapter V: Interpretation and Analysis**

### **Test Boring**

Results of the Test Boring are shown in Table 4.1. In general, the uppermost 7 meters of Boring B-1 consisted of weathered limestone fragments in a ferruginous sand and clayey matrix. From 3.5 to 6 meters the samples consisted of silty sand and weathered limestone fragments. The N-values generally increased with depth from 5 to 19. From 6 to 21.5 meters the borings encountered highly weathered limestone that exhibited highly variable consistency indicated by SPT N-values ranging from 4 to 65. The attempt to collect core samples from this transition zone proved unsuccessful because the boring encountered three large, open cavities from 21.5 to 27.4 meters depth. Only two indurated recrystallized limestone fragments were recovered from a depth of 25 meters.

### **Rock Core and Thin Sections**

Much of the Aymamón Limestone cores from this mogote karst zone are well-indurated, recrystallized and well-cemented limestone. Samples were mostly packstone and less commonly wackestone and grainstone textures. Core and thin section samples showed a great variety of pore types; including fabric selective and non-fabric selective types. Most of the porosity is vuggy and mouldic with much less intraparticle porosity. Vug and mouldic porosities develop as a result of the dissolution of more unstable aragonitic fossils. Large vugs filled or partially filled with red-brown silt-size particles are common, occurring in distinct zones and generally increasing in abundance toward the surface. The type of pore was controlled by the mineralogy of the constituent fossils when the dissolution occurred. The fossils in the core samples included calcareous algae, benthic foraminifers, and echinoderms that have a calcite skeletal composition and corals, mollusks, and other fragments that have an aragonite skeletal composition.

## **Mineral Identification**

XRD analyses showed that the mineralogy of the carbonate samples consisted of calcite, high magnesium calcite and dolomite. The staining technique performed on thin sections produced an intense red color on the thin sections, which indicated that the present mineralogy of the carbonate constituents is dominantly calcite.

## **Bulk Density**

The bulk density of the analyzed core samples and core fragment recovered in the Monte Verde boring were determined by measuring their weights and determining their displacement volumes. Density of the core samples is mostly controlled by the macro-porosity, especially since the samples had low micro-porosities and are all composed of calcite, which has a density of 2,700 Kg/m<sup>3</sup>. Accordingly, the data from Table 4.14 shows that the NC-5 sample from 21.5 meters had the highest density value and the lowest macro-porosity value and the NC-5 sample from 27.5 meters had the lowest density value and the highest macro-porosity value. The density value for the sample from 27.5 meters however, was too high for the corresponding estimated macro-porosity. A similar problem is seen in the NC-5 Samples at 20, 21.5 and 23 meters showed the similar density values but macro-porosity values that ranged from 1 to 19%. These data suggest that the methodology to estimate macro-porosity percentage was not accurate. The method appears to have over estimated the porosity, because the density values do not directly correspond to the macro-porosity values. Corresponding total porosity values for the measured density of core fragments recovered in the Monte Verde boring are shown in Table 4.14. The total porosities were calculated using a maximum density of 2,700 Kg/m<sup>3</sup>, the density of calcite.

## **Elastic Properties of the Aymamón Limestone Core Samples**

The stress-strain loading curves of the samples show classic nonlinear behavior at low stress loads caused by volume decrease probably by reduction of micro-porosity. For core samples from 20m, 23m and, 27.5m, this non linearity occurs over about 50% of their elastic strength that ranged from 0.00003 to 0.0001 GPa. The core sample from 21.5m had much greater elastic strength but showed the same nonlinearity over the first 0.005 GPa which was only a small portion of its elastic strength. Young modulus of elasticity,  $E$ , increased consistently from the shallower samples to the deepest. Al-Shayea (2004) attributed the increase in Young modulus  $E$  to an increase in the density and Palchik and Hatzor (2002) attributed this increase to decreasing porosity. Given the similar composition of the four samples, density variations should be directly proportional to the porosity. Neither total porosity nor density could be related to the measured value of the elastic constants, in fact the least dense, highest porosity core sample tested gave the greatest value for Young's modulus. Similarly the measured value of Poisson's ratio does not show any systematic relation to density nor porosity. The value of Poisson's ratio for the sample from 20 meters was anomalously lower, by an order of magnitude, than the other tested samples. This may be attributed to the testing method and raises into question the validity of the results for this sample. The rigidity shows a similar increase with depth of sample to Young's modulus. The bulk modulus on the other hand does not. The bulk modulus does show a systematic increase with decreasing micro-porosity other than for the sample from 20 meters which was affected by the anomalous value of Poisson's ratio. It seems unlikely that micro-porosity directly controls the elastic compressibility of the limestone, especially in light of the lack of impact of macro-porosity on the elastic properties of the rock. The micro-porosity may be acting as a proxy for the crystallinity and density of the rock matrix. The inter-pore limestone

matrix density may be the factor controlling limestone elastic compressibility and the seismic wave velocities.

### **Comparison of the Calculated Seismic Velocities with MASW and CHS methods**

The MASW derived shear wave velocities from 17 – 29 meters depth are considerably faster than those calculated for the NC-5 core samples over similar depth ranges. The reason for this is not clear, because the NC-5 core samples came from a different locality than the field-measured analysis and may not be representative of the limestone that lie at these depths at the Monte Verde site. Core samples from these depths at Monte Verde were not collected because the boring encountered mega-voids or macro-pores from 21.5 to 27.4 meters depth. Despite the occurrence of macro-voids over this depth range the field-measured shear wave velocity increased from 1,257 to 1,486 m/sec. The fastest calculated seismic velocity corresponds to the sample from 27.5 meters that had the greatest macro-porosity. These observations suggest that macro-porosity has little effect on seismic wave velocity in the Aymamón Limestone. The increased seismic velocity in limestones with greater macro-porosities may be related to recrystallization of the surrounding rock matrix into a more dense crystalline mass.

Average compressional and shear seismic velocities obtained by Suelos, Inc. using the seismic cross-hole method were compared to the compressional and shear seismic velocities obtained from lab measurements (Table 4.17). The average calculated lab seismic wave velocities are within the same order of magnitude to those derived using the Cross Hole Seismic method. The elastic modulus, Poisson's ratio, and shear modulus derived from the Cross Hole Seismic dynamic analyses (Table 4.18) compare within the same order of magnitude with those determined with the unconfined compression static analyses, especially the core sample from 21.5 meters.

## **Chapter VI: Discussions and Conclusions**

The initial goal of this project was to investigate the physical properties of the Aymamón Limestone Formation that control its seismic wave velocity in order to address problems related to karst-sinkhole detection. To accomplish this goal,

- A surface wave seismic study was undertaken at the Monte Verde Urbanization's basketball court where serious subsidence of the court has occurred to delineate the extent of dissolution.
- A test boring was drilled at the basketball court in order to correlate the derived seismic velocity profiles with the subsurface geology of the site.
- Limestone core samples from the Aymamón Formation were collected to perform laboratory tests in order determine their elastic properties, since no recovery was obtained from the test boring.
- Cores samples were also used to make descriptions and petrographic analyses to better characterize the physical properties of the Aymamón Limestone.

The MASW technique proves to be a good assessment tool in areas with known or suspected dissolution at depths ranging from ~8 to 20 meters below ground surface. The rate of change of the shear wave velocity was observed to decrease at depths greater than ~20 meters, as compared to the rate of change of the velocity at shallower depths. This rate of change of the shear wave velocity may be indicative the occurrence of macro-porosity at depth. The increased seismic velocity in limestone with greater macro-porosities may be related to recrystallization of the surrounding rock matrix into a more dense crystalline mass. The comparison conducted in this thesis was based on dataset obtained at different locations. The surface wave shear wave

velocities were obtained using geophysical techniques at the Monte Verde Urbanization and the rock samples used for the lab measurements were obtained elsewhere along the Puerto Rico North Coast Aymamón Limestone, so caution must be used in the interpretation these results.

The Aymamón Limestone Formation is consider by Monroe (1980) to be the most uniform in lithology and thickness of all the Tertiary formations cropping out in northern Puerto Rico. The tested samples in this study showed the same mineralogical composition. The average calculated seismic wave velocities from the tested samples (21.5, 23, and 27.5 m) and the elastic parameters determined and calculated compares closely to those obtained from cross hole seismic measurements made by Suelos, Inc. from other formations across the northern coast of Puerto Rico. We can conclude that the use of seismic wave velocities determined at the field to back calculate the elastic constants is viable, as they compared well with laboratory static measurements. Although we tested a small number of samples, according to these comparisons, the data obtained from the samples may be representative of the Aymamón and Aguada Limestone Formations.

The measured value of Poisson's ratio for the sample from 20 meters was anomalously lower, by an order of magnitude, than the other tested samples. This may be attributed to the testing method and raises into question the validity of the elastic constants and the seismic wave velocities results for this sample. However, the remaining three samples provided consistent results that compare well with field derived data. Thus, the results of this study have contributed to a better characterization of the Aymamón Limestone Formation that will enhance the interpretation of subsurface seismic data in mogote karst sinkhole investigations.

## References

- Al-Shayea, N.A., 2004, Effects of testing methods and conditions on the elastic properties of limestone rock, *Engineering Geology*, v. 74, p. 139-156.
- American Society for Testing and Materials, 2004, Standard Practices for Preparing Rock Core Specimens and Determining Dimensional and Shape Tolerances (ASTM D 4543-04), ASTM Committee D18 on Soil and Rock, p. 1-5.
- American Society for Testing and Materials, 2002, Standard Test Method for Elastic Moduli of Rock Core Specimens in Uniaxial Compression (ASTM D 3148-02), ASTM Committee D18 on Soil and Rock, p. 1-6.
- American Society for Testing and Materials, 1999, Standard Test Method for Penetration Test and Split-Barrel Sampling of Soils (ASTM D 1586-99), ASTM Committee D18 on Soil and Rock, p. 1-5.
- Briggs, R.P., 1966, The blanket sands of northern Puerto Rico: : *in* Third Caribbean Geological Conference, Kingston, Jamaica, 1962, Transactions, Jamaica Geological Survey Publications 95, p. 60-69.
- Briggs, R.P., and Gordon, W. A., 1961, Oil and gas possibilities of northern Puerto Rico, Puerto Rico Mining Commission, San Juan, p 40.
- Choquette, P.W., and Pray, L.C., 1970, Geologic nomenclature and classification of porosity in sedimentary carbonates: American Association of Petroleum Geologists Bulletin, v. 54, p. 207-250.
- Donnelly, T.W., 1964, Evolution of eastern Greater Antillean island arc: American Association of Petroleum Geologists Bulletin, v. 48, no. 5, p. 680-696.
- Dunham, R.J., 1962, Classification of carbonate rocks according to depositional texture, *in* Ham, W.E., ed., Classification of carbonate rocks, A.A.P.G. Memoir, 1, p. 62-84, 108-121.
- Hartley, J.R., 1989, Subsurface Geology of the Tertiary Carbonate Rocks: Northwestern Puerto Rico, Thesis M.S. University of New Orleans, p. 97-99, 113, 170-171.
- Isenberg, 1972, Bulk modulus and shear modulus, Relationships between elastic properties, p. 22.
- Krushensky, R.D., and Schellekens, J.H., 2000, Geology, geochemistry, Geophysics, Mineral Occurrences and Mineral Resource Assessment for the Commonwealth of Puerto Rico, U.S. Geological Survey, Open-File Report 98-38, p. 25-39.

- Meyerhoff, H.A., Krieg, E.A., Closs, J.D., and Taner, I., 1983, Petroleum potential of Puerto Rico: unpublished report, Associated Resource Consultants, Inc. and Edward A. Krieg and Associates, Inc.
- Miotke, F.D., 1973, The subsidence of the surfaces between mogotes in Puerto Rico east of Arecibo (transalted from German by W.H. Monroe): *Caves and Karst*, v. 15, no. 1, p. 1-12.
- Monroe, W.H., 1980a, Relief map of Puerto Rico showing principal physiographic provinces: U.S. Geological Survey Professional Paper 1159, scale 1:240,000.
- Monroe, W.H., 1980b, Some tropical landforms of Puerto Rico: U.S. Geological Survey Professional Paper 1159, Washington D.C., p. 39.
- Monroe, W.H., 1980, Geology of the Middle Tertiary Formations of Puerto Rico, U.S. Geological Survey Professional Paper 953, p. 11-66, 52-59, 93.
- Monroe, W.H., 1976, The karst landforms of Puerto Rico, US Geological Survey Professional Paper 899, p.10-19.
- Monroe, W.H., 1973, Stratigraphy and petroleum possibilities of Middle Tertiary rocks in Puerto Rico, reply to discussions, *A.A.P.G.*, v. 57, no. 6, p. 1086-1099.
- Monroe, W.H., 1973, Geologic map of the Bayamón quadrangle, Puerto Rico: U.S. Geological Survey Miscellaneous Geologic Investigations Map I-751, scale 1:20,000.
- Palchik, V. and Hatzor, Y.H., 2002, Crack damage stress as a composite function of porosity and elastic matrix stiffness in dolomites and limestones, *Engineering Geology*, v. 63, p. 233-245.
- Quiñones-Márquez, F., Gómez-Gómez, F., and Allen, Z., 1984, Puerto Rico groundwater resources, National Water Summary, US Geological Survey Water Supply Paper 2275, p. 367-372.
- Ramírez, W., 2000, Dolomitization and Evolution of the Puerto Rico North Coast Confined Aquifer System, Thesis Ph.D. Tulane University, p. 102, 218-221.
- Scharlach, R.A., 1990, Depositional History of Oligocene-Miocene Carbonate Rocks, Surface of Northeastern Puerto Rico, Thesis M.S. University of New Orleans, p.129.
- Ward, W.C., Scharlach, R.A., and Hartley, J.R., *in press*, Geology of the North Coast groundwater province of Puerto Rico. *in*: Renken, R.A., and others, Geology and Hydrogeology of the Caribbean-Islands Aquifer System of the Commonwealth of Puerto Rico and the U.S. Virgin Islands, U.S. Geological Survey Professional Paper 1419.



**APPENDIX A**

**RESULTS OF THE UNCONFINED COMPRESSIVE  
STRENGTH TEST**

Table A-1  
Sample data  
Aymamón Limestone Formation  
Unconfined Compressive Strength Test

<b>Core NC-5</b>	<b>Diameter (in)</b>	<b>Length (in)</b>	<b>Area (in<sup>2</sup>)</b>	<b>Velocity (mm/min)</b>	<b>Load (lbf)</b>	<b>Peak Load (lbf)</b>	<b>Peak Load (N)</b>
20 m	2.8900	2.8555	6.5564	0.15	40,015.99	9,059	40,296.44
21.5 m	2.8495	2.3200	6.3739	0.3	40,015.99	24,102	107,211
23 m	2.8915	3.6345	6.5632	0.15	40,015.99	6,299	28,019.35
27.5 m	2.8862	3.94	6.5392	0.35	40,015.99	16,906	75,201.63

Table A-2  
Sample data  
Aymamón Limestone Formation  
Unconfined Compressive Strength Test – Poisson's ratio  
Sample Number: NC-5 20 m  
do = 2.8900 in    Lo= 2.8555 in

<b>P (Lbf)</b>	<b>df (in)</b>	<b>Δd (in)</b>	<b>Et</b>	<b>Lf (in)</b>	<b>ΔL (in)</b>	<b>ε</b>	<b>Poisson's ratio (v)</b>
0	2.8900	0	0	2.8555	0	0	0
448	2.8900	0	0	2.8607	0.0052	0.0018	0
896	2.8900	0	0	2.8620	0.0065	0.0023	0
1351	2.8900	0	0	2.8630	0.0075	0.0026	0
1793	2.8900	0	0	2.8637	0.0082	0.0029	0
2252	2.8900	0	0	2.8645	0.0090	0.0032	0
2692	2.8900	0	0	2.8652	0.0097	0.0034	0
3147	2.8900	0	0	2.8660	0.0105	0.0037	0
3577	2.8900	0	0	2.8665	0.0110	0.0039	0
4045	2.8900	0	0	2.8672	0.0117	0.0041	0
4482	2.8902	0.0002	0.00007	2.8678	0.0123	0.0043	0.016
4945	2.8902	0.0002	0.00007	2.8685	0.0130	0.0046	0.015
5373	2.8902	0.0002	0.00007	2.8690	0.0135	0.0047	0.015
5844	2.8902	0.0002	0.00007	2.8697	0.0142	0.0050	0.014
6293	2.8902	0.0002	0.00007	2.8702	0.0147	0.0051	0.014
6754	2.8906	0.0006	0.0002	2.8710	0.0155	0.0054	0.04
7193	2.8908	0.0008	0.0003	2.8717	0.0162	0.0057	0.05
7643	2.8910	0.0010	0.0003	2.8725	0.0170	0.0060	0.05
8099	2.8916	0.0016	0.0005	2.8735	0.0180	0.0063	0.08
8555	2.8922	0.0022	0.0008	2.8742	0.0187	0.0065	0.12
8990	2.8926	0.0026	0.0009	2.8790	0.0235	0.0082	0.11
9059	2.8930	0.0030	0.0010	2.8820	0.0265	0.0093	0.11

Table A-3  
Sample data  
Aymamón Limestone Formation  
Unconfined Compressive Strength Test – Poisson's ratio  
Sample Number: NC-5 21.5 m  
do = 2.8495 in Lo = 2.32 in

<b>P (Lbf)</b>	<b>df (in)</b>	<b>Δd (in)</b>	<b>Et</b>	<b>Lf (in)</b>	<b>ΔL (in)</b>	<b>ε</b>	<b>Poisson's ratio (v)</b>
0	2.8495	0	0	2.32	0	0	0
450	2.8507	0.0012	0.0004	2.3215	0.0015	0.0006	0.67
890	2.8511	0.0016	0.0006	2.3228	0.0028	0.0012	0.50
1355	2.8511	0.0016	0.0006	2.3240	0.0040	0.0017	0.35
1794	2.8511	0.0016	0.0006	2.3250	0.0050	0.0022	0.27
2245	2.8511	0.0016	0.0006	2.3260	0.0060	0.0026	0.23
2697	2.8511	0.0016	0.0006	2.3270	0.0070	0.0030	0.20
3133	2.8511	0.0016	0.0006	2.3278	0.0078	0.0034	0.18
3586	2.8517	0.0022	0.0008	2.3287	0.0087	0.0038	0.21
4041	2.8517	0.0022	0.0008	2.3295	0.0095	0.0041	0.20
4520	2.8517	0.0022	0.0008	2.3303	0.0103	0.0044	0.18
4948	2.8519	0.0024	0.0008	2.3310	0.0110	0.0047	0.17
5384	2.8521	0.0026	0.0009	2.3317	0.0117	0.0050	0.18
5835	2.8521	0.0026	0.0009	2.3325	0.0125	0.0054	0.17
6312	2.8521	0.0026	0.0009	2.3332	0.0132	0.0057	0.16
6726	2.8521	0.0026	0.0009	2.3337	0.0137	0.0059	0.15
7179	2.8521	0.0026	0.0009	2.3345	0.0145	0.0063	0.14
7637	2.8521	0.0026	0.0009	2.3352	0.0152	0.0065	0.14
8118	2.8521	0.0026	0.0009	2.3360	0.0160	0.0069	0.13
8528	2.8521	0.0026	0.0009	2.3365	0.0165	0.0071	0.13
9019	2.8521	0.0026	0.0009	2.3372	0.0172	0.0074	0.12
9465	2.8527	0.0032	0.0011	2.3377	0.0177	0.0076	0.14
9887	2.8537	0.0042	0.0015	2.3385	0.0185	0.0080	0.19
10333	2.8627	0.0132	0.0050	2.3392	0.0192	0.0083	0.60
10781	2.8649	0.0154	0.0054	2.3397	0.0197	0.0085	0.59
11244	2.8659	0.0164	0.0060	2.3405	0.0205	0.0088	0.68
11728	2.8669	0.0174	0.0061	2.3413	0.0213	0.0092	0.65
12141	2.8675	0.0180	0.0063	2.3417	0.0217	0.0094	0.67
12570	2.8679	0.0184	0.0065	2.3440	0.0240	0.0103	0.63
13019	2.8687	0.0192	0.0067	2.3445	0.0245	0.0105	0.64
13497	2.8699	0.0204	0.0072	2.3453	0.0253	0.0109	0.66
13939	2.8721	0.0226	0.0080	2.3457	0.0257	0.0111	0.71
14410	2.8741	0.0246	0.0090	2.3462	0.0262	0.0113	0.76
14830	2.8753	0.0258	0.0091	2.3467	0.0267	0.0115	0.78
15302	2.8837	0.0342	0.0120	2.3475	0.0275	0.0118	1
15713	2.8863	0.0368	0.0129	2.3480	0.0280	0.0121	1

16186	2.8867	0.0372	0.0131	2.3487	0.0287	0.0124	1
16641	2.8867	0.0372	0.0131	2.3495	0.0295	0.0127	1
17090	2.8869	0.0374	0.0131	2.3500	0.0300	0.0129	1
17537	2.8883	0.0388	0.0136	2.3507	0.0307	0.0132	1
17940	2.8885	0.0390	0.0137	2.3515	0.0315	0.0136	1
18886	2.8887	0.0392	0.0137	2.3538	0.0338	0.0146	0.94
19336	2.8893	0.0398	0.0140	2.3560	0.0360	0.0155	0.90
19787	2.8895	0.0400	0.0140	2.3568	0.0368	0.0159	0.88
20230	2.8897	0.0402	0.0141	2.3572	0.0372	0.0160	0.88
20682	2.8901	0.0406	0.0142	2.3577	0.0377	0.0162	0.88
21149	2.8905	0.0410	0.0144	2.3585	0.0385	0.0166	0.87
21581	2.8913	0.0418	0.0147	2.3592	0.0392	0.0169	0.87
22029	2.8949	0.0454	0.0159	2.3598	0.0398	0.0172	0.93
22478	2.8977	0.0482	0.0171	2.3605	0.0405	0.0175	0.97
24102	2.9233	0.0738	0.0259	2.3642	0.0442	0.0191	1.4

Table A-4  
Sample data  
Aymamón Limestone Formation  
Unconfined Compressive Strength Test – Poisson's ratio  
Sample Number: NC-5 23 m  
do = 2.8915 in Lo = 3.6345 in

<b>P (Lbf)</b>	<b>df (in)</b>	<b>Δd (in)</b>	<b>Et</b>	<b>Lf (in)</b>	<b>ΔL (in)</b>	<b>ε</b>	<b>Poisson's ratio (ν)</b>
0	2.8915	0	0	3.6345	0	0	0
452	2.8916	0.0001	0.00003	3.6363	0.0018	0.0005	0.06
895	2.8916	0.0001	0.00003	3.6373	0.0028	0.0008	0.04
1347	2.8916	0.0001	0.00003	3.6385	0.0040	0.0011	0.03
1920	2.8918	0.0002	0.00007	3.6395	0.0050	0.0014	0.05
2250	2.8923	0.0008	0.0003	3.6410	0.0065	0.0018	0.17
2697	2.8930	0.0015	0.0005	3.6423	0.0078	0.0021	0.24
3145	2.8937	0.0022	0.0008	3.6435	0.0090	0.0025	0.32
3588	2.8944	0.0029	0.0010	3.6445	0.0100	0.0028	0.36
4045	2.8950	0.0035	0.0012	3.6458	0.0113	0.0031	0.39
4493	2.8957	0.0042	0.0014	3.6468	0.0123	0.0034	0.41
4940	2.8964	0.0049	0.0017	3.6477	0.0132	0.0036	0.47
5395	2.8971	0.0056	0.0019	3.6487	0.0142	0.0039	0.49
5842	2.8978	0.0063	0.0022	3.6497	0.0152	0.0042	0.52
6299	2.8993	0.0078	0.0023	3.6510	0.0165	0.0045	0.51

Table A-5  
Sample data  
Aymamón Limestone Formation  
Unconfined Compressive Strength Test – Poisson's ratio  
Sample Number: NC-5 27.5 m  
do = 2.8862 in Lo= 3.9400 in

<b>P (Lbf)</b>	<b>df (in)</b>	<b>Δd (in)</b>	<b>Et</b>	<b>Lf (in)</b>	<b>ΔL (in)</b>	<b>ε</b>	<b>Poisson's ratio (v)</b>
0	2.8862	0	0	3.9400	0	0	0
448	2.8862	0	0	3.9410	0.0010	0.0003	0
880	2.8864	0.0002	0.00007	3.9420	0.0020	0.0005	0.14
1347	2.8866	0.0004	0.0001	3.9430	0.0030	0.0008	0.12
1796	2.8866	0.0004	0.0001	3.9437	0.0037	0.0009	0.11
2240	2.8868	0.0006	0.0002	3.9445	0.0045	0.0011	0.18
2697	2.8868	0.0006	0.0002	3.9453	0.0053	0.0013	0.15
3145	2.8868	0.0006	0.0002	3.9460	0.0060	0.0015	0.13
3583	2.8872	0.0010	0.0003	3.9465	0.0065	0.0016	0.19
4046	2.8874	0.0012	0.0004	3.9473	0.0073	0.0018	0.22
4503	2.8876	0.0014	0.0005	3.9477	0.0077	0.0019	0.26
4945	2.8876	0.0014	0.0005	3.9483	0.0083	0.0021	0.24
5380	2.8876	0.0014	0.0005	3.9490	0.0090	0.0023	0.22
5844	2.8878	0.0016	0.0005	3.9495	0.0095	0.0024	0.21
6301	2.8878	0.0016	0.0005	3.9500	0.0100	0.0025	0.20
6734	2.8878	0.0016	0.0005	3.9505	0.0105	0.0027	0.18
7177	2.8882	0.0020	0.0007	3.9510	0.0110	0.0028	0.25
7634	2.8884	0.0022	0.0008	3.9515	0.0115	0.0029	0.28
8100	2.8886	0.0024	0.0008	3.9520	0.0120	0.0030	0.27
8536	2.8888	0.0026	0.0009	3.9527	0.0127	0.0032	0.28
9013	2.8888	0.0026	0.0009	3.9532	0.0132	0.0034	0.26
9455	2.8892	0.0030	0.0010	3.9537	0.0137	0.0035	0.29
9886	2.8894	0.0032	0.0011	3.9540	0.0140	0.0036	0.31
10332	2.8896	0.0034	0.0012	3.9545	0.0145	0.0037	0.32
10795	2.8900	0.0038	0.0013	3.9550	0.0150	0.0038	0.34
11244	2.8902	0.0040	0.0014	3.9555	0.0155	0.0039	0.36
11705	2.8902	0.0040	0.0014	3.9560	0.0160	0.0041	0.34
12148	2.8904	0.0042	0.0015	3.9565	0.0165	0.0042	0.36
12577	2.8910	0.0048	0.0017	3.9570	0.0170	0.0043	0.39
13022	2.8912	0.0050	0.0017	3.9575	0.0175	0.0044	0.39
13495	2.8916	0.0054	0.0019	3.9580	0.0180	0.0046	0.41
13942	2.8920	0.0058	0.0020	3.9585	0.0185	0.0047	0.43
14411	2.8924	0.0062	0.0021	3.9590	0.0190	0.0048	0.44
14833	2.8928	0.0066	0.0023	3.9592	0.0192	0.0049	0.47
15294	2.8932	0.0070	0.0024	3.9597	0.0197	0.0050	0.48
15724	2.8938	0.0076	0.0026	3.9602	0.0202	0.0051	0.51

16181	2.8942	0.0080	0.0028	3.9607	0.0207	0.0052	0.54
16646	2.8944	0.0082	0.0028	3.9612	0.0212	0.0054	0.52
16906	2.8946	0.0084	0.0029	3.9618	0.0218	0.0055	0.53

Table A-6  
Sample data  
Aymamón Limestone Formation  
Unconfined Compressive Strength Test – Stress  
Sample Number: Core NC-5

Core ID	Depth (m)	P (lbf)	A (in <sup>2</sup> )	P/A	Stress ( $\sigma$ ) (psi)
NC-5	20	9,059	6.5564	9,059/6.5564	1,381.7
NC-5	21.5	24,102	6.3739	24,102/6.3739	3,781.4
NC-5	23	6,299	6.5632	6,299/6.5632	959.7
NC-5	27.5	16,906	6.5392	16,906/6.5392	2,585.3

Table A-7  
Sample data  
Aymamón Limestone Formation  
Unconfined Compressive Strength Test – Strain  
Sample Number: Core NC-5

Core ID	Depth (m)	$\Delta L$ (in)	Lo (in)	$\Delta L/Lo$	Strain ( $\epsilon$ ) (%)
NC-5	20	0.0265	2.8555	0.0265/2.8555	0.0093
NC-5	21.5	0.0442	2.32	0.0442/2.32	0.0191
NC-5	23	0.0165	3.6345	0.0165/3.6345	0.0045
NC-5	27.5	0.0218	3.94	0.0218/3.94	0.0055

Table A-8  
Sample data  
Aymamón Limestone Formation  
Unconfined Compressive Strength Test – Young's Modulus  
Sample Number: Core NC-5

Core ID	Depth (m)	Stress ( $\sigma$ ) (psi)	Strain ( $\epsilon$ ) (%)	$\sigma / \epsilon$	Young's modulus (E) (psi)	Young's modulus (E) (GPa)
NC-5	20	1,381.7	0.0093	1,381.7/0.0093	148,570	1.02
NC-5	21.5	3,781.4	0.0191	3,781.4/0.0191	197,979	1.37
NC-5	23	959.7	0.0045	959.7/0.0045	213,267	1.47
NC-5	27.5	2,585.3	0.0055	2,585.3/0.0055	470,055	3.24

Table A-9  
Sample data  
Aymamón Limestone Formation  
Unconfined Compressive Strength Test – Shear Modulus  
Sample Number: Core NC-5

Core ID	Depth (m)	Young's modulus (E) (GPa)	Poisson's ratio ( $\nu$ )	Shear Modulus ( $\mu$ ) (GPa)
NC-5	20	1.02	0.029	0.50
NC-5	21.5	1.37	0.37	0.50
NC-5	23	1.47	0.27	0.58
NC-5	27.5	3.24	0.29	1.3



Table A-10  
Sample data  
Aymamón Limestone Formation  
Unconfined Compressive Strength Test – Bulk Modulus  
Sample Number: Core NC-5

Core ID	Depth (m)	Young's modulus (E) (GPa)	Poisson's ratio ( $\nu$ )	Bulk Modulus (K) (GPa)
NC-5	20	1.02	0.029	0.36
NC-5	21.5	1.37	0.37	1.74
NC-5	23	1.47	0.27	1.06
NC-5	27.5	3.24	0.29	2.6

Table A-11  
Sample data  
Aymamón Limestone Formation  
Unconfined Compressive Strength Test – S-wave Velocity  
Sample Number: Core NC-5

Core ID	Depth (m)	Shear Modulus ( $\mu$ ) (Pa)	Density ( $\rho$ ) ( $\text{Kg/m}^3$ )	S-wave Velocity ( $V_s$ ) (m/s)
NC-5	20	497,742,491.3	2,460	450
NC-5	21.5	498,181,421.9	2,510	446
NC-5	23	578,907,142.1	2,490	482
NC-5	27.5	1,256,168,605	2,290	740

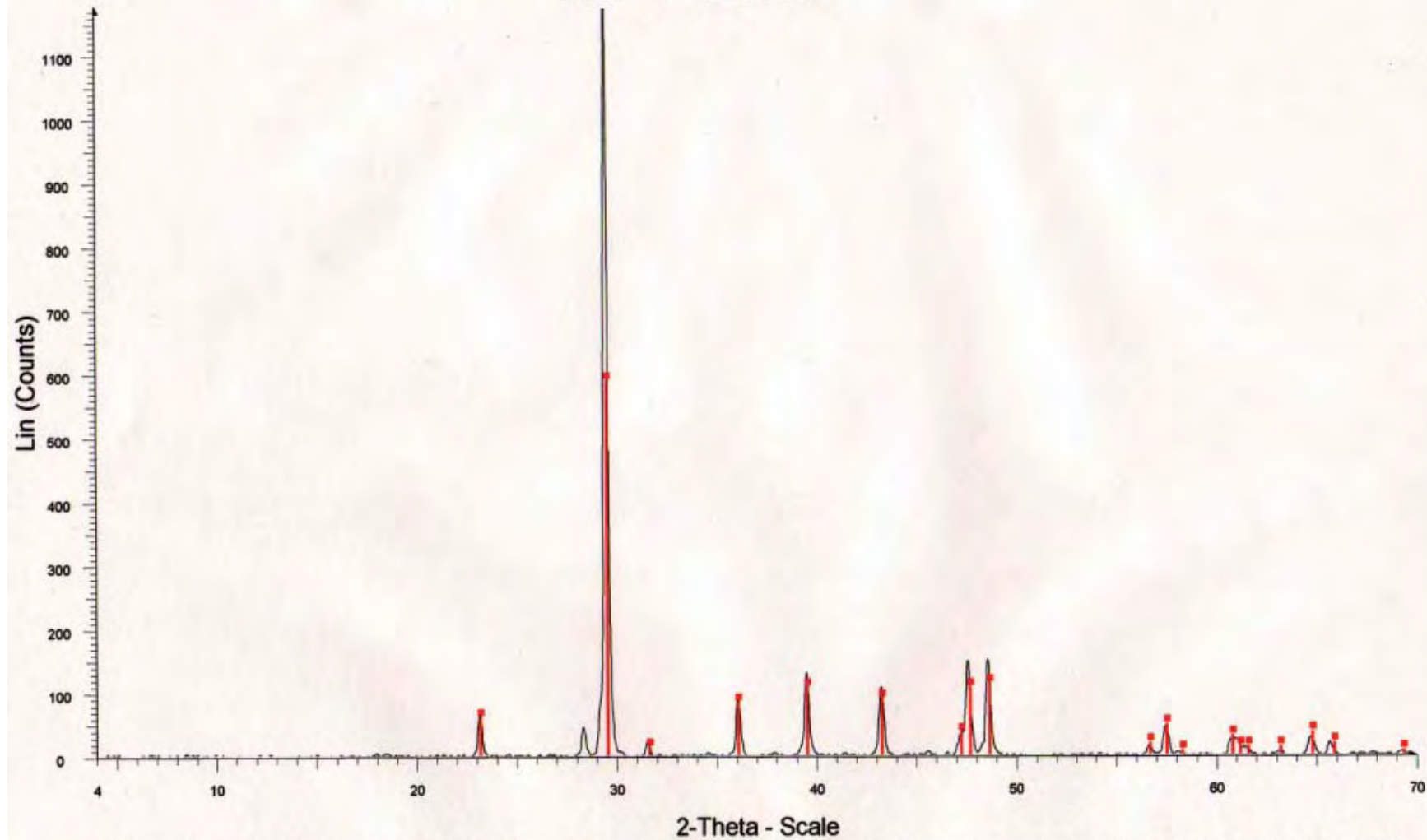
Table A-12  
Sample data  
Aymamón Limestone Formation  
Unconfined Compressive Strength Test – P-wave Velocity  
Sample Number: Core NC-5

Core ID	Depth (m)	Young's Modulus (E) (Pa)	Poisson's ratio (v)	Density ( $\rho$ ) (Kg/m <sup>3</sup> )	P-wave Velocity (Vp) (m/s)
NC-5	20	1,024,354,047	0.029	2,460	646
NC-5	21.5	1,365,017,096	0.37	2,510	981
NC-5	23	1,470,424,141	0.27	2,491	859
NC-5	27.5	3,240,915,002	0.29	2,295	1,360

# **APPENDIX B**

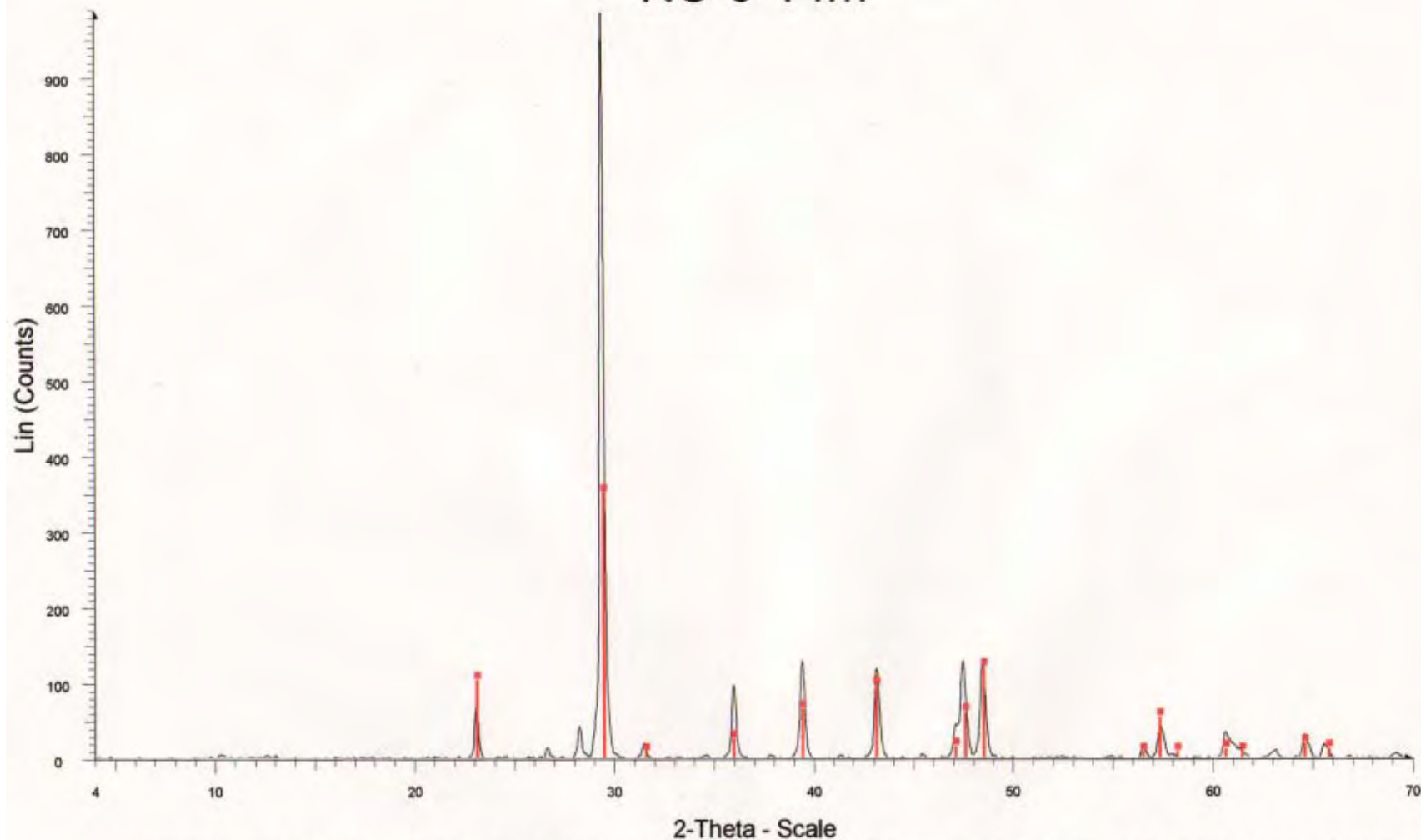
## **XRD RESULTS**

# NC-4-32.3m



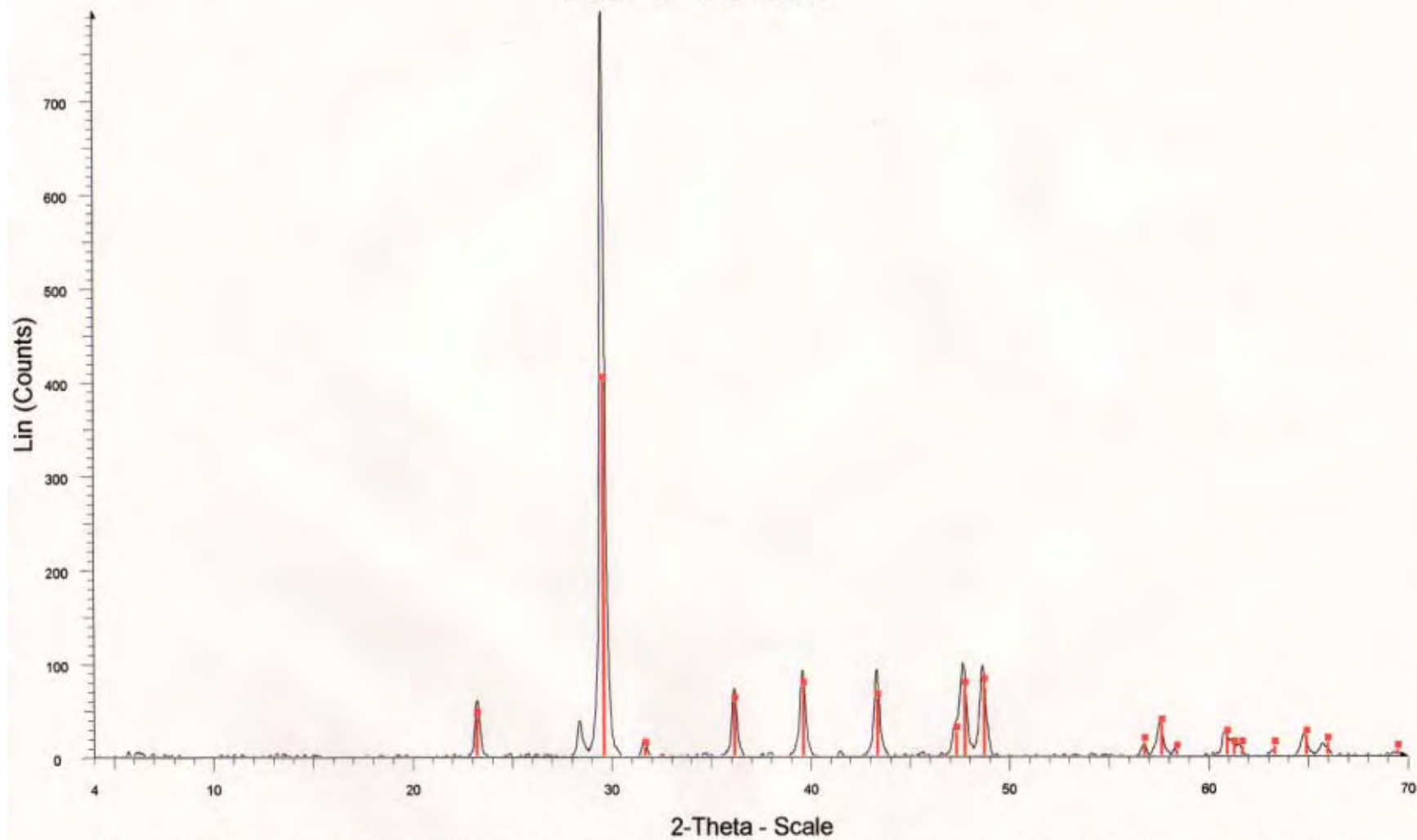
Vanessa Rosario / NC-4-32.3m - File: NC-4-32.3m.RAW - Type: 2Th/Th locked - Start: 4.000 ° - End: 70.000 ° - Step: 0.020 ° - Step time: 1. s - Temp.: 25 °C (Room) - Time Started: 28 s - 2-Theta: 4.000  
 Operations: Background 1.000,1.000 | Smooth 0.150 | Import  
 89-1304 (C) - Magnesium calcite, syn - (Mg<sub>0.03</sub>Ca<sub>0.97</sub>)(CO<sub>3</sub>) - Y: 50.00 % - d x by: 1. - WL: 1.54056 - Hexagonal (Rh) - a 4.97800 - b 4.97800 - c 16.96900 - alpha 90.000 - beta 90.000 - gamma 120.000

# NC-9-14m



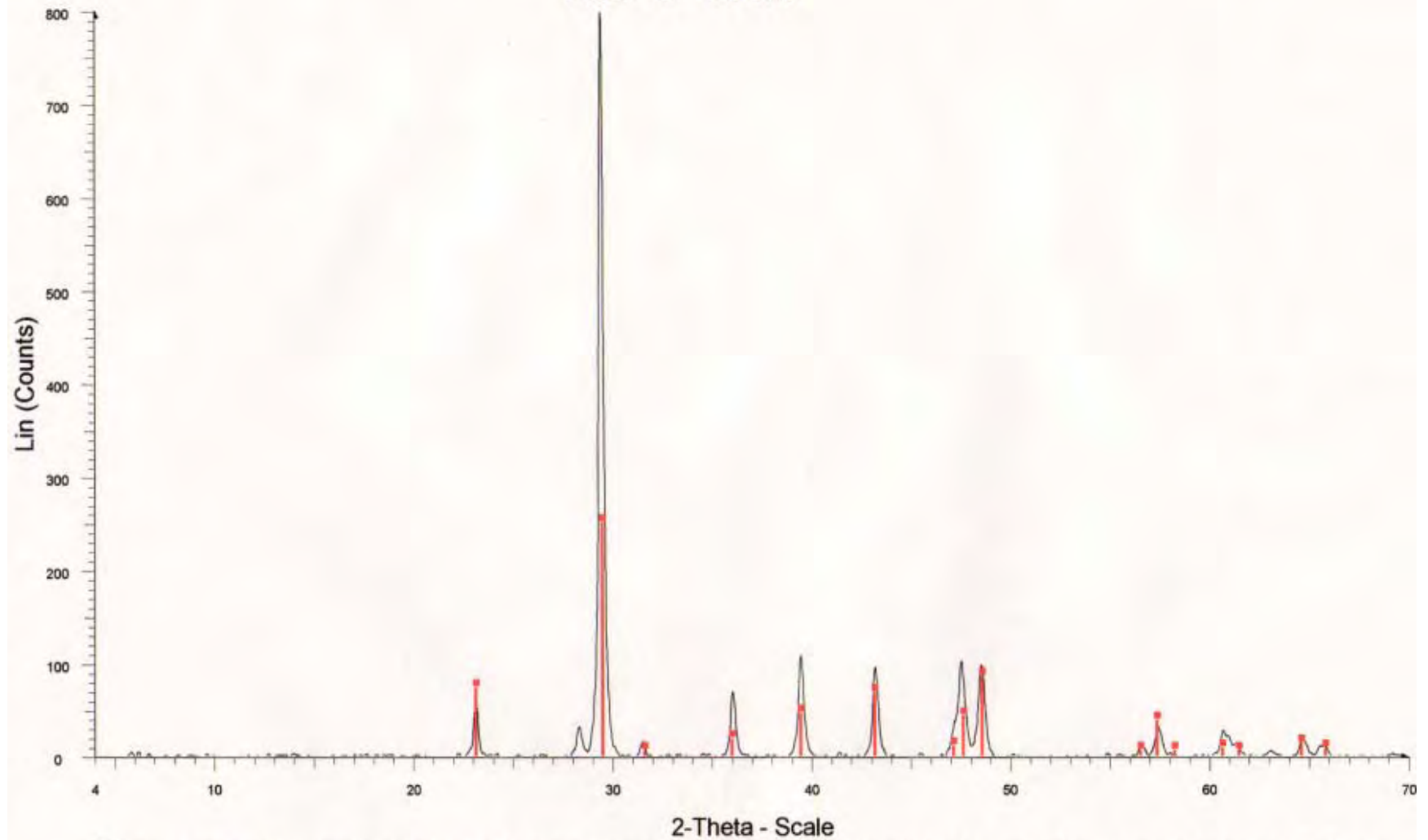
Vanessa Rosario / NC-9-14m - File: NC-9-14m.RAW - Type: 2Th/Th locked - Start: 4.000 ° - End: 70.000 ° - Step: 0.020 ° - Step time: 1. s - Temp.: 25 °C (Room) - Time Started: 46 s - 2-Theta: 4.000 ° -  
 Operations: Background 1.000,1.000 | Smooth 0.150 | Import  
 24-0027 (D) - Calcite - CaCO3 - Y: 35.42 % - d x by: 1. - WL: 1.54056 - Hexagonal (Rh) - a 4.99000 - b 4.99000 - c 17.00200 - alpha 90.000 - beta 90.000 - gamma 120.000 - Primitive - R-3c (167) - 6 - 3

NC-9-15.5m



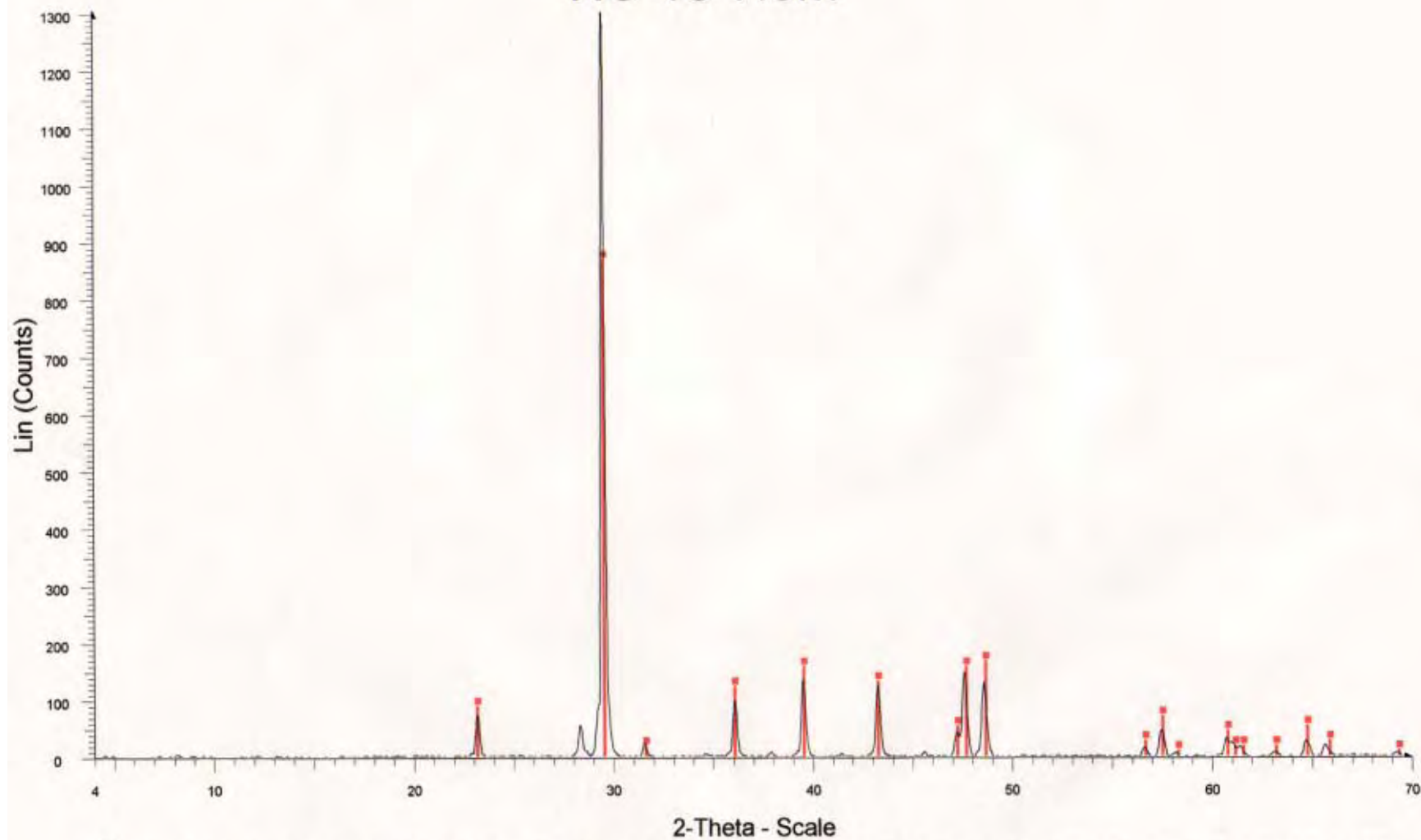
Vanessa Rosario / NC-9-15.5m - File: NC-9-15.5m.RAW - Type: 2Th/Th locked - Start: 4.000 ° - End: 70.000 ° - Step: 0.020 ° - Step time: 1. s - Temp.: 25 °C (Room) - Time Started: 16 s - 2-Theta: 4.000  
Operations: Background 1.000,1.000 | Smooth 0.150 | Import  
86-2335 (C) - Calcite magnesian - (Mg.064Ca.936)(CO<sub>3</sub>) - Y: 50.00 % - d x by: 1. - WL: 1.54056 - Hexagonal (Rh) - a 4.96730 - b 4.96730 - c 16.96310 - alpha 90.000 - beta 90.000 - gamma 120.000 - F

# NC-9-17m



Vanessa Rosario / NC-9-17m - File: NC-9-17m.RAW - Type: 2Th/Th locked - Start: 4.000 ° - End: 70.000 ° - Step: 0.020 ° - Step time: 1. s - Temp.: 25 °C (Room) - Time Started: 16 s - 2-Theta: 4.000 ° -  
 Operations: Background 1.000,1.000 | Smooth 0.150 | Import  
 24-0027 (D) - Calcite - CaCO3 - Y: 31.25 % - d x by: 1. - WL: 1.54056 - Hexagonal (Rh) - a 4.99000 - b 4.99000 - c 17.00200 - alpha 90.000 - beta 90.000 - gamma 120.000 - Primitive - R-3c (167) - 6 - 3

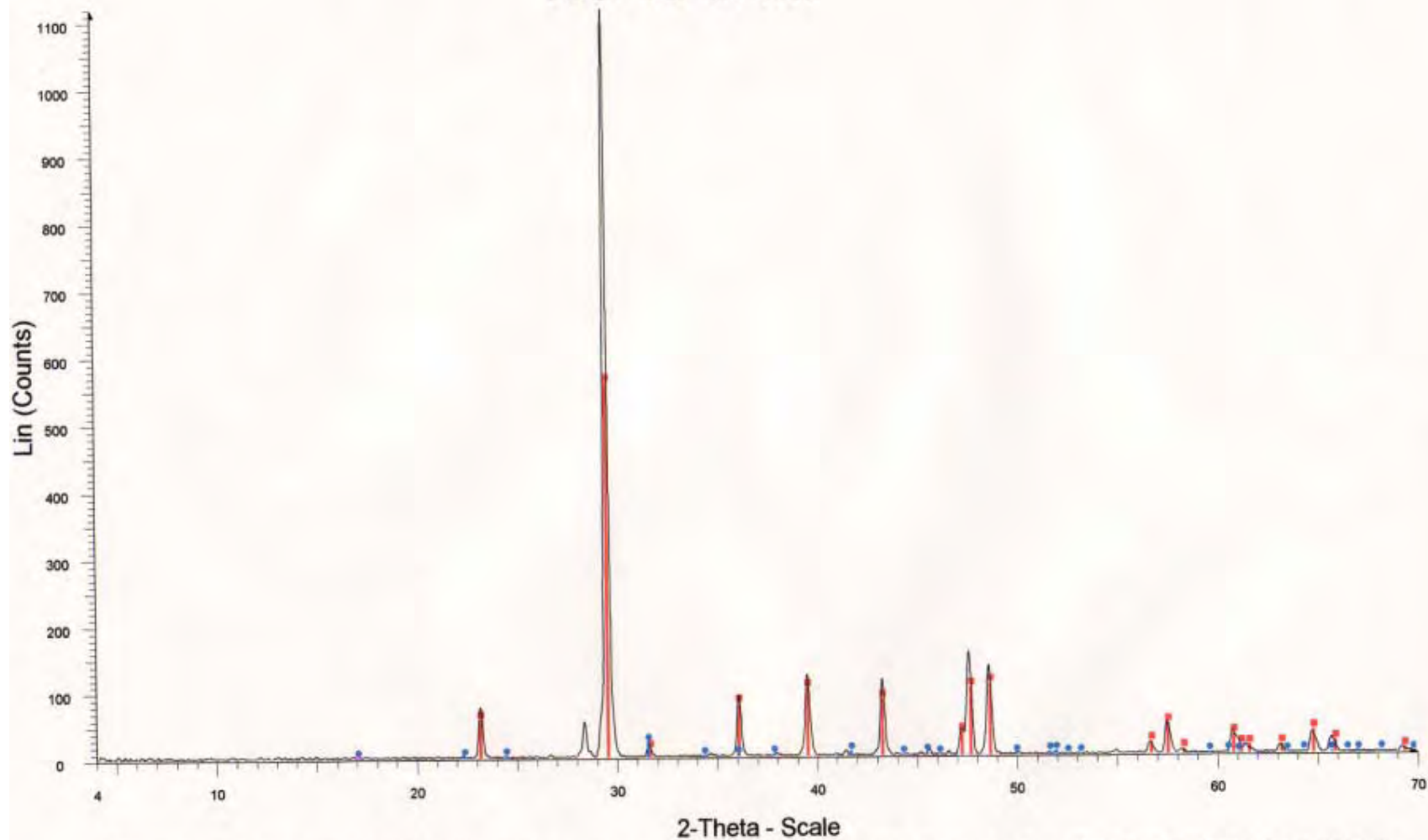
NC-10-7.9m



Vanessa Rosario / NC-10-7.9m - File: NC-10-7.9m.RAW - Type: 2Th/Th locked - Start: 4.000 ° - End: 70.000 ° - Step: 0.020 ° - Step time: 1. s - Temp.: 25 °C (Room) - Time Started: 16 s - 2-Theta: 4.000  
Operations: Background 1.000,1.000 | Smooth 0.150 | Import  
89-1304 (C) - Magnesium calcite, syn - (Mg<sub>0.03</sub>Ca<sub>0.97</sub>)(CO<sub>3</sub>) - Y: 66.67 % - d x by: 1, - WL: 1.54056 - Hexagonal (Rh) - a 4.97800 - b 4.97800 - c 16.98800 - alpha 90.000 - beta 90.000 - gamma 120.000

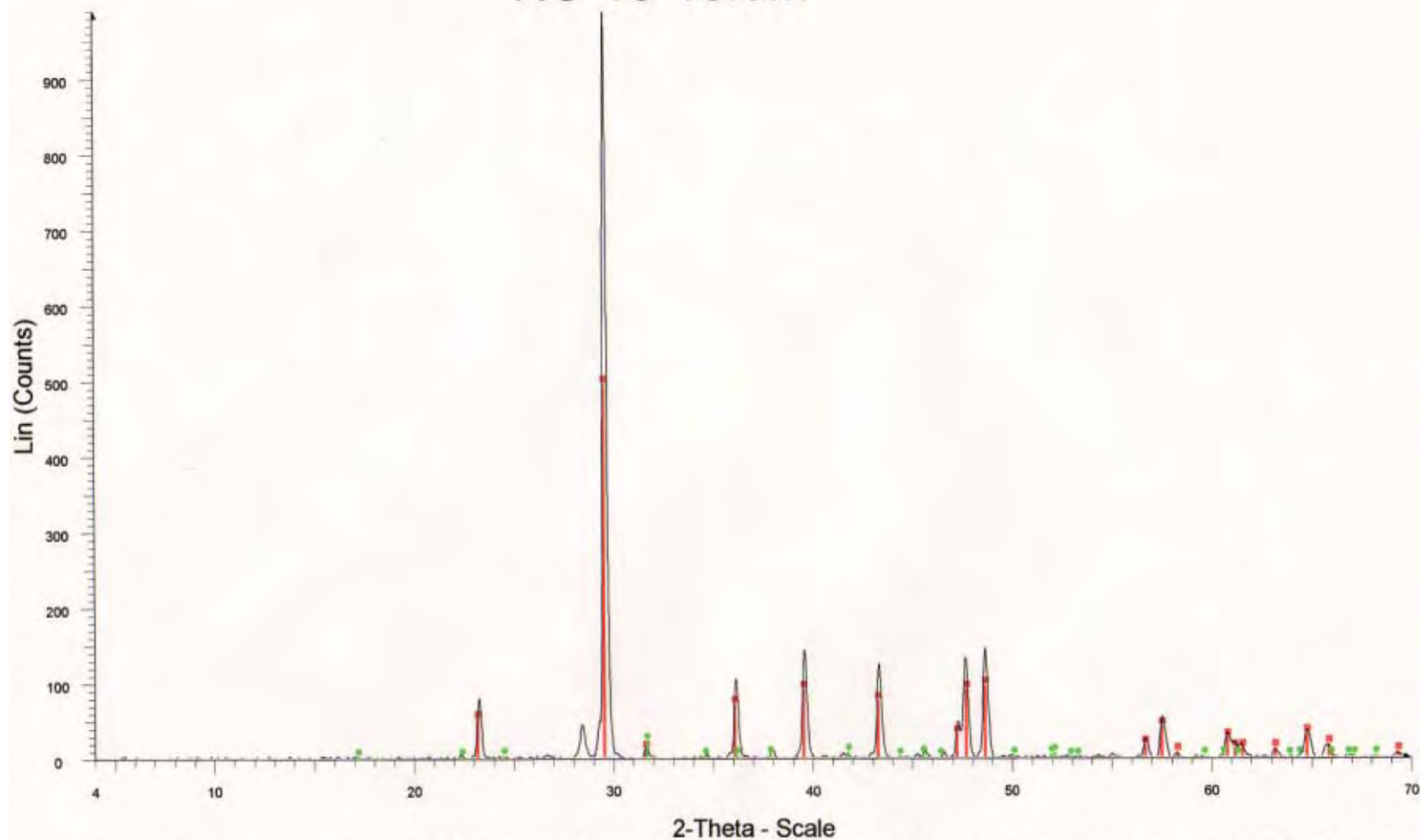


# NC-10-9.4m



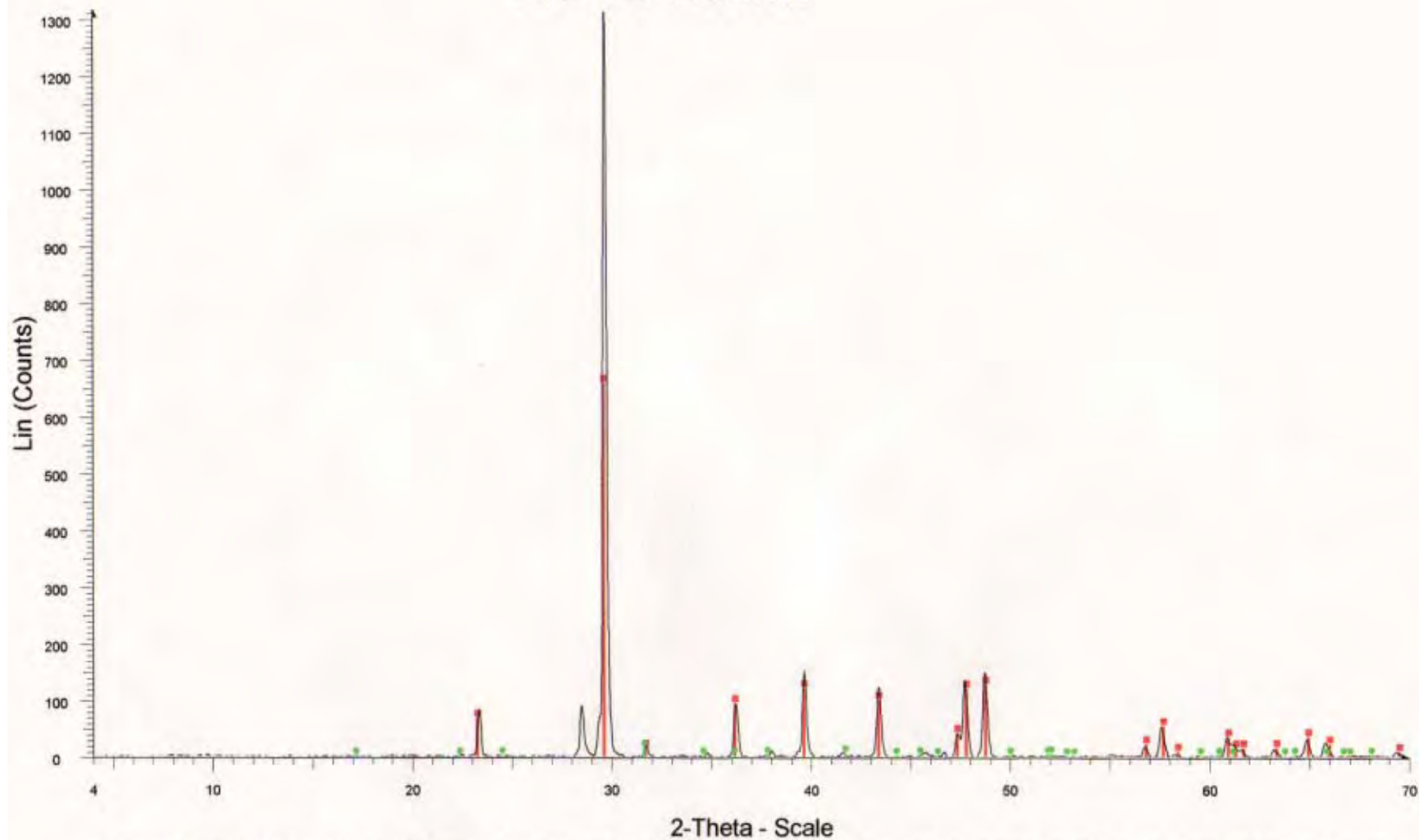
Vanessa Rosario / NC-10-9.4m - File: NC-10-9.4m.RAW - Type: 2Th/Th locked - Start: 4.000 ° - End: 70.000 ° - Step: 0.020 ° - Step time: 1. s - Temp.: 25 °C (Room) - Time Started: 16 s - 2-Theta: 4.000  
 Operations: Background 1.000,1.000 | Background 1.000,1.000 | Smooth 0.150 | Import  
 89-1304 (C) - Magnesium calcite, syn -  $(\text{Mg}_{0.03}\text{Ca}_{0.97})(\text{CO}_3)$  - Y: 49.98 % - d x by: 1. - WL: 1.54056 - Hexagonal (Rh) - a 4.97800 - b 4.97800 - c 16.98800 - alpha 90.000 - beta 90.000 - gamma 120.000  
 79-1344 (C) - Dolomite -  $\text{CaMg}(\text{CO}_3)_2$  - Y: 1.91 % - d x by: 0.9958 - WL: 1.54056 - Hexagonal (Rh) - a 4.77770 - b 4.77770 - c 15.73000 - alpha 90.000 - beta 90.000 - gamma 120.000 - Primitive - R-3 (

# NC-10-10.9m



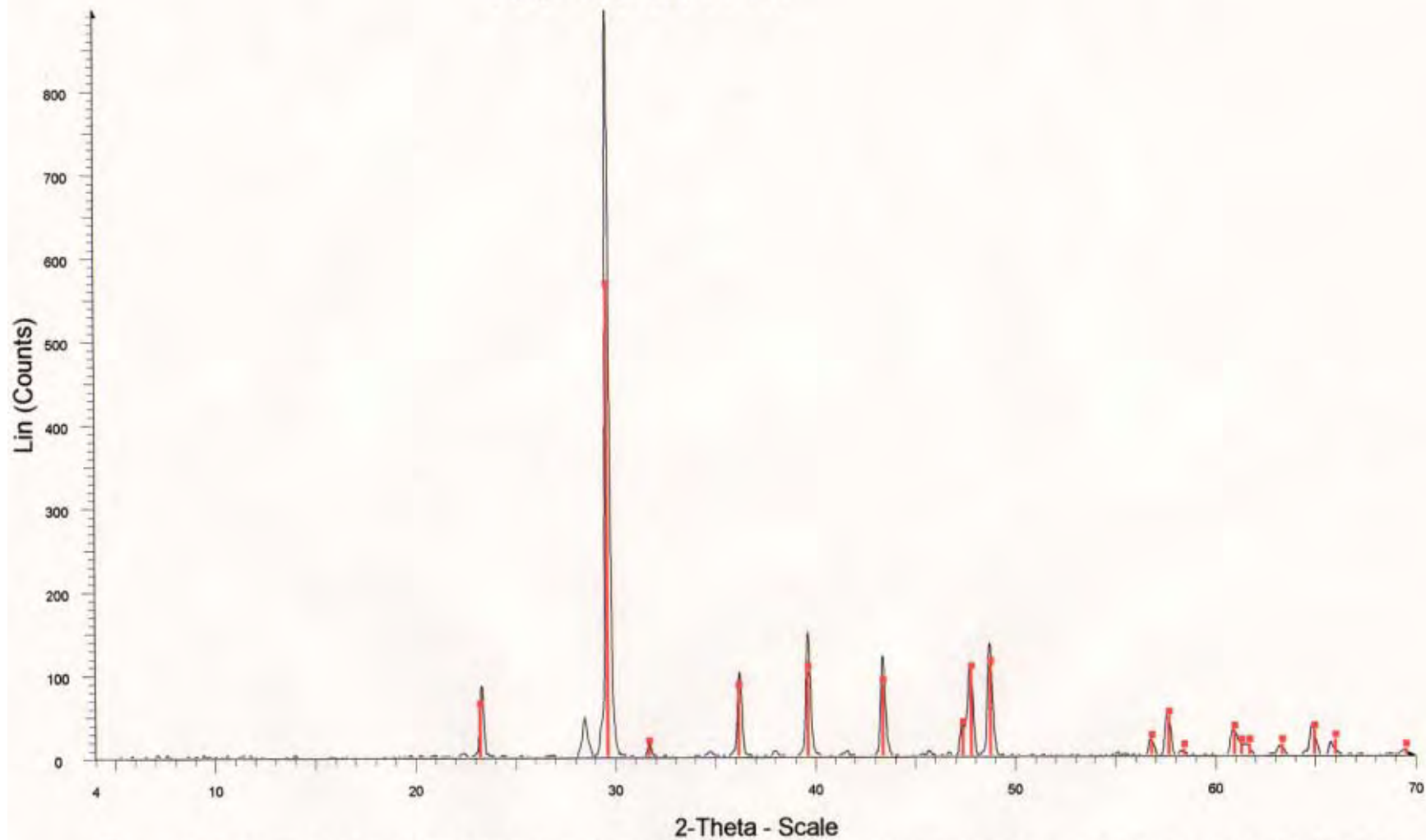
Vanessa Rosario / NC-10-10.9m - File: NC-10-10,9m1.RAW - Type: 2Th/Th locked - Start: 4.000 ° - End: 70.000 ° - Step: 0.020 ° - Step time: 1. s - Temp.: 25 °C (Room) - Time Started: 16 s - 2-Theta: 4.1  
 Operations: Background 1.000,1.000 | Smooth 0.150 | Import  
 89-1304 (C) - Magnesium calcite, syn - (Mg<sub>0.03</sub>Ca<sub>0.97</sub>)(CO<sub>3</sub>) - Y: 50.00 % - d x by: 1, - WL: 1.54056 - Hexagonal (Rh) - a 4.97800 - b 4.97800 - c 16.98800 - alpha 90.000 - beta 90.000 - gamma 120.000  
 79-1346 (C) - Dolomite - CaMg(CO<sub>3</sub>)<sub>2</sub> - Y: 2.08 % - d x by: 0.9979 - WL: 1.54056 - Hexagonal (Rh) - a 4.76360 - b 4.76360 - c 15.58200 - alpha 90.000 - beta 90.000 - gamma 120.000 - Primitive - R-3 (C)

# NC-10-26.2m



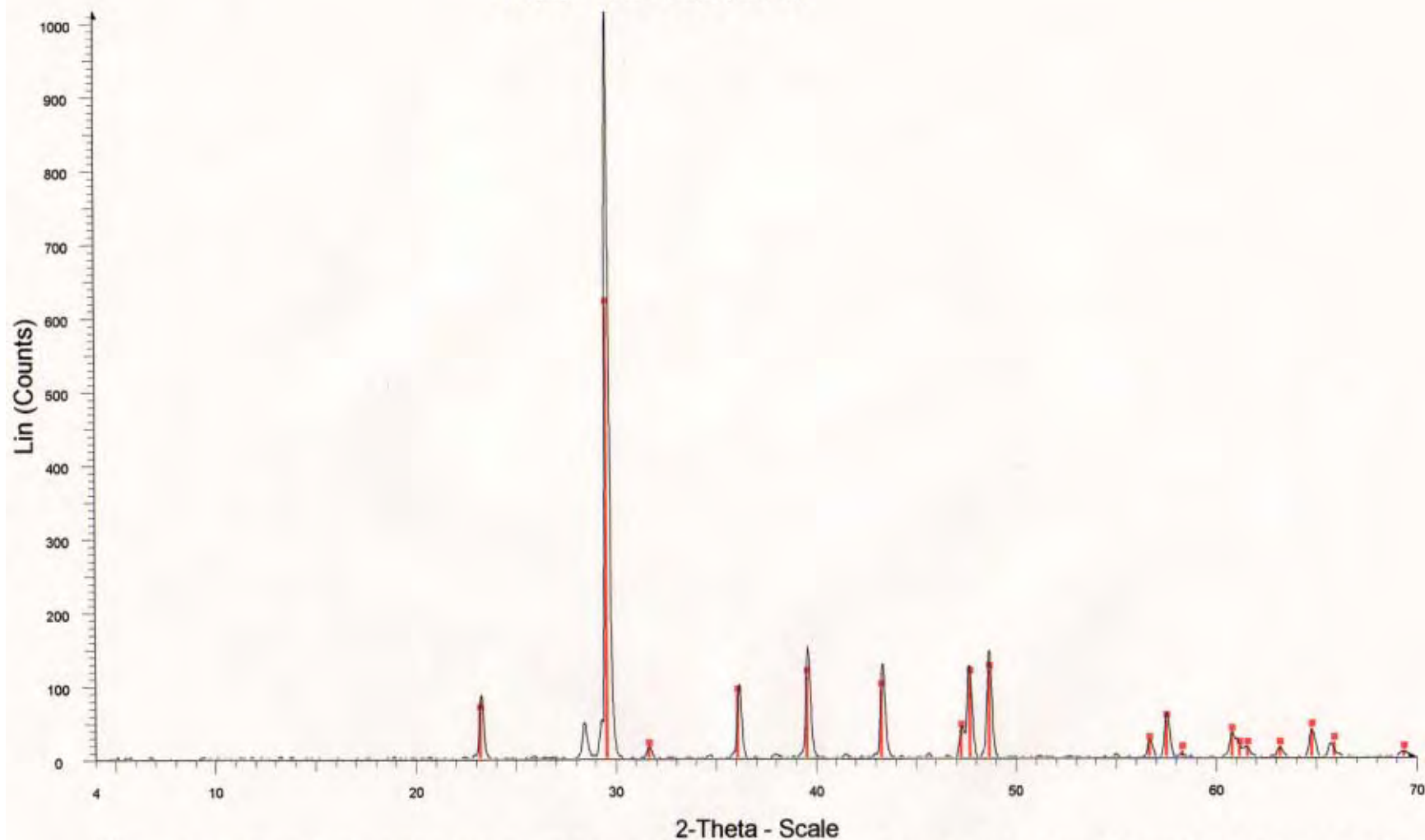
Vanessa Rosario / NC-10-26.2m - File: NC-10-26,2m.RAW - Type: 2Th/Th locked - Start: 4.000 ° - End: 70.000 ° - Step: 0.020 ° - Step time: 1. s - Temp.: 25 °C (Room) - Time Started: 19 s - 2-Theta: 4.01  
 Operations: Background 1.000,1.000 | Smooth 0.150 | Import  
 86-2335 (C) - Calcite magnesian - (Mg<sub>0.064</sub>Ca<sub>0.936</sub>)(CO<sub>3</sub>) - Y: 50.00 % - d x by: 1. - VL: 1.54056 - Hexagonal (Rh) - a 4.96730 - b 4.96730 - c 16.96310 - alpha 90.000 - beta 90.000 - gamma 120.000 - F  
 79-1346 (C) - Dolomite - CaMg(CO<sub>3</sub>)<sub>2</sub> - Y: 1.04 % - d x by: 1. - VL: 1.54056 - Hexagonal (Rh) - a 4.76380 - b 4.76380 - c 15.58200 - alpha 90.000 - beta 90.000 - gamma 120.000 - Primitive - R-3 (148)

# NC-10-27.7m



Vanessa Rosario / NC-10-27.7m - File: NC-10-27.7m.RAW - Type: 2Th/Th locked - Start: 4.000 ° - End: 70.000 ° - Step: 0.020 ° - Step time: 1, s - Temp.: 25 °C (Room) - Time Started: 16 s - 2-Theta: 4.0  
 Operations: Background 1.000,1.000 | Smooth 0.150 | Import  
 86-2335 (C) - Calcite magnesian - (Mg<sub>0.64</sub>Ca<sub>0.936</sub>)(CO<sub>3</sub>) - Y: 62.50 % - d x by: 1, - WL: 1.54056 - Hexagonal (Rh) - a 4.96730 - b 4.96730 - c 16.96310 - alpha 90.000 - beta 90.000 - gamma 120.000 - F

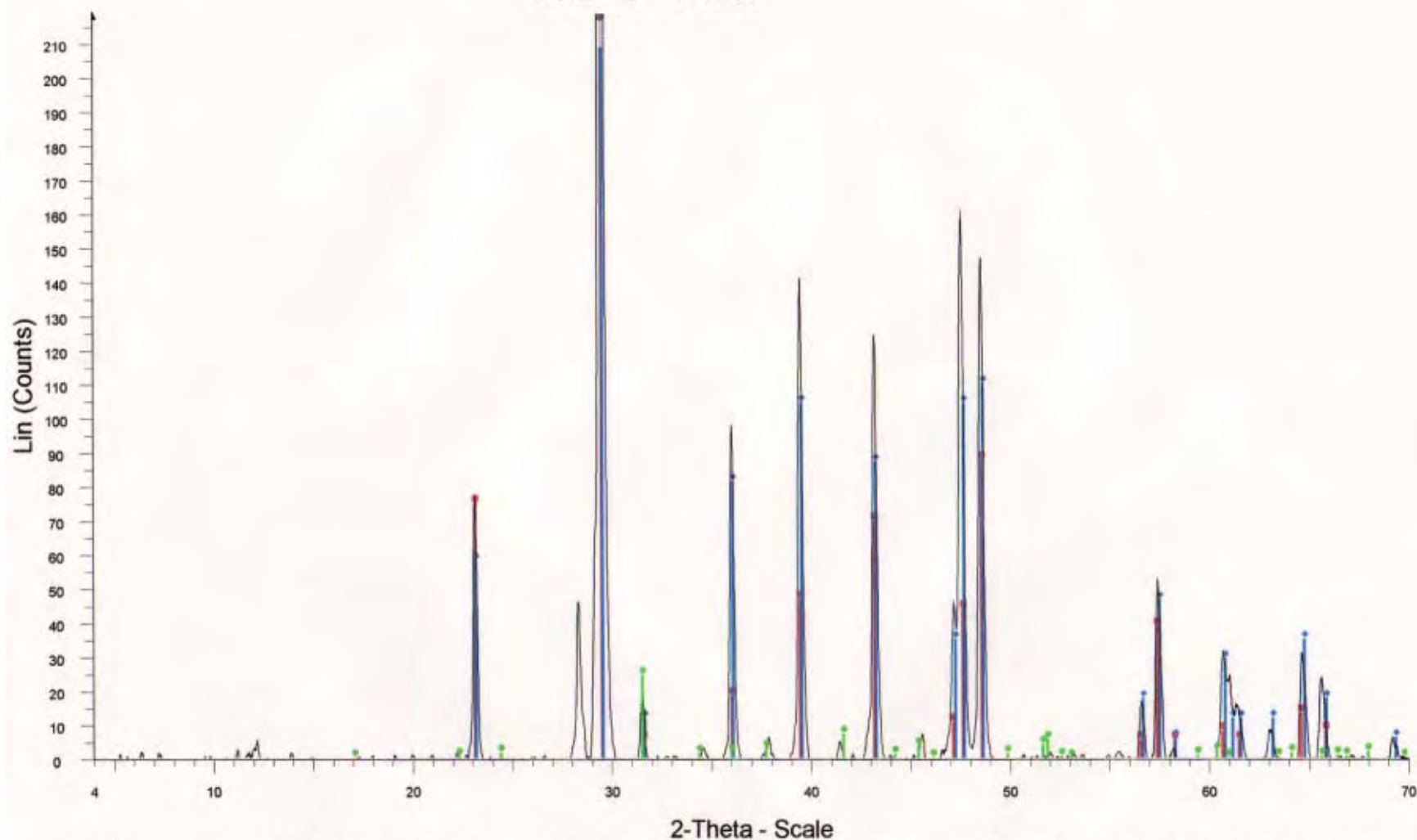
# NC-10-29.2m



Vanessa Rosario / NC-10-29.2m - File: NC-10-29,2m.RAW - Type: 2Th/Th locked - Start: 4.000 ° - End: 70.000 ° - Step: 0.020 ° - Step time: 1. s - Temp.: 25 °C (Room) - Time Started: 14 s - 2-Theta: 4.0  
 Operations: Background 1.000,1.000 | Smooth 0.150 | Import  
 89-1304 (C) - Magnesium calcite, syn - (Mg<sub>0.03</sub>Ca<sub>0.97</sub>)(CO<sub>3</sub>) - Y: 60.42 % - d x by: 1. - VL: 1.54056 - Hexagonal (Rh) - a 4.97800 - b 4.97800 - c 16.98800 - alpha 90.000 - beta 90.000 - gamma 120.000



# NC-5-14m



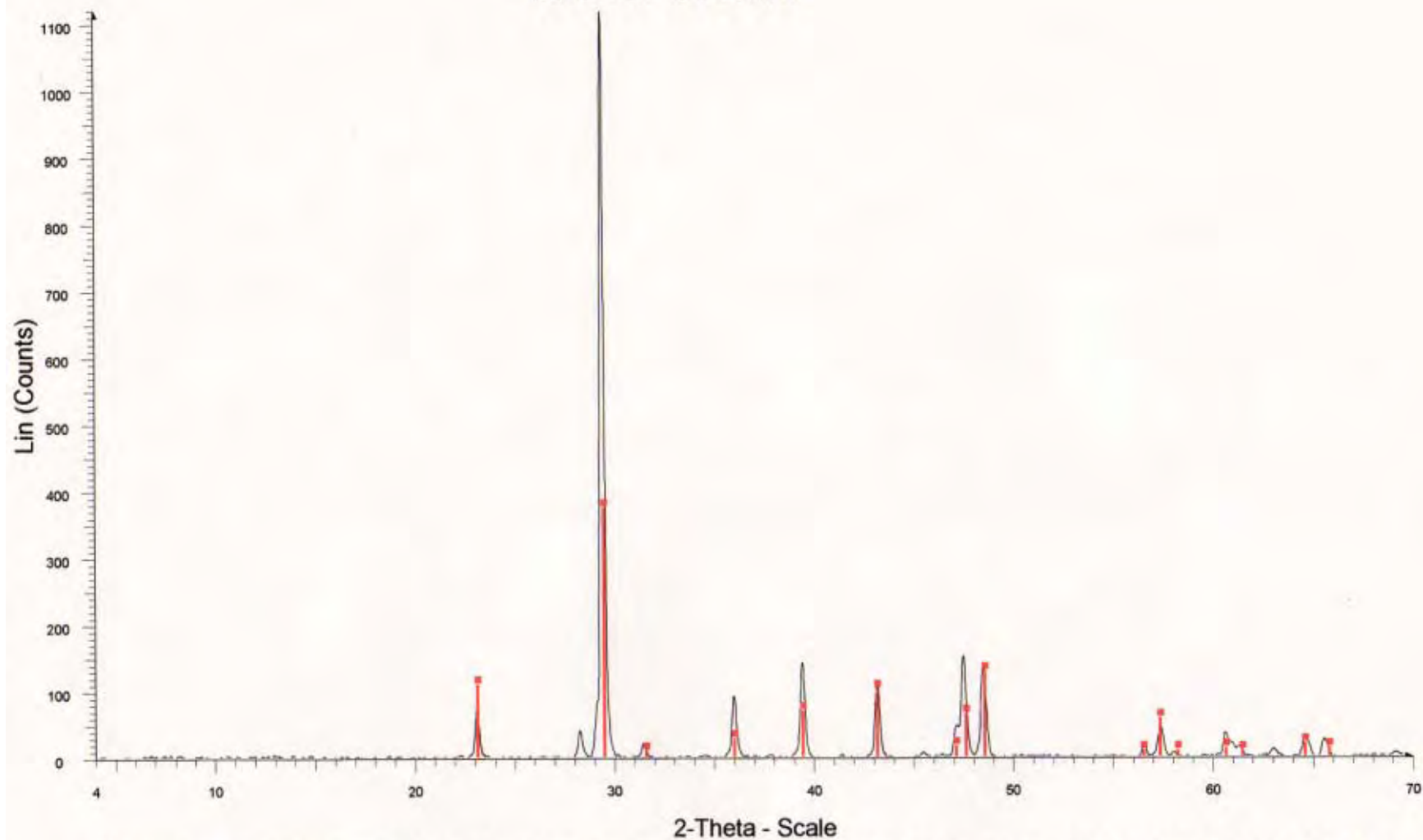
Vanessa Rosario / NC-5-14m - File: NC-5-14m.RAW - Type: 2Th/Th locked - Start: 4.000 ° - End: 70.000 ° - Step: 0.020 ° - Step time: 1. s - Temp.: 25 °C (Room) - Time Started: 16 s - 2-Theta: 4.000 ° - Operations: Background 1.000,1.000 | Smooth 0.150 | Import

24-0027 (D) - Calcite -  $\text{CaCO}_3$  - Y: 22.22 % - d x by: 1. - WL: 1.54056 - Hexagonal (Rh) - a 4.99000 - b 4.99000 - c 17.00200 - alpha 90.000 - beta 90.000 - gamma 120.000 - Primitive - R-3c (167) - 6 - 3

89-1304 (C) - Magnesium calcite, syn -  $(\text{Mg}_{0.03}\text{Ca}_{0.97})(\text{CO}_3)$  - Y: 50.00 % - d x by: 1. - WL: 1.54056 - Hexagonal (Rh) - a 4.97800 - b 4.97800 - c 16.98800 - alpha 90.000 - beta 90.000 - gamma 120.000 - Primitive - R-3 (148)

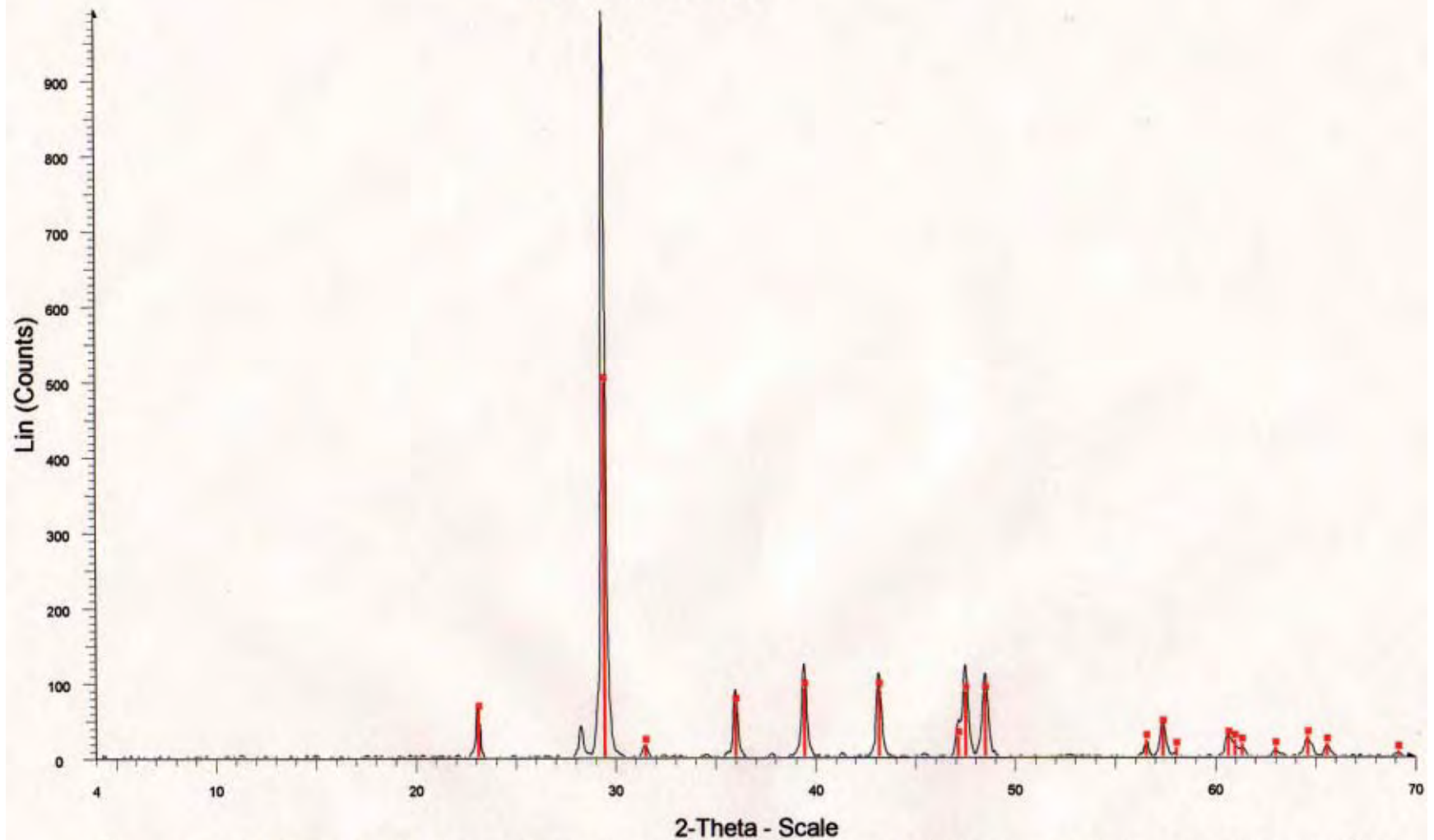
79-1345 (C) - Dolomite -  $\text{CaMg}(\text{CO}_3)_2$  - Y: 2.08 % - d x by: 1. - WL: 1.54056 - Hexagonal (Rh) - a 4.77030 - b 4.77030 - c 15.65300 - alpha 90.000 - beta 90.000 - gamma 120.000 - Primitive - R-3 (148)

# NC-5-15.5m



Vanessa Rosario / NC-5-15.5m - File: NC-5-15,5m.RAW - Type: 2Th/Th locked - Start: 4.000 ° - End: 70.000 ° - Step: 0.020 ° - Step time: 1. s - Temp.: 25 °C (Room) - Time Started: 16 s - 2-Theta: 4.000  
Operations: Background 1.000,1.000 | Smooth 0.150 | Import  
24-0027 (D) - Calcite - CaCO<sub>3</sub> - Y: 33.33 % - d x by: 1. - WL: 1.54056 - Hexagonal (Rh) - a 4.99000 - b 4.99000 - c 17.00200 - alpha 90.000 - beta 90.000 - gamma 120.000 - Primitive - R-3c (167) - 6 - 3

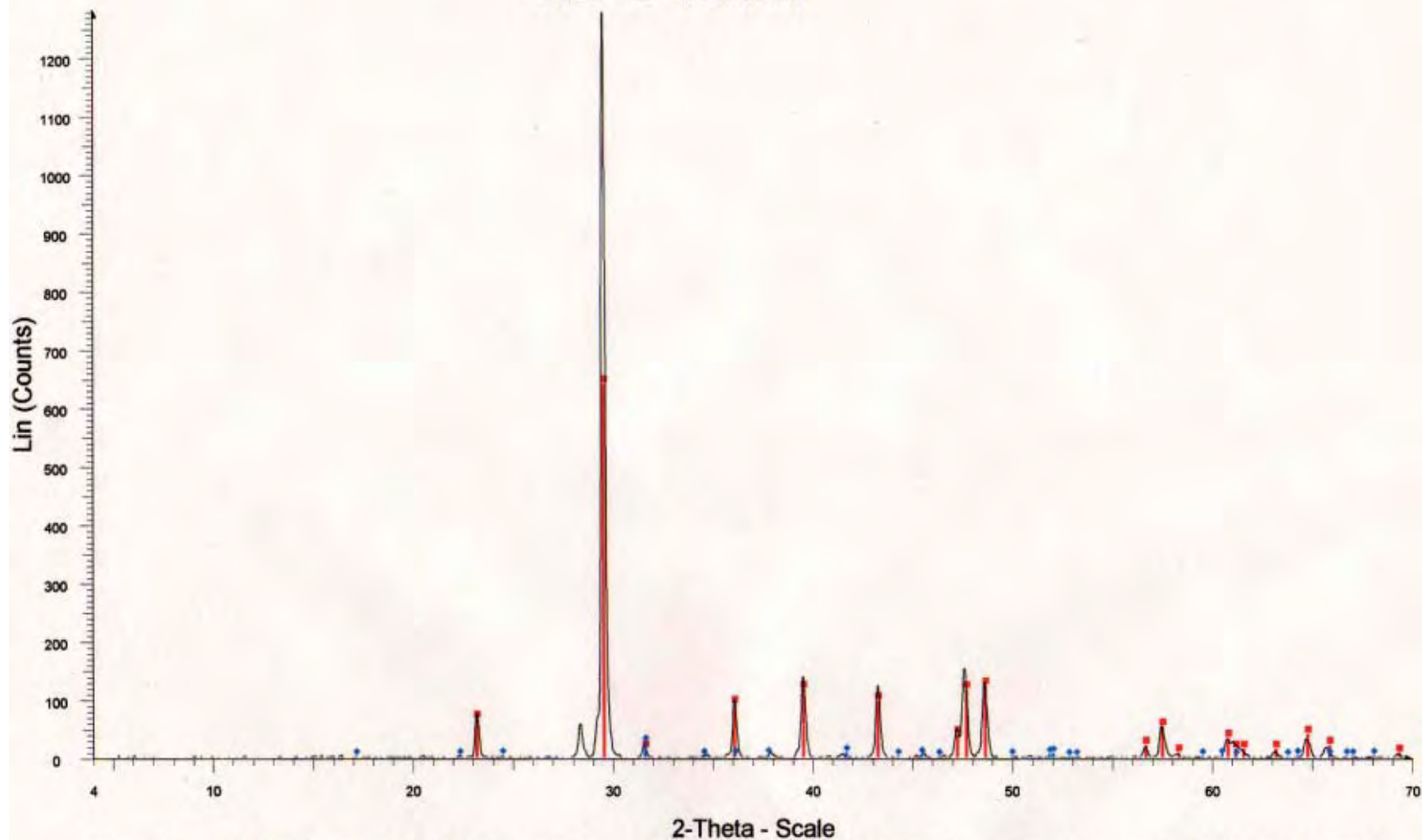
# NC-5-17m



Vanessa Rosario / NC-5-17m - File: NC-5-17m.RAW - Type: 2Th/Th locked - Start: 4.000 ° - End: 70.000 ° - Step: 0.020 ° - Step time: 1. s - Temp.: 25 °C (Room) - Time Started: 16 s - 2-Theta: 4.000 ° -  
 Operations: Background 1.000,1.000 | Smooth 0.150 | Import  
 05-0586 (\*) - Calcite, syn - CaCO<sub>3</sub> - Y: 50.00 % - d x by: 1. - WL: 1.54056 - Hexagonal (Rh) - a 4.98900 - b 4.98900 - c 17.06200 - alpha 90.000 - beta 90.000 - gamma 120.000 - Primitive - R-3c (167) - t

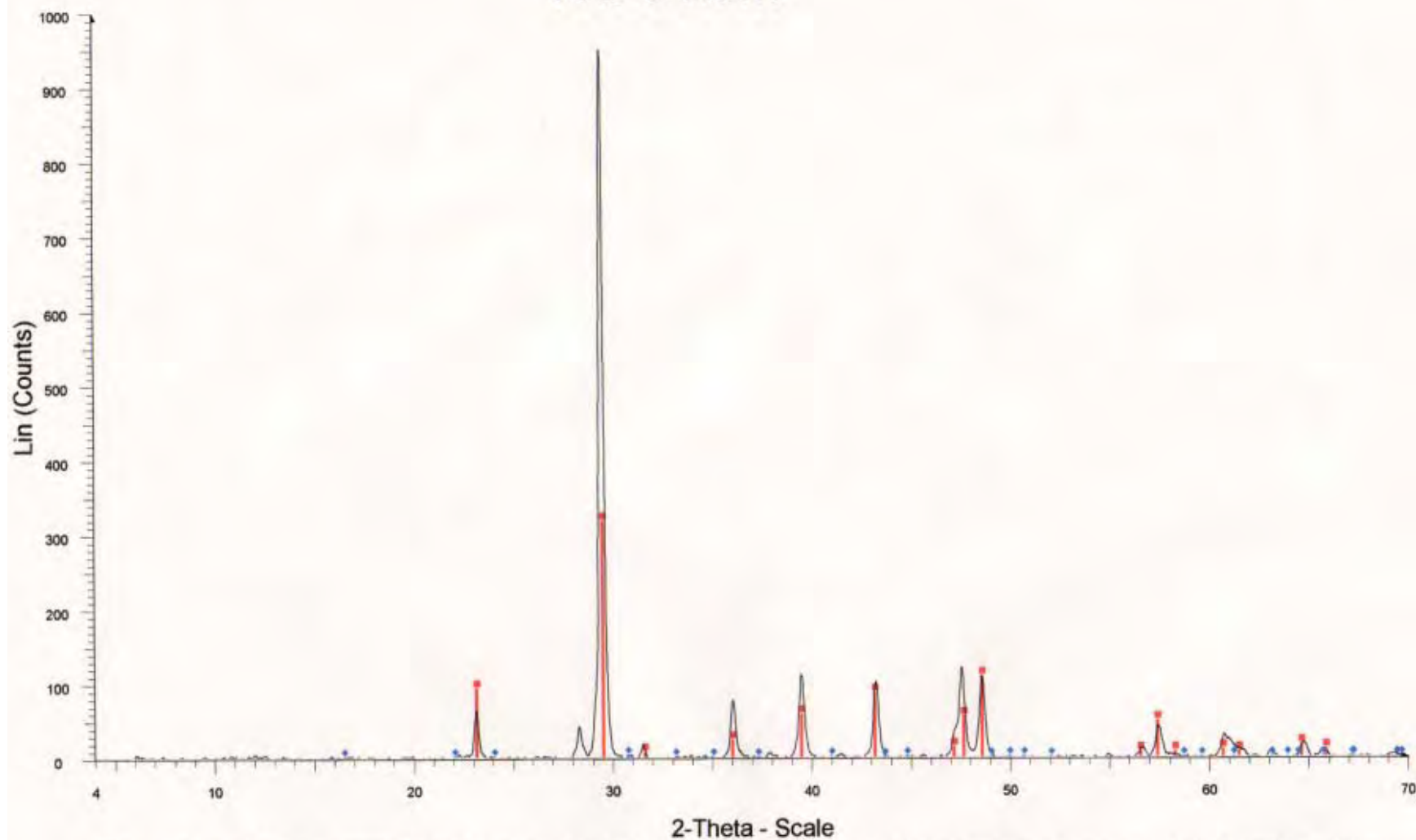


# NC-5-18.5m



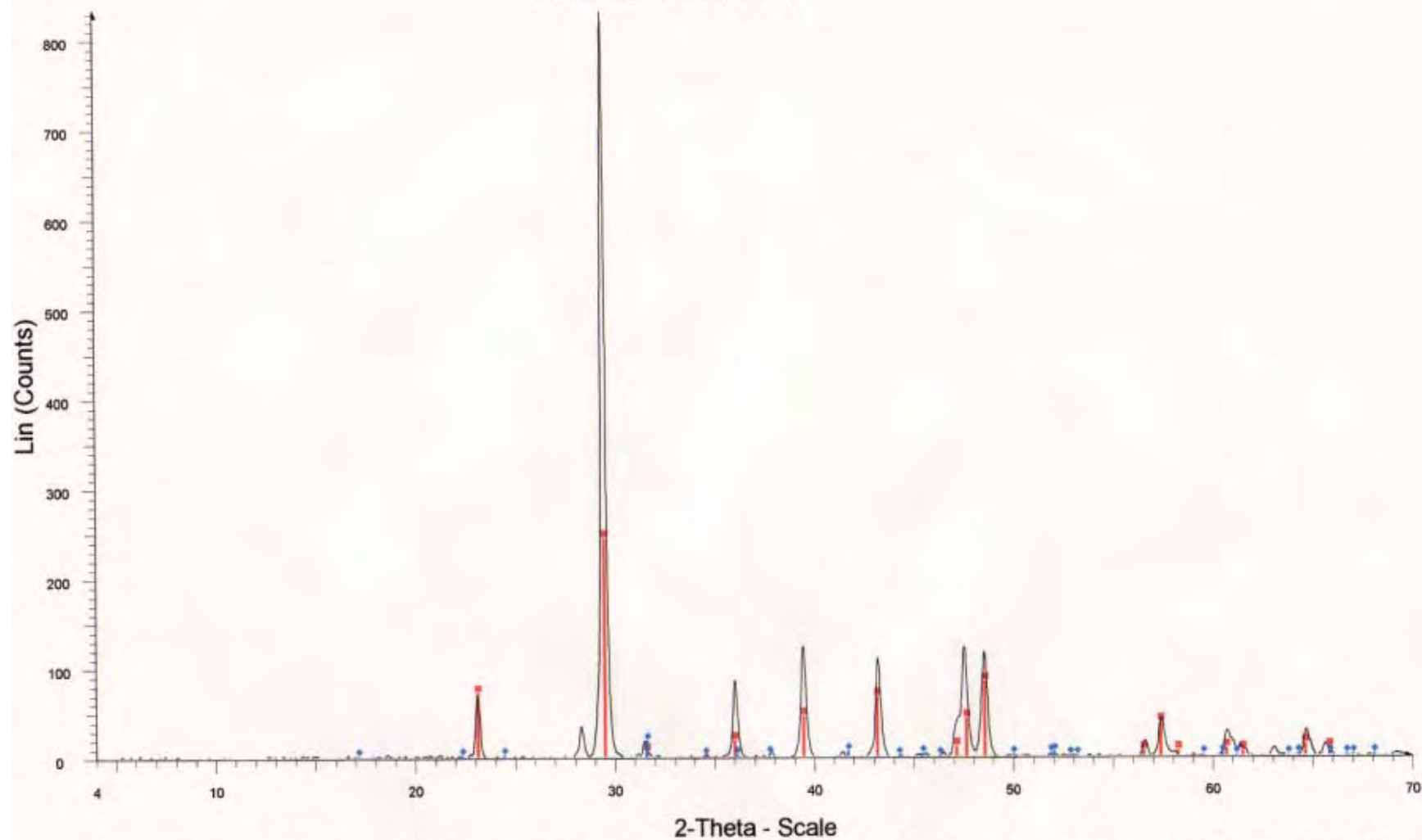
Vanessa Rosario / NC-5-18.5m - File: NC-5-18,5m.RAW - Type: 2Th/Th locked - Start: 4.000 ° - End: 70.000 ° - Step: 0.020 ° - Step time: 1. s - Temp.: 25 °C (Room) - Time Started: 16 s - 2-Theta: 4.000  
 Operations: Background 1.000,1.000 | Smooth 0.150 | Import  
 ■ 89-1304 (C) - Magnesium calcite, syn - (Mg<sub>0.03</sub>Ca<sub>0.97</sub>)(CO<sub>3</sub>) - Y: 50.00 % - d x by: 1. - WL: 1.54056 - Hexagonal (Rh) - a 4.97800 - b 4.97800 - c 16.98800 - alpha 90.000 - beta 90.000 - gamma 120.000  
 ◆ 79-1346 (C) - Dolomite - CaMg(CO<sub>3</sub>)<sub>2</sub> - Y: 1.84 % - d x by: 1. - WL: 1.54056 - Hexagonal (Rh) - a 4.76360 - b 4.76360 - c 15.58200 - alpha 90.000 - beta 90.000 - gamma 120.000 - Primitive - R-3 (148)

# NC-5-20m



Vanessa Rosario / NC-5-20m - File: NC-5-20m.RAW - Type: 2Th/Th locked - Start: 4.000 ° - End: 70.000 ° - Step: 0.020 ° - Step time: 1. s - Temp.: 25 °C (Room) - Time Started: 16 s - 2-Theta: 4.000 ° -  
 Operations: Background 1.000,1.000 | Smooth 0.150 | Import  
 24-0027 (D) - Calcite -  $\text{CaCO}_3$  - Y: 33.33 % - d x by: 1. - WL: 1.54056 - Hexagonal (Rh) - a 4.99000 - b 4.99000 - c 17.00200 - alpha 90.000 - beta 90.000 - gamma 120.000 - Primitive - R-3c (167) - 6 - 3  
 73-2444 (C) - Dolomite -  $\text{CaMg}(\text{CO}_3)_2$  - Y: 0.25 % - d x by: 1. - WL: 1.54056 - Hexagonal (Rh) - a 4.82280 - b 4.82280 - c 16.22700 - alpha 90.000 - beta 90.000 - gamma 120.000 - Primitive - R-3 (148)

# NC-5-21.5m

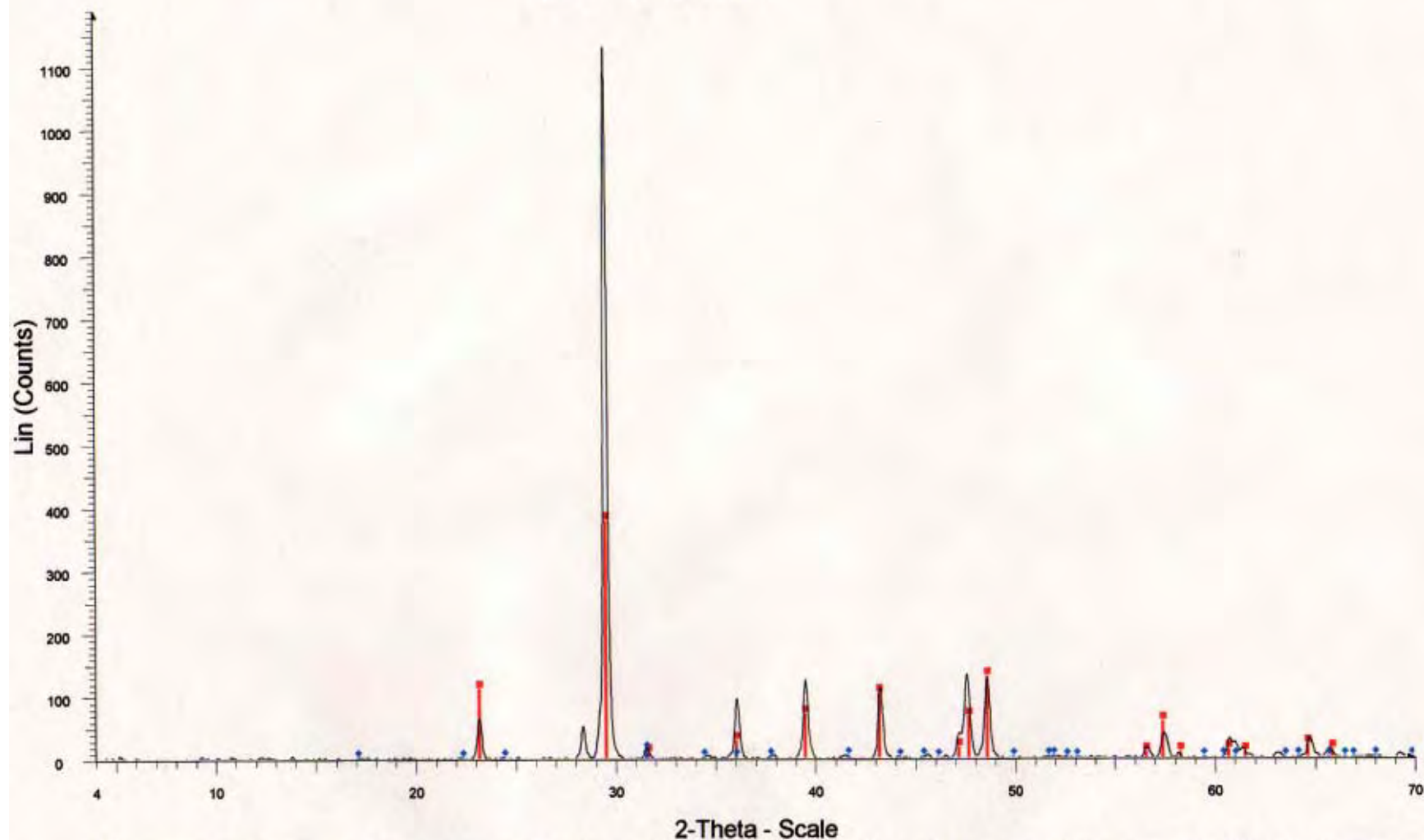


Vanessa Rosario / NC-5-21.5m - File: NC-5-21.5m.RAW - Type: 2Th/Th locked - Start: 4.000 ° - End: 70.000 ° - Step: 0.020 ° - Step time: 1. s - Temp.: 25 °C (Room) - Time Started: 16 s - 2-Theta: 4.000  
 Operations: Background 1.000,1.000 | Smooth 0.150 | Import

24-0027 (D) - Calcite -  $\text{CaCO}_3$  - Y: 29.17 % - d x by: 1. - WL: 1.54056 - Hexagonal (Rh) - a 4.99000 - b 4.99000 - c 17.00200 - alpha 90.000 - beta 90.000 - gamma 120.000 - Primitive - R-3c (167) - 6 - 3

79-1346 (C) - Dolomite -  $\text{CaMg}(\text{CO}_3)_2$  - Y: 2.00 % - d x by: 1. - WL: 1.54056 - Hexagonal (Rh) - a 4.76360 - b 4.76360 - c 15.58200 - alpha 90.000 - beta 90.000 - gamma 120.000 - Primitive - R-3 (148)

# NC-5-23m

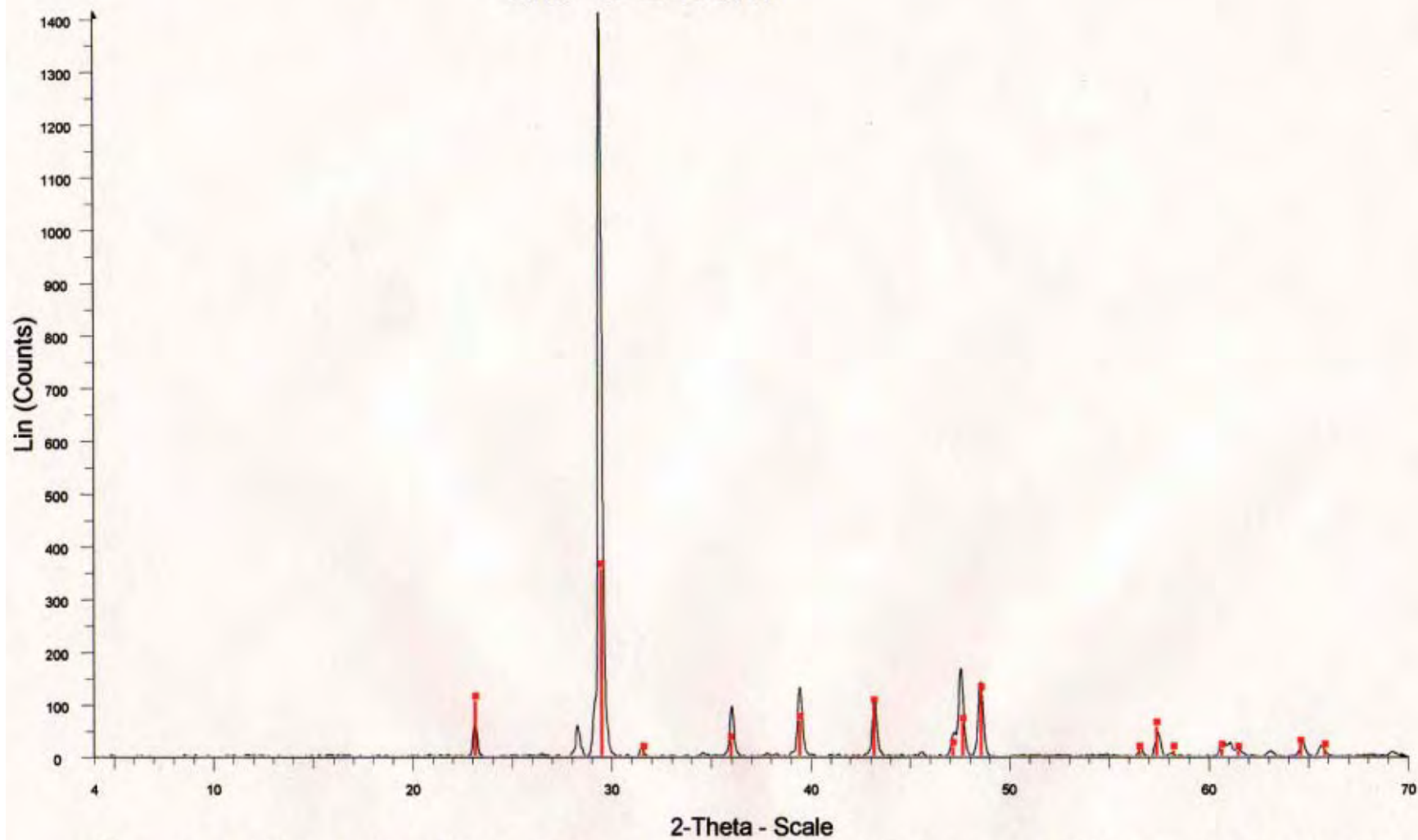


Vanessa Rosario / NC-5-23m - File: NC-5-23m.RAW - Type: 2Th/Th locked - Start: 4.000 ° - End: 70.000 ° - Step: 0.020 ° - Step time: 1. s - Temp.: 25 °C (Room) - Time Started: 16 s - 2-Theta: 4.000 ° -  
 Operations: Background 1.000,1.000 | Smooth 0.150 | Import

24-0027 (D) - Calcite -  $\text{CaCO}_3$  - Y: 33.33 % - d x by: 1. - WL: 1.54056 - Hexagonal (Rh) - a 4.99000 - b 4.99000 - c 17.00200 - alpha 90.000 - beta 90.000 - gamma 120.000 - Primitive - R-3c (167) - 6 - 3

79-1345 (C) - Dolomite -  $\text{CaMg}(\text{CO}_3)_2$  - Y: 1.04 % - d x by: 1. - WL: 1.54056 - Hexagonal (Rh) - a 4.77030 - b 4.77030 - c 15.65300 - alpha 90.000 - beta 90.000 - gamma 120.000 - Primitive - R-3 (148)

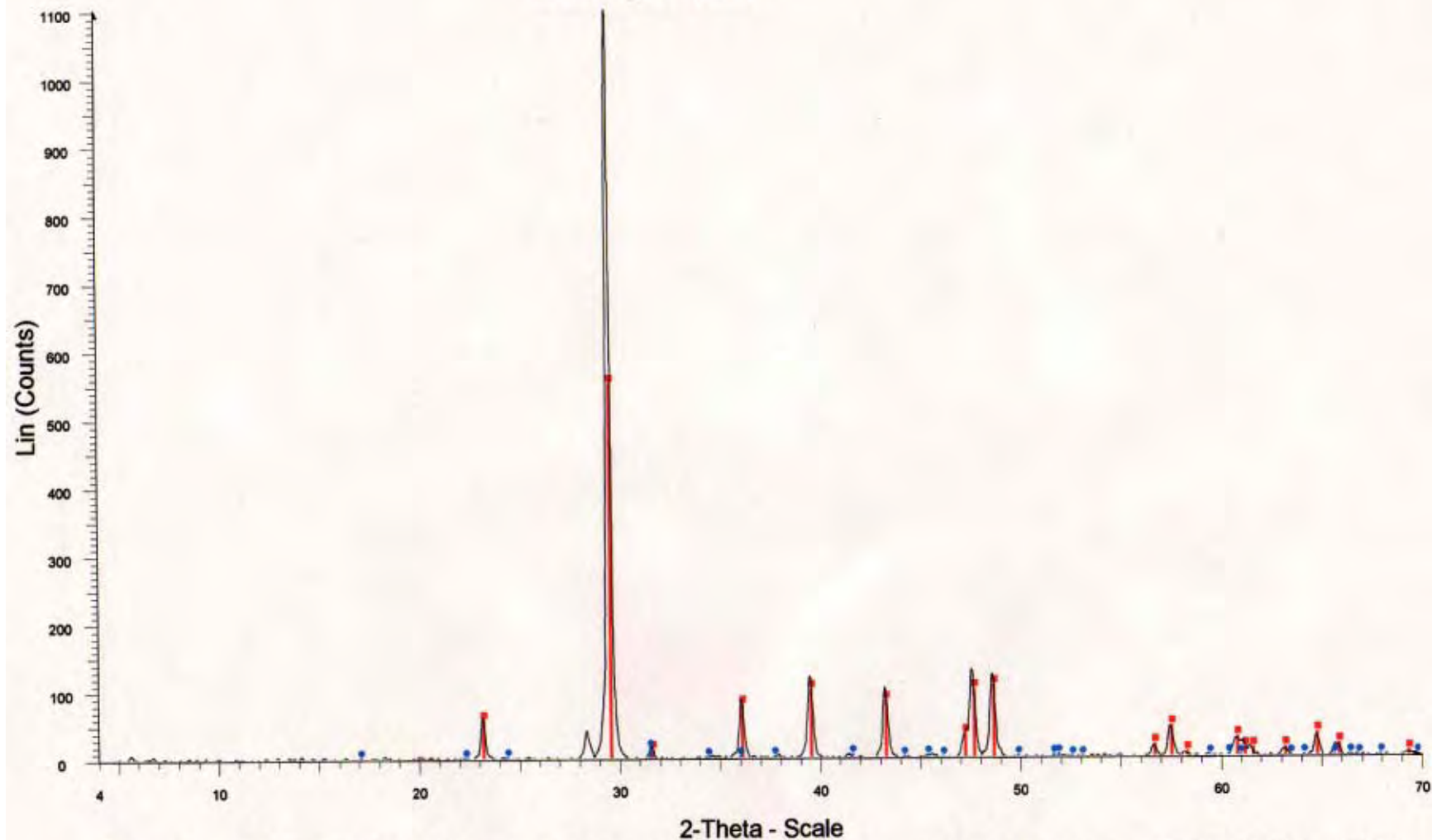
NC-5-24.5m



Vanessa Rosario / NC-5-24.5m - File: NC-5-24,5m.RAW - Type: 2Th/Th locked - Start: 4.000 ° - End: 70.000 ° - Step: 0.020 ° - Step time: 1. s - Temp.: 25 °C (Room) - Time Started: 18 s - 2-Theta: 4.000  
Operations: Background 1.000,1.000 | Smooth 0.150 | Import  
24-0027 (D) - Calcite -  $\text{CaCO}_3$  - Y: 25.00 % - d x by: 1. - VL: 1.54056 - Hexagonal (Rh) - a 4.99000 - b 4.99000 - c 17.00200 - alpha 90.000 - beta 90.000 - gamma 120.000 - Primitive - R-3c (167) - 6 - 3

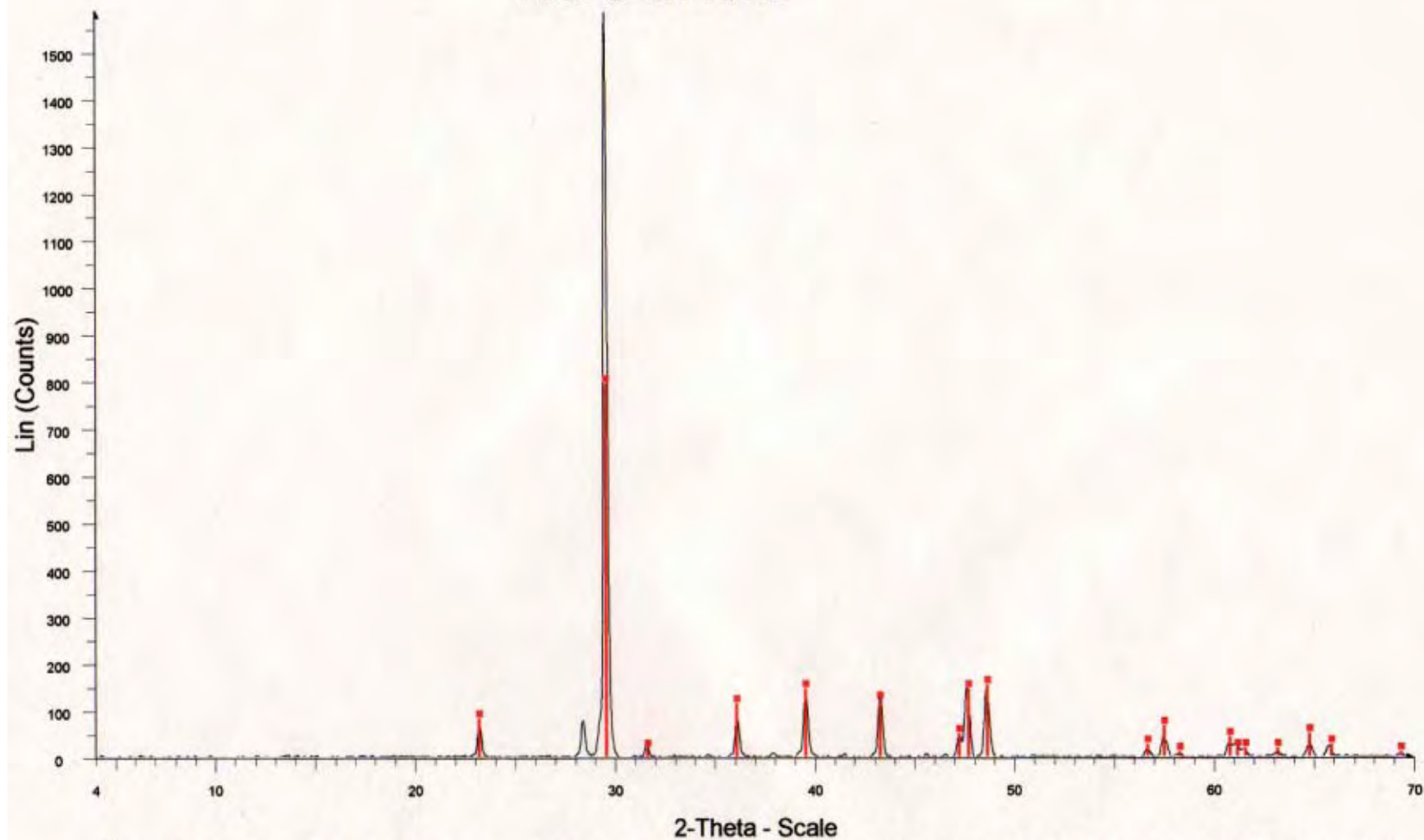


# NC-5-26m



Vanessa Rosario / NC-5-26m - File: NC-5-26m.RAW - Type: 2Th/Th locked - Start: 4.000 ° - End: 70.000 ° - Step: 0.020 ° - Step time: 1. s - Temp.: 25 °C (Room) - Time Started: 16 s - 2-Theta: 4.000 ° -  
 Operations: Background 1.000,1.000 | Smooth 0.150 | Import  
 89-1304 (C) - Magnesium calcite, syn -  $(\text{Mg}_{0.03}\text{Ca}_{0.97})(\text{CO}_3)$  - Y: 50.00 % - d x by: 1. - WL: 1.54056 - Hexagonal (Rh) - a 4.97800 - b 4.97800 - c 16.98800 - alpha 90.000 - beta 90.000 - gamma 120.000  
 79-1345 (C) - Dolomite -  $\text{CaMg}(\text{CO}_3)_2$  - Y: 1.23 % - d x by: 1. - WL: 1.54056 - Hexagonal (Rh) - a 4.77030 - b 4.77030 - c 15.65300 - alpha 90.000 - beta 90.000 - gamma 120.000 - Primitive - R-3 (148)

NC-5-27.5m



Vanessa Rosario / NC-5-27.5m - File: NC-5-27.5m.RAW - Type: 2Th/Th locked - Start: 4.000 ° - End: 70.000 ° - Step: 0.020 ° - Step time: 1. s - Temp.: 25 °C (Room) - Time Started: 16 s - 2-Theta: 4.000  
Operations: Background 1.000,1.000 | Smooth 0.150 | Import  
89-1304 (C) - Magnesium calcite, syn - (Mg<sub>0.03</sub>Ca<sub>0.97</sub>)(CO<sub>3</sub>) - Y: 50.00 % - d x by: 1. - WL: 1.54056 - Hexagonal (Rh) - a 4.97800 - b 4.97800 - c 16.98800 - alpha 90.000 - beta 90.000 - gamma 120.000